Damage Modelling of Reinforced Concrete Bridge Piers under Flood and Log Impact

A thesis submitted in fulfilment of the requirements for the degree of Doctor of Philosophy

Maryam Nasim

BEng (Civil & hydraulic), KNTU of Technology, Tehran,

MEngSc (Offshore Structures), Shand University of Technology, Tabriz

School of Engineering

College of Science, Engineering and Health

RMIT University

DECLARATION

I certify that except where due acknowledgement has been made, the work is that of the author alone; the work has not been submitted previously, in whole or in part, to qualify for any other academic award; the content of the thesis is the result of work which has been carried out since the official commencement date of the approved research program; any editorial work, paid or unpaid, carried out by a third party is acknowledged; and, ethics procedures and guidelines have been followed. I acknowledge the support I have received for my research through the provision of an Australian Government Research Training Program and Bushfire and Natural Hazard CRC Scholarship.

Maryam Nasim

20 November 2019

ACKNOWLEDGEMENT

First and the most I would like to express my sincerest gratitude to my principal research supervisor, Professor Sujeeva Setunge, for her excellent guidance throughout entire PhD steps and in my professional development. I am grateful to have had the opportunity to engage in various academic activities and develop a range of skills that I know will benefit me greatly in the future.

I am also grateful to my second supervisors, Dr Hessam Mohseni, Dr Tariq Maqsood and Dr Shiwei Zhou, for their support to complete this research. I would like to thank them for making themselves available for any meeting and discussion about ideas and provide insightful comments and positive criticisms that have enhanced the quality of my research.

I greatly appreciate the support provided from the industry research partners of the project and my greatest thanks go to the people contributed from VicRoads and BNH-CRC.

I am greatly indebted to my dear mother, Farideh Zeinali, and dear father, Hassan Nasim, for their unconditional love and support in every moment of my lifetime. My father's inspiration and lifestyle attitude and my mother's continuous love and encouragement made this possible to complete this research.

I offer my deepest gratitude to my Husband, Hossein Senobar, for his love and encouragement and support during my time at university which the completion of my PhD would not have been possible without him.

I would like to send my greatest love to my kids, Benita and Emma, for being patient and a great motivation to finish my thesis with precious results. I would also like to acknowledge the support and love from my dear brother Miad Nasim.

Finally, I thank RMIT staff and friends, and my CRC colleagues group members for providing assistance and encouragements during my research journey.

DEDICATION

I would like to dedicate this work to:

My dear daughters: Benita & Emma Senobar

My dear mother: Farideh Zeinali Guravan

My dear dad: Hassan Nasim

My dear husband: Hossein Senobar.

LIST OF PUBLICATION

Journal Papers:

1) Nasim M., Setunge S., Mohseni H., Zhou Sh. (2018) "An investigation into the water flow pressure distribution on the bridge pier under flood loading" *Structure and Infrastructure Engineering Journal*, 15:2, 219-229, DOI: 10.1080/15732479.2018.1545792

2) Nasim, M., Setunge, S, Maqsood, T., Mohseni, H. (2019) "A Comparative Study of Deflection and Energy-Based Approaches on Damage Estimation of an RC Flexural Element", Manuscript Submitted in Advances in Structural Engineering, under review

3) Nasim, M., Setunge, S, Maqsood, T. (2019) "Effect of the Mass of a Free-Dropped-Hammer on Dynamic Response of a Reinforced Concrete Beam", manuscript submitted in International Journal of Civil Engineering.

4) Nasim, M., Setunge, S, Maqsood, T. (2019), Effect of the Mass of a Free-Dropped-Hammer on Dynamic Response of a Reinforced Concrete Beam" manuscript is ready to be submitted

Conference Papers:

1) Nasim M., Setunge S., Mohseni H., Zhou Sh, Dissanayake A., "An Investigation to the Behaviour of water flow on Bridge Pier in Flood Event" Australian Bridge Conference (2017), Melbourne, Australia.

2) Nasim M., Setunge S., Mohseni H., Zhou Sh**, "**Computational Investigation on the Piers of a U-Slab Bridge under Raising Flood Intensity" IABMAS (2018), Melbourne, Australia.

3) Nasim M., Setunge S., "Vulnerability Assessment for the RC Beam Exposed to Monotonic Loading Using Different Damage Indexes", CSTX (2019) Barcelona, Spain.

Abstract

Australia has suffered from the loss of life and extreme damage to infrastructure from natural hazards such as bushfire, flood etc. Floods are Australia's costliest disasters on bridges, one of the most important components of highway and railway transportation network. Therefore, safety and serviceability of bridges have always been a great concern to the practice and profession of civil engineering. The resilience of critical infrastructures such as roads and bridges is vital in evacuation support activities for during, before and after disaster response and recovery. In addition, bridges have a significant impact on the resilience of road infrastructure and the damage to bridges could significantly increase the vulnerability of the community served by the transportation infrastructure. Therefore, understanding the factors which affect the resilience of bridge structures, is extremely important to ensure the design specifications, as well as maintenance regimes for bridge structures. Furthermore, considering the resilience and vulnerability of structures is vital during, before and after disasters. Roads Corporation of Victoria (VicRoads) has identified that older structures consisting of U-slab decks are vulnerable to flood loading. The proposed project will focus on understanding damages to U-slab bridges exposed to flood loading.

The vulnerable element of the case study U-slab bridges has been identified using a simplified analysis using Space-Gass. This analysis indicated that the superstructure of a U slab structure is quite robust under flood loading and slender piers can be vulnerable. Water flow pressure on the piers has been studied using Computational Fluid Dynamics (CDF) methodology to examine the pressure distribution on piers with two different cross-sectional shapes. This work has demonstrated that the pressure distribution on a bridge pier under flood loading can be simulated using a uniformly distributed load. Further, it is noted that the

magnitude of the flood-induced force is significantly affected by the geometry of the pier cross-section.

Considering the concrete plasticity damage (CPD) modelling, nonlinear analysis has been conducted to evaluate the damage behaviour of the piers, and a simple damage index based on energy absorbed, which can be derived from a standard finite element modelling output, has been introduced. Based on that different damage levels of a bridge pier under flood loading damage indices have been derived.

Based on the review of practice and the literature review the log or moving object impact is likely to be occurring during flood loading. Therefore, a comprehensive investigation has been conducted to understand the structural response of a moving object impact, i.e., log impact. Using a validated model, the general relationship between different aspects of the structural response has been studied. Moreover, the bridge damage response during log impact has been studied, and the numerical results have been compared to provisions of different design standards. This study has concluded that the current provisions of design standards on the log or any moving object impact on bridges under flood loading could be unconservative and will require a systematic study considering the varying mass of impacts and the geometry of bridge piers.

TABLE OF CONTENTS

List of Figures

List of Tables

Abbreviation

AASHTO…..……. American Association of State Highway and Transportation Officials
ALLDMD…..……. The Whole Model's Damage Dissipated Energy
ANN…..…… Artificial Neural Networks
AS…...…… Australian Standards
BITRE ……. Bureau of Infrastructures, Transport and Rational Economics
CDP…….…… Concrete Damage Plasticity
CFD …….……. Computational Fluid Dynamics
DDE ……. Damage Dissipated Energies
DI.…… Damage Index
Dis …… Damage Indices
DL ……... Damage Level
DLs …… Damage Levels
DMIF…….……...…… Dynamic Multiplier of Impact Force
DWT……... Dead-Weight Tonnage of The Vessel
FEM ……..…..……Finite Element Method
FEMA ……..Federal Emergency Management Agency
FDM ……..Finite-Difference Method
FDR ……...… Flexural Damage Ratio
FSI……..…….…...… Fluid-Structure Interaction
FVM …….. Finite-Volume Method
GDP…… Global Damage Parameter
LES ……. Large-Eddy Simulation
MO …… Moving Object
PIV…….…… Particle Image Velocimetry
RC……...…. Reinforced Concrete
SDOF……... Single Degree of Freedom
URANS……...……...……. Unsteady-Reynolds-Averaged Navier-Stokes
UDL …….…… Uniformly Distributed Static Load
VOF……...……. Volume of Fluid

LIST OF SYMBOLS AND NOMENCLATURE

Notation/Symbol	***Definition***
p	*Pressure*
ρ	*Fluid density*
V_f	*Fluid velocity*
u	*The velocity component in the fluid flow direction (x)*
t	*Time*
T	*Temperature*
k	*Thermal conductivity*
Φ	*Viscous-dissipation function*
Q	*The vector of conserved variables*
F	*Vector of fluxes*
V	*Volume of the control volume element*
A	*The surface area of the control volume element*
C_d	*Drag coefficient*
f_{cu}	*Ultimate compression strength of concrete*
f_{ct}	*Tensile strength of concrete*
E_c	*The module of elasticity of concrete*
ν	*Poisson ratio*
$\acute{f}_c$	*The compression strength of concrete*
f_y	*Steel yield stress*
E_s	*The module of elasticity of steel*
f_{b0}	*Initial equibiaxial compressive yield stress*

f_{c0}	*Initial axial compressive yield stress*
$\widetilde{\delta_T}$	*Total deformation*
$\widetilde{\delta_e}$	*Elastic deformation*
$\widetilde{\delta_{Tr}}$	*Residual deformation*
δ_i	*Displacement of the mid-span in loading step i*
δ_{uj}	*Ultimate deformation of the mid-span in each DL, j (j=1,2,3)*
DDE_i	*Damage dissipated energy in loading step i*
DDE_{uj}	*Ultimate damage dissipated-energy*
A_s	*Streel cross-sectional area*
σ_t	*Tensile stress*
σ_c	*Compressive stress*
d_t	*Tensile damage variable*
d_c	*Compressive damage variables*
E_0	*Initial module of elasticity*
ε_t	*Tensile strain*
ε_c	*Compressive strain*
$\varepsilon_t^{\sim pl}$	*Tensile plastic strain*
$\varepsilon_c^{\sim pl}$	*Compressive plastic strain*
g	*Gravitational acceleration*
h	*Impactor height*
d	*Displacement of the hammer*
ξ	*Damping ratio*

δ_n	*the nth amplitude of the response curve*
m	*Number of conservative cycles in the response curve*
E_{total}	*Total energy*
β	*Constant coefficient of total energy*
φ_m	*Factor of mass*
m_h	*Mass of the hammer*
m_b	*Mass of the beam*
G	*Peak acceleration of the impact*
T_b	*The beam thickness*
H	*The drop height*
D_{max}	*Maximum deformation*
D_u	*Ultimate deformation*
C_d	*Drag coefficient*
A_d	*The area of the surface facing the flow*
V_f	*Fluid Velocity*
v_{ih}	*The velocity of the impact*
$\hat{k}$	*Effective contact stiffness*
m_l	*The mass of the object*
DWT	*The dead-weight tonnage of the vessel*
S	*Stopping distance of the object*
v_ω	*The velocity of wave propagation in concrete*
l	*Wave propagation length*
t_p	*Wave propagation time*

F_{ip}	*The peak impact force*
φ_{pi}	*The dimensionless factor of the peak impact forces*

CHAPTER 1

Introduction and Research Background

1 Introduction and Research Background

Whether from a bushfire, flood, severe storm, earthquake, or even tsunami, Australia has suffered from the loss of life and extreme damage to infrastructure from natural hazards and as our communities grow, so does the potential for more significant losses in these areas. Pritchard (2013) emphasized that the current standards (AS 5100:2004) do not cover extreme flood loads.

Floods have the highest damage potential of all kinds of natural disaster worldwide and affect the highest number of people.

Figure 1-1: Average annual cost of natural disasters by state and territory, 1967-2005 (BITRE, 2001b)

State and territory	Flood	Severe storms	Cyclones	Earthquakes	Bushfires	Total
		Cost ($ million in 2005 Australian dollars)[a]				
NSW	172.3	217.1	0.6	145.7	23.9	559.6
VIC	40.2	23.8	0.0	0.0	36.7	100.6
QLD	124.5	46.7	99.3	0.0	0.7	271.2
SA	19.3	16.7	0.0	0.0	13.0	49.0
WA	4.7	13.0	43.3	3.1	4.6	68.7
TAS	6.9	1.2	0.0	0.0	11.5	19.5
NT	9.1	0.4	138.5	0.3	0.0	148.3
ACT	0.0	0.5	0.0	0.0	9.7	10.2
Australia	**376.9**	**325.2**[b]	**281.6**	**149.1**	**100.1**	**1232.9**
Share of total *(per cent)*[c]	30.9	26.7	23.1	12.2	8.2	100.0

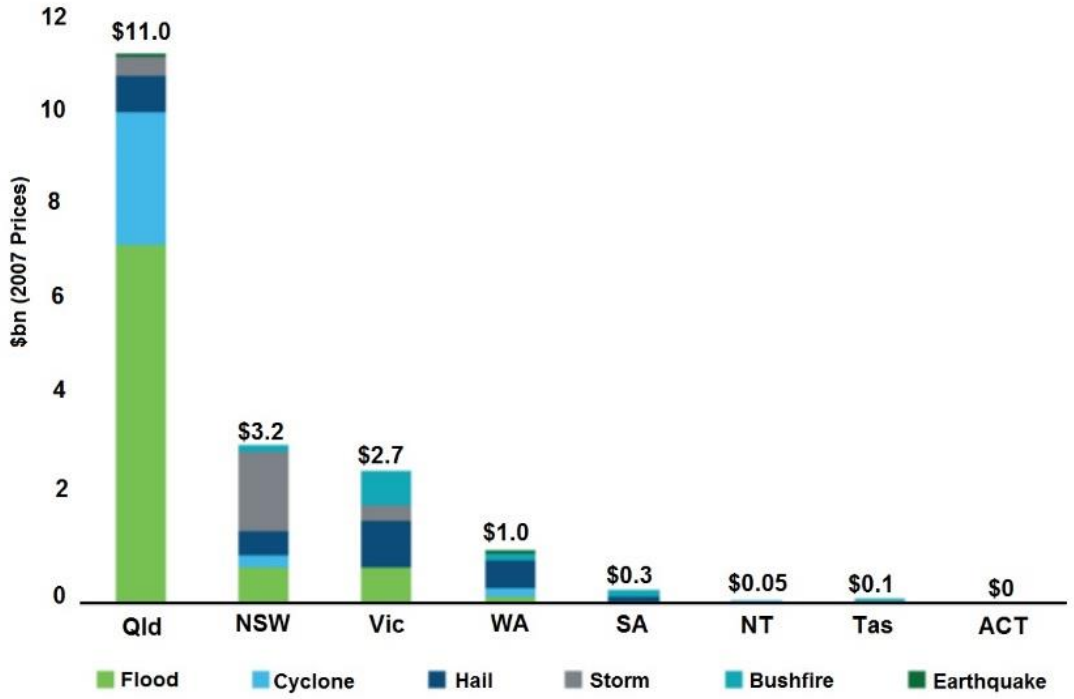

Figure 1-2: Total economic cost of natural disasters, by state, average 2007-2016 ($bn) (*Deloitte Access Economics, (2017). Building resilience to natural disasters in our states and territories*)

Figure 1-1, by BITRE's (Bureau of Infrastructures, Transport and Rational Economics) research group; represents the average annual cost of natural disasters by states and territory between 1967 and 2005. These data indicate that during this period, floods are Australia's the most costly disaster type, accounting for 29 per cent of total natural disaster costs over the period 1967–1999 (BITRE, 2001b). Severe storms and cyclones inflicted the most economic damage, followed by flood. Climate change has increased the risk from extreme events and the update of this table that includes data for the years 2007 to 2013 – during extreme climate events in QLD, VIC, SA and NSW – will be of great interest to this project. However, Australian Business Roundtable for Disaster Resilience & Safer Communities prepared Figure 1-2 to present aggregated costs of various natural hazards. Deloitte Access Economics, (2017) reports

the amount of loss of urban structures during natural hazards and based on this information, the loss from the flood is considered especially in Queensland state. These costs are expected to be doubled by 2030 and to increase to an average of $23 billion per year by 2050, see Figure 1-3.

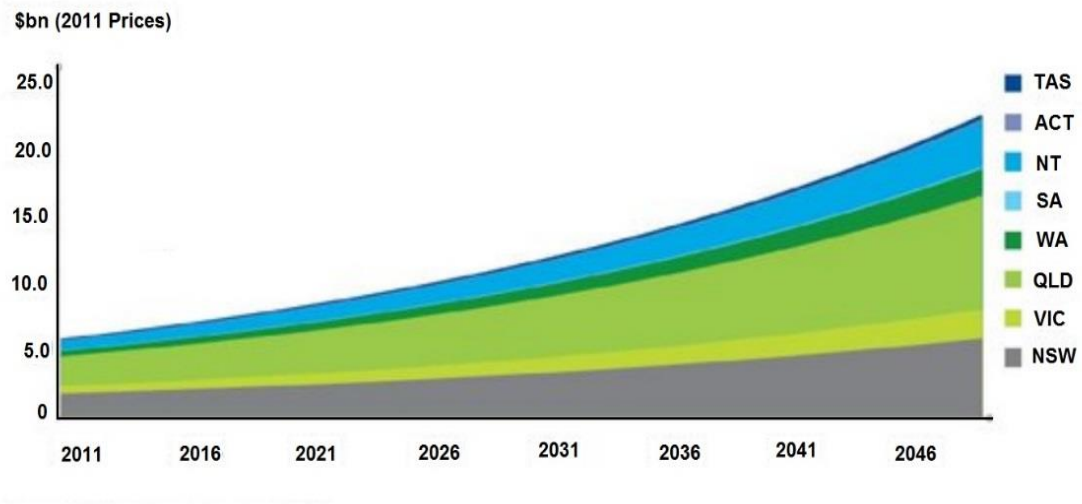

Figure 1-3: Forecast of the total economic cost of natural disasters 2011-2050, (Deloitte Access Economics, (2017). Building resilience to natural disasters in our states and territories)

Bridges are important components of highway and railway transportation systems. Therefore, safety and serviceability of bridges have always been a great concern to the practice and profession of civil engineering. Experience indicates that bridges are extremely vulnerable to natural and human-made hazards such as earthquakes, floods, high wind, blast and vehicle/vessel impact at bridge piers (Prasad Gautham Ganesh, 2011). Damage of bridges due to such extreme events may cause significant disruption of the normal functionality of transportation systems, and thus may result in major economic losses to the society and affect the greatest number of people.

The resilience of critical infrastructures such as roads and bridges is vital in evacuation support activities for disaster response and recovery (Oh, Deshmukh, & Hastak, 2010). Bridge

structures have a major impact on the resilience of road infrastructure and the damage to bridges could increase the vulnerability of the community served by the road infrastructure significantly. During an emergency event, the community relies on road infrastructure to enable them to evacuate the area quickly. During the re-building period after a disaster, bridges play a major role in ensuring access to the affected areas. Therefore, understanding the major factors which affect the resilience of the bridge structures is extremely important to ensure that the design specifications, as well as maintenance regimes for bridge structures, consider the resilience and vulnerability of structures during a disaster.

The major damage due to these events is identified as abutment scouring, failure of the deck and girders due to the impact of floating items and loss of bridge approaches (Kalendher, 2017). The damage will depend on the structural configuration of the bridge as well as exposure scenarios. During flood events, authorities are faced with the challenge of making appropriate decisions regarding traffic control on bridges. Remaining the bridges open during a disaster plays a vital role in disaster recovery. Nevertheless, considerable casualties and property loss can happen if bridges are in danger of collapse are not closed in a timely manner (C.-C. Hung & Yau, 2014), so there is a strong demand for an effective safety evaluation method for bridges during flood events. Roads Corporation of Victoria (VicRoads) has identified that older structures such as U-slab bridges are vulnerable during flooding. Hence, to fully understand the structural damage under different scenarios, the proposed research, is focusing on the understanding of the vulnerability of the U-Slab bridge structures as a case study when it is exposed to flood or any impact of a floating object. The methodology proposed in this study, developed can be used as a generic approach for vulnerability assessment of similar bridges.

Major failure mechanisms of river bridges have earlier been identified as deck and the bridge approach, pier abutment scouring, significantly built up of mud and debris on the structure and approaches, log impact on the piers and bridge deck, cracks in the abutment wing walls and misalignment of abutment headstock connection to piles (Lebbe, Lokuge, Setunge, & Zhang, 2014).

Drag and uplift forces and the vortices effect on these forces on the bridge decks have been studied experimentally and with CFD simulation models (Kerenyi, Sofu, & Guo, 2009). Numerical simulations show that uplift force can be greater than the weight of the bridge deck for about 20-30% of the time during a wave period, for the case study of wave load on the bridge deck of the Biloxi Bay Bridge during Hurricane Katrina, (Xiao, Huang, & Chen, 2010). Basically, the CFD-based simulations give a reliable perspective about the distribution of flood-induced stress within the structure.

During the extreme flood, bridges are exposed to the debris and log load, which is considered in design codes in Australia by the ultimate limit state with a 2000-year return interval design flood. This provision means that most of the bridges over waterways will be designed for overtopping; therefore, the design flood loads required to be revised. Jempson (2000), has done further research on debris and flood loads on superstructure according to the limit state philosophy and presents a series of design charts and tables. Further, he developed a new methodology for the calculation of overturning moments that accounts for the correct line of action of the drag and lift forces (Jempson, 2000).

1.1 Research Aims and Objective

The major aim of the conducted research is to understand the vulnerability of U-slab bridge structures under flood loading. Figure 1-4 presents a schematic U-slab bridge structure commonly used in Victoria, Australia.

Figure 1-4: U-Slab Bridge Located in Victoria, Australia

These older structures have slender bridge piers at close intervals. The research objectives cover three major areas.

1) Understanding the effect of the distributions of hydrodynamic flood force on bridge piers.
2) Understanding the effect of floating moving object impact on bridge piers.

3) Understanding the effect of the mass of the objects on the impact forces and damage to bridge piers.

At the beginning of the research, a preliminary analysis was undertaken to understand the most vulnerable part of the structure under flood loading. Outcomes of this combined with extensive consultation with the road cooperation of Victoria narrowed the scope down to the vulnerability of the U-slab bridge piers under flood and object impact.

Subsequently, a computational fluid dynamics analysis was conducted to understand the force distribution on piers under flood loading. This was followed by the static failure element analysis to understand the effect of the flood loading on the U-slab piers damage behaviour.

Finally, the impact of objects on the U-slab piers was analysed using dynamic analysis of impact.

The outcome develops an understanding of the behaviour of U-slab piers under flood loading and the impact of floating objects, also it develops a generic methodology for vulnerability analysis of bridge structures under varying flood loading and impact of objects of varying mass.

1.2 Significance of Research

The research presented here develops a method to understand the effect of flood and object impact on bridge piers.

The work develops an understanding of the failure modes of bridge piers under flood and moving object impact and develops a method to estimate the damages.

Outcomes are valuable in identifying the vulnerability of the structures under flood loading and levels of damages.

1.3 Research Questions

The research presented here has addressed the following questions.

1) What are the failure modes of a U-Slab Bridge exposed to flood?

2) What are the typical loadings to be considered in analyses of the effect of the flood on bridges?

3) How can we create a numerical model to analyse the effect of flood loading on U-Slab bridges?

4) How can we establish damage models for the bridge under flood and log impact loading?

5) What are the failure criteria for concrete elements under fluid pressure and log impact?

6) What parameters influence the failure of piers under flood loading?

1.4 Research Gap

1) Current Australian standards do not comprehensively cover extreme flood loading due to rapid changes in intervals of hazards caused by climate change.
2) Managing authorities need to understand the damage behaviour of bridges under flood loading.

3) Literature does not cover comprehensive damage responses for bridges under different flood conditions and different parameters.
4) The impact loading from a log and other objects are not comprehensively covered with different codes such as AS5100, and it is assumed as a quasi-static loading. However, the dynamic behaviour of an object impact on the structure needs to be understood to quantify the likelihood of failure.
5) The equivalent static impact force proposed by AASHTO is currently independent of pier geometry. This needs to be further explored.
6) Hydrodynamic forces generated by floodwater flow needs to be considered for understanding the response of structures.

Research scope developed to address the gaps identified from practical literature and review, are addressed as,

1) Investigate the vulnerability and the instability behaviour of U-slab bridge as a case study under extreme flood, and the dynamic effect of a moving object (MO) impact during exposure to extreme flood events, on the piers and the deck.

2) Study into the recognition of the failure modes and likely mechanisms of failure. Also, the vulnerable components and factors influencing failure.

3) Develop a numerical model for the piers, deck and simulation of the moving object impact.

4) Calculate dynamic and static forces on bridges structures due to different flood velocities.

5) Present an overall methodology as a generic method for damage response and make a decision in enhancing the resilience of U-slab bridges, exposed to flood loading, for wider application.

1.5 Preliminary work

A preliminary study was conducted to understand the vulnerability of the U-slab deck under flood loading. This preliminary work included an analysis of the flood and object impact on the U-slab deck of the case study bridge. Figure 1-5 presents the case study structure and the configurations.

The outcome of the analysis demonstrated that the U-slab deck is less vulnerable to lateral flood and floating object impact compared to the I-girder deck reported by (Lebbe et al., 2014). Further, it was clear that the slender piers of the structure would be more vulnerable under flood and object impact. Therefore, a decision was made to focus the research on the piers of the U-slab bridge structure.

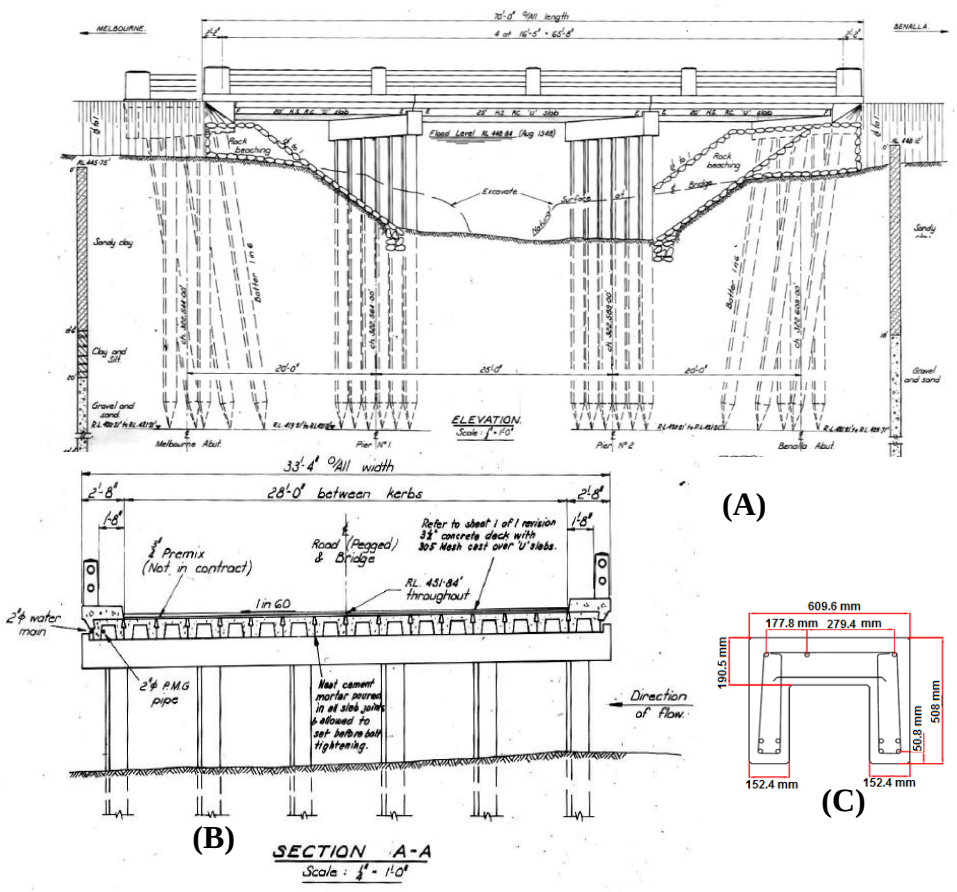

Figure 1-5: (A) Typical U-slab Bridge in Melbourne, (B) the bridge section and (C) the deck elements cross-sectional detail

1.6 Thesis outline

Based on the Study rationales, the thesis is categorized into four principal chapters. Chapter 2 provides a comprehensive study on the nature of the hydro-dynamic, and hydro-static loading exerted from the flood on bridge piers. In design standards, a simplified analysis method is adopted where researchers consider the effect of the flood on a distributed load. In this chapter, a detailed analysis is undertaken to ascertain the loading applied and the effect of the geometry of the pier on the applied load using a computational fluid dynamics approach. The study explored the effect of flood velocity on the load applied on the piers. This study has been

published in Structure and Infrastructure Engineering (Nasim, Setunge, Mohseni, & Zhou, 2018).

Chapter 3 focuses on damage to the bridge piers under flood loading. This commenced with the estimation of the damage induced on a reinforced concrete structural element utilising a finite element methodology to calculate the structural damage and response when it is under incremental flood pressure. An incremental static analysis, employing ABAQUS/Standard is conducted to compare the deflection-based method and the dissipated-damage-energy method, to calculate and predict structural damage. The influence of the degree-of-freedom of the structure is investigated on the failure scenario of the system. This study is submitted to Advances in Structural Engineering in Nov 2019 and is under review.

Chapter 4 is an introduction to Chapter 5, which is a preamble to establish the methodology of impact modelling. The methodology of numerical simulation is presented and validated with some experimental results from the literature. The dynamic behaviour of a reinforced concrete beam with similar geometry of our study is modelled and analysed by conducting ABAQUS/Explicit package, and the effect of the mass of the impactor is studied to fully understand the structural responses. The results validated our methodology, and the work has been submitted to Archives of Civil and Mechanical Engineering in Nov 2019 and is under review.

Chapter 5 provides a very comprehensive parametric study on the influence of the mass and velocity of a moving object, to examine the structural dynamic responses in terms of maximum impact forces resulting from the impact of the moving object. In this chapter, the maximum design impact forces are compared with provisions of design standards such as

AS5100 and AASHTO. The results have shown the necessity of considering moving object impact in the design procedure. The result of this work will be submitted to a journal for publishing.

The flowchart presented in next page describe the research methodology and outline different steps carried out in this study.

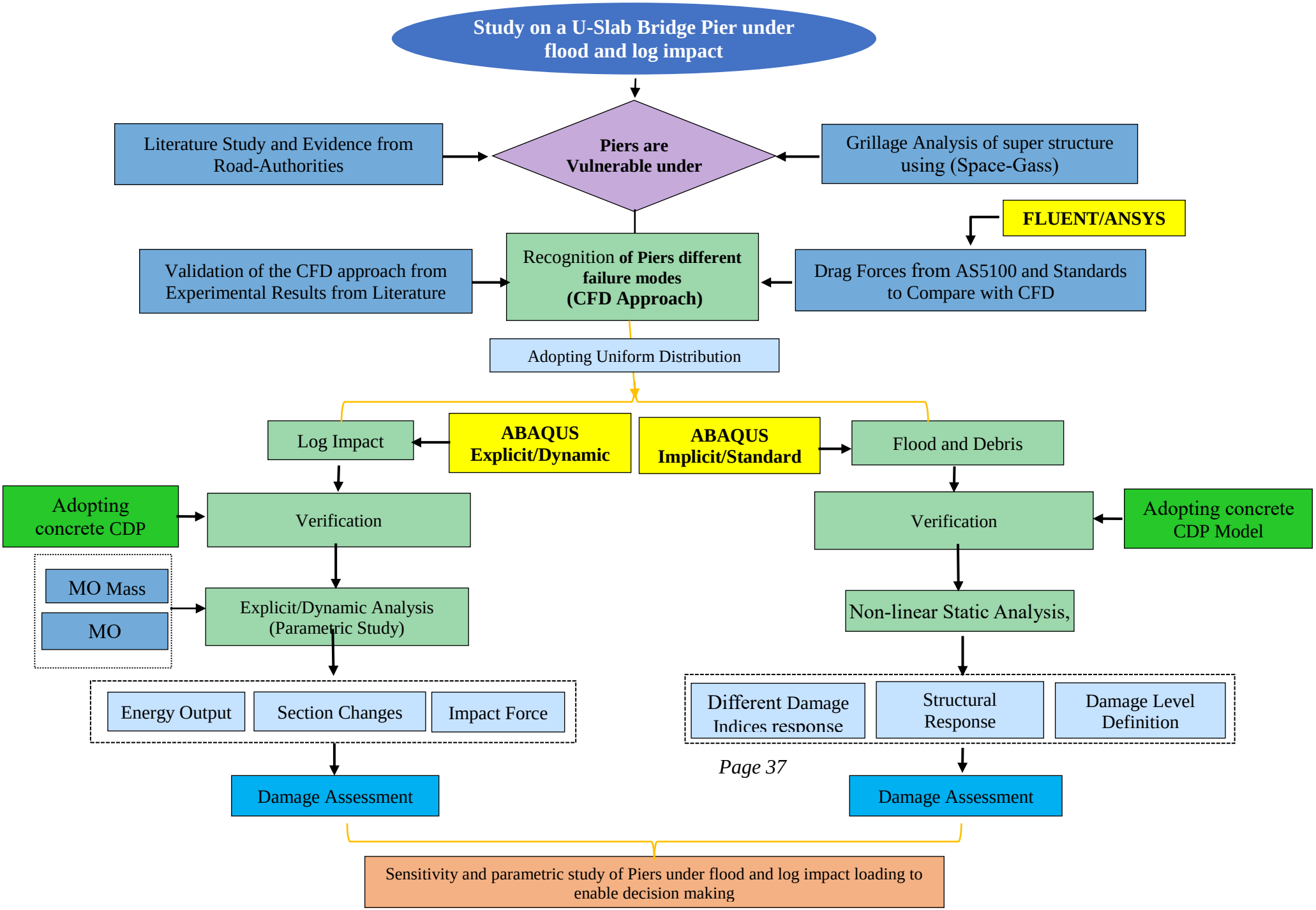
Study on a U-Slab Bridge Pier under flood and log impact
Literature Study and Evidence from Road-Authorities
Piers are Vulnerable under
Grillage Analysis of super structure using (Space-Gass)
FLUENT/ANSYS
Validation of the CFD approach from Experimental Results from Literature
Recognition of Piers different failure modes (CFD Approach)
Drag Forces from AS5100 and Standards to Compare with CFD
Adopting Uniform Distribution
Log Impact
ABAQUS Explicit/Dynamic
ABAQUS Implicit/Standard
Flood and Debris
Adopting concrete CDP
Verification
Adopting concrete CDP Model
Verification
MO Mass
MO
Explicit/Dynamic Analysis (Parametric Study)
Non-linear Static Analysis,
Energy Output
Section Changes
Impact Force
Different Damage Indices response
Structural Response
Damage Level Definition
Damage Assessment
Damage Assessment
Sensitivity and parametric study of Piers under flood and log impact loading to enable decision making

CHAPTER 2

An Investigation of Water-Flow Pressure Distribution on Bridge Piers under Flood Loading

Statement of Authorship

Journal paper title:	An Investigation of Water-Flow Pressure Distribution on Bridge Piers under Flood Loading
Status:	Published
Reference:	M Nasim, S Setunge, SW Zhou, H Mohseni, 'An investigation of water-flow pressure distribution on bridge piers under flood loading', Structure and Infrastructure Engineering, 15:219-229, 2019.
Name:	Maryam Nasim
Position:	PhD Scholar
Contribution:	Corresponding Author, Collecting and interpreting data, performing analysis, preparing figures and writing the manuscript
Name of author:	Sujeeva Setunge
Position:	Professor, Deputy Dean Research and Innovation School of Engineering, RMIT University
Contribution:	Supervising research, assisting in manuscript preparation and reviewing
Name of author:	Shiwei Zhou,
Position:	Lecturer, School of Engineering, RMIT University
Contribution:	Editing and reviewing the manuscript
Name of author:	Hessam Mohseni,
Position:	Lecturer, School of Engineering, RMIT University
Contribution:	Editing and reviewing the manuscript

2 An investigation of water-flow pressure distribution on bridge piers under flood loading

Synopsis

In order to quantify the vulnerability of bridge piers under flood loading, it is essential to understand the types of loading applied on bridge piers under flood. A review of the literature indicated that there is a gap in knowledge in this space with most studies assuming a simplified uniformly distributed static load (UDL) on a bridge pier. In this research, ANSYS-FLUENT is employed to carry out a computational fluid dynamic analysis. This analysis indicated that the assumption of a UDL is appropriate for representing flood loading. However, the shape of the pier affected the magnitude of the load applied.

Abstract

This study simulates the flood effect on piers using a finite volume method in the ANSYS-FLUENT package. The pier is modelled as a non-structural column with a rectangular and a circular cross-section. To simplify the methodology, the pier, as well as the bed and sidewalls, is assumed to be non-slip boundaries for the fluid domain. A crucial feature of this investigation is the consideration of the effect of water while it is flowing around an object like a bridge pier and the distribution of pressure along with the pier height. A numerical model is proposed to explore the influence of variation of velocity on the hydrodynamic force and pressure distribution exerted on piers. A significant finding is that the shape of the pier cross-section has a significant effect on the fluid pressure exerted on bridge piers under flood loading. It is noted that the AS5100 method is appropriate for a conservative estimation of the pressure on

rectangular piers, whereas the technique will have a risky safety margin for bridge piers with a circular cross-section and need to be used with caution.

Keywords: Flood loading; Computational fluid dynamics; Finite volume methods; Bridge piers; Shape effect; Hydraulics; Hydrodynamics; Flood hazard

2.1 Introduction and Literature Review

Resistance to flood and debris loading are critical parameters affecting the design of bridges under flood loading. The increase in flood intensity during the past decades because of global warming has led researchers to revise bridge design codes. Flow around a cylinder is a topic of numerous experimental and numerical studies. Water flow is a very complex phenomenon and still needs to be considered in future research. A comprehensive survey of the behaviour of fluid flow around piers is essential for the prediction of water flow distribution and the evaluation of a bridge's response. Using a computational fluid dynamics (CFD) method, in this study, the water flow distribution is demonstrated in comparison with the equation proposed in the standards.

Bridges under flood loading have been studied in numerous literature. The design and research on riverine bridges have various aspects of being investigated. Some researchers consider the structural behaviour and focus on structural modelling, ignoring the water flow dynamic behaviour. On the other hand, other researchers have focused on the water flow dynamic aspects, including drag forces, different parameters of fluids such as drag coefficients, Reynolds numbers and various methodologies of computational modelling. Although fluid behaviour is entirely complicated and needs more study, the fluid-structure interaction (FSI) is

another factor which has been studied by different researchers. Moreover, the scouring effect and fluid-soil interactions are other areas of CFDs taken into consideration by engineers.

The following literature review covered various aspects of fluid dynamics, and it was noted there is a lack of research addressing the effect of fluid load on a fixed object such as a bridge pier. Simulating the fluid pressure on a bridge pier and understanding the methods of numerical modelling to investigate structural behaviour are the main objectives of the research.

2.1.1 Bridge Damage History

Historical data show that two types of the most costly natural disasters in Australia from 1967 to 1999 are riverine flooding (approximately $314 million per annum) and severe storm damage (roughly $284.2 million per annum) reported by (Melbourne & Water, 2005). Over the last 30 years, numerous bridges around the world have been damaged by flooding. For example, the Schoharie Creek Bridge (Storey, Chris, Delatte, & Norbert, 2003) in New York was destroyed in 1987, the Hatchie Bridge (M. Cao, Liu, & Meng, 2009) in Tennessee was demolished in April 1989, and the Hintze Ribeiro Bridge (Sousa & Bastos, 2013) in Portugal was damaged in 2001, all due to floods. The Walnut Street Bridge in the United States collapsed in 1996 because of flood intensity (Lee & Sternberg, 2008). The CPR Bonnybrook Bridge in Canada failed due to water flow pressure and scouring, which exceeded the bridge's structural instability in a flood event in 2014 (Ebrahimi et al., 2016). The damage to these bridges was entirely or partially attributed to damage to the piers caused by unexpected flood loading on the structure or scouring.

However, in order to investigate a bridge pier's failure, understanding of the water flow distribution is essential. Water flow force on the piers in a significant majority of bridges built

across rivers is calculated using the methods specified in design codes. Although scouring, as a result of a flood, is one of the most critical phenomena which cause bridges to lose their stability, water flow pressure as well as debris and log impacts, can cause structural damage and failure. Therefore, the distribution of water flow pressure is the focus of this study. To understand this further, the effect of water pressure beyond the effects of other phenomena during flood loading is investigated.

2.1.2 A Review of Fluid-Structure Interaction (FSI) Studies

Previous studies of the effects of floods on bridge piers have mainly focused on fluid loadings as a result of the fluid-structure interaction (FSI). The concept of FSI considers the stability of oscillatory interaction of some deformable or floating structures with an internal or surrounding fluid flow. It is one of the crucial considerations in the design of many engineering systems, e.g. bridges and aircraft. Several studies concentrate on the effect of hydrodynamic pressure on the seismic response of bridge piers (Arnold et al., 1977; Gao & Zhu, 2006; F. Li, Chen, & Wang, 2008; Y.-c. Li, 1990; Xue-kui, Xi, & Hui, 2006; Yoshihiro & Robert, 1988). Wang, Zou, Xu, & Luo (2015) investigated the water current around piers and the coupling effects between solid and fluid interfaces using FSI methods. Einstein & El-Samni, (1949) measured the dynamic loadings on a rough wall and found that even in the case of an extremely high relative roughness, the drag force on protrusions can be determined based on the logarithmic friction formula, which is a logarithmic function of roughness, fluid velocity and its geometrical parameters.

Ataei & Padgett (2015) investigated the vulnerability of a coastal bridge under hurricane conditions and determined how the different factors in modelling of the fluid-structure influenced the bridge's response. Aghaee & Hakimzadeh, (2010) simulated the turbulent flow

around a vertical circular pier with consideration of the coupling of pressure and velocity, and the vortexes around the pier were investigated using the Reynolds-averaged Navier-Stokes equation and the space-averaged Navier-Stokes equations.

2.1.3 A Review of Scouring and Fluid-Soil Interaction Studies

In relation to the study of fluid interactions with soil, some researchers have studied the fluid around piers to calculate and observe the scouring behaviour of the soil around piers (see (Gaudio, Tafarojnoruz, & Calomino, 2012) and (Ferraro, Tafarojnoruz, Gaudio, & Cardoso, 2013)). For a long time, due to the complexity of the fluid and structures involved, this issue has been studied experimentally. In an experimental investigation of the velocity around a pier, the response to the forward and backward flow was investigated to predict the local scour (Beheshti & Ataie-Ashtiani, 2009). Ghodsi & Beheshti (2018) developed a methodology to optimise the scour depth around a complex bridge pier. Tubaldi et al. (2017) developed a novel probabilistic framework for the computation of the vulnerability of bridge-pier during scouring using a Markovian approach to account for memory effects in scouring development. Kerenyi et al., (2009) conducted an analysis of sediment transport and its influence on scouring with consideration of shape optimisation of piers, with the aim of minimising scour and pier erosion, and concluded that the evaluation of active or passive counter-measures could mitigate further damage. Numerical simulation of rectangular and circular piers to understand the vortex around a pier and the scour response has been carried out for different cylinder heights (Ou Zhiliang, 2007).

2.1.4 Numerical and Experimental Studies of Water Flow Characteristics

Numerous studies of 3-D simulations and experimental investigations of bridge pier underflow have been conducted to simulate water flow velocity. However, in the last few decades, the numerical modelling of the flow around piers has been a growing field of investigation. Catalano et al. (2003) performed a large-eddy simulation (LES) of the flow around a circular cylinder at high Reynolds numbers. The methodology's accuracy is typical for high Reynolds numbers considering a very complex turbulent flow. Kuroda et al. 2007) studied the flow around a rectangular cylinder using LES and then compared the results with particle image velocimetry (PIV) data. A 3-D LES of the turbulent flow around a cylindrical pier is presented in (Wei & Huhe, 2006). Advances in the use of LES to study flow around bodies are reviewed in (Z. Yang, 2015). Darg and up-lift loadings, together with their vortex effects on bridge decks, have been studied experimentally and numerically (Kerenyi et al., 2009). The drag coefficient is the other research area which researchers have focused on recently, and the experimental studies conducted and discussed to reduce the drag coefficient is by (Hamed, Vega, Liu, & Chamorro, 2017).

Rezaeiha et al., (2017) performed an extensive set of unsteady-Reynolds-averaged Navier-Stokes (URANS) simulations to study the impact of the cylinder, serving as different aerodynamic parameters and Reynolds number. Malizia et al. (2016) performed several CFD simulation of a cylinder at low Reynolds (3,900) and sub-critical Reynolds numbers (140,000). They found the best agreement at low Reynolds numbers for (URANS) k-ω, based on grid-sensitivity analysis and validation with wind tunnel measurements available in the literature for two Reynolds numbers. The drag coefficient of flow around rectangular, semi-circular-nosed, and 90-degree wedged-nosed and circular piers has been calculated numerically using the finite

element method (Almasri & Moqbel, 2017). These researchers recommended that the AASHTO drag coefficient values should be revised for different circumstances, especially under severe conditions. Yuce and Kareem, (2016) numerically studied the fluid flow around bluff bodies such as circular and square cross-sectional bodies for different Reynolds numbers and examined the drag forces using a k-ω turbulence closure model.

In the present study, the k-ω turbulence concept is used to model a non-structured model underwater flow. This concept gives a reasonable response in comparison with some experimental data of Yuce and Kareem (2016).

2.1.5 A Review of Computational Fluid Mechanics (CFD)

Fluid mechanics use numerical analysis to solve fluid problems. CFD is used for a wide range of calculations of fluid to determine its characteristics, considering the fluid boundary conditions. CFD-based simulation can be used for a wide range of hydraulic problems, including the assessment of drag force for bridge piers, for shape optimisation and the evaluation of active or passive countermeasures for damage mitigation (Kerenyi et al., 2009). Such simulations based on CFD are reliable and have distinct advantages. CFD can assist in the assessment of lift and drag loading on flooded decks to calculate pressure as a function of velocity.

The complex fluid-soil interactions under the effects of floods are governed by the Navier–Stokes equations in which the conservation of mass, momentum and energy are taken into account. Numerical methods, such as the finite-volume method (FVM), the finite-difference method (FDM), and the finite element method (FEM), have been developed to effectively discretise and solve these equations (Mattiussi, 1997, 2000). The classical FDM approach to

the discretisation of field problems is based on the use of finite difference formulae to approximate locally the derivatives entering the expression of differential operators. A structured grid of points is defined first usually a very regular one, and a local field quantity are attached to each point. Then, for each of these points, the differential operators appearing in the problem's equations are given a discrete expression using the above-mentioned finite difference formula. FVM is a numerical method to discretise the field equations of a problem by subdividing the problem domain into cells and compiling the field equations in the integral form of these cells (Calomino, Tafarojnoruz, De Marchis, Gaudio, & Napoli, 2015).

On the other hand, the FEM is an analytical tool for solid mechanics, and its first formulation was based on a direct physical approach (Burnett, 1987; Fletcher, 1984). Given its flexibility concerning FD methods, and the good results produced, the FE approach was applied to many other fields, with variations required by the nature of the new problems (Mattiussi, 2000). For example, Hung and Wang (1987) used FDM to calculate the distribution of non-linear hydrodynamic pressures on the vertical and inclined surfaces of dams. The FVM combines the advantages of FEM for geometric flexibility and FDM for simple discrete computation (C. Chen, Liu, & Beardsley, 2003). As FVM uses less computational memory and provides high calculation efficiency, it is especially suitable for the turbulent flows featured with high Reynolds numbers, and source term dominates flows (Patankar, 1980). Using the Volume of Fluid (VOF)-based method in FLOW-3D (a general CFD software), numerical model simulations were conducted for bridge constructions using four different types of bridge openings located in a compound channel and it was discovered that the ability and performance of the model are affected by various bridge configurations and shapes (Kocaman, Seckin, & Erduran, 2010).

Computational methods for solving the Navier-Stokes equations are primarily classified into two categories: density-based methods and pressure-based methods, depending on whether the fluid is compressible or incompressible, Miettinen and Siikonen, (2015) addressed the full application of both approaches. Many existing techniques (Pulliam & Steger, 1980) solve the continuity equation for the density (as a primary variable) and then specify the pressure (as a secondary variable) using the equation of state. Therefore, they are called density-based methods. However, a pressure-based method, where the pressure is used as a primary variable, has no restrictions associated with specific flow regimes (Hirt, Amsden, & Cook, 1974). The present pressure-based method is an extension of the procedure of (Rhie & Chow, 1983), which was originally developed to solve incompressible Navier-Stokes equations. The FLUENT package is able to consider both methods, and in our study, incompressible fluid is assumed for analysis; therefore, the present study uses a pressure-based approach.

2.2 Methodology

The methodology of this paper adopts a CFD approach. This work was carried out to determine how the total water flow pressure can change during fluid velocity alterations. The two models represented rectangular and circular cylinders and were developed numerically to understand the change in fluid pressure and its distribution when there is an increase in fluid velocity. In this study, an FVM is used to determine the distribution of pressure on the piers of the cuboid and cylindrical shapes for a wide range of flood velocities. Conservation laws apply to an infinitesimally small control volume or to an infinitesimal fluid system to analyse fluid motion. There are three basic differential equations of fluid motion, summarised as follows:

2-1: *Continuity:* $$\frac{\partial p}{\partial t} + \nabla.\left(\rho V_f\right) = 0$$

2-2: *Momentum (Navier-Stokes)*: $\rho \frac{dV}{dt} = \rho g - \nabla p + \nabla . \tau_{ij}$

2-3: *Energy:* $\rho \frac{d\hat{u}}{dt} + p(\nabla . V) = \nabla . (k \nabla T) + \Phi$

where p is the pressure, ρ is the fluid density, V_f represents the fluid velocity, τ_{ij} is shear stress, t is time, T is temperature, k is thermal conductivity, and Φ is a viscous-dissipation function derived from:

2-4: $\Phi = \mu \left[2(\frac{\partial u}{\partial x})^2 + 2(\frac{\partial v}{\partial y})^2 + 2(\frac{\partial w}{\partial z})^2 + (\frac{\partial v}{\partial x} + \frac{\partial u}{\partial y})^2 + (\frac{\partial w}{\partial y} + \frac{\partial v}{\partial z})^2 + (\frac{\partial u}{\partial z} + \frac{\partial w}{\partial x})^2 \right]$

where, μ is the dynamic viscosity coefficient, u, v, z are the velocity component in the fluid flow directions (x, y, z), (White, 2011).

Numerical FVM analysis is the most appropriate modern approach. In this method, to solve differential equations, equations are written in a conservative form before solving over the discrete control volumes. One of the most significant advantages of such discretisation is the guarantee of flux conservation using a particular control volume, as shown below:

2-5: $\boldsymbol{\frac{\partial}{\partial t} \iiint Q \, dV + \iint F \, dA = 0}$

where Q is the vector of conserved variables, F is the vector of fluxes, V is the volume of the control volume element, and A is the surface area of the control volume element (Patankar, 1980).

Depending on the flow conditions, hydrostatic and hydrodynamic loads are generally applied to bridges (Coulbourne, 2011). These loads depend on the flow velocity, and hydrodynamic load can be transferred to hydrostatic load for simplification when the speed is less than 10 m/s,

according to the ASCE standard (ASCE, 1994). However, AS 5100 does not have such restrictions.

Two major hydrodynamic loads of fluid flow proceeding over an object can split into drag (horizontal load or aligned with the fluid streamlines) and uplift forces (vertical load or perpendicular to the fluid streamlines) as shown in Figure 2-1. The active and most critical hydrodynamic loads on a pier as a cylinder are drag and lateral loadings.

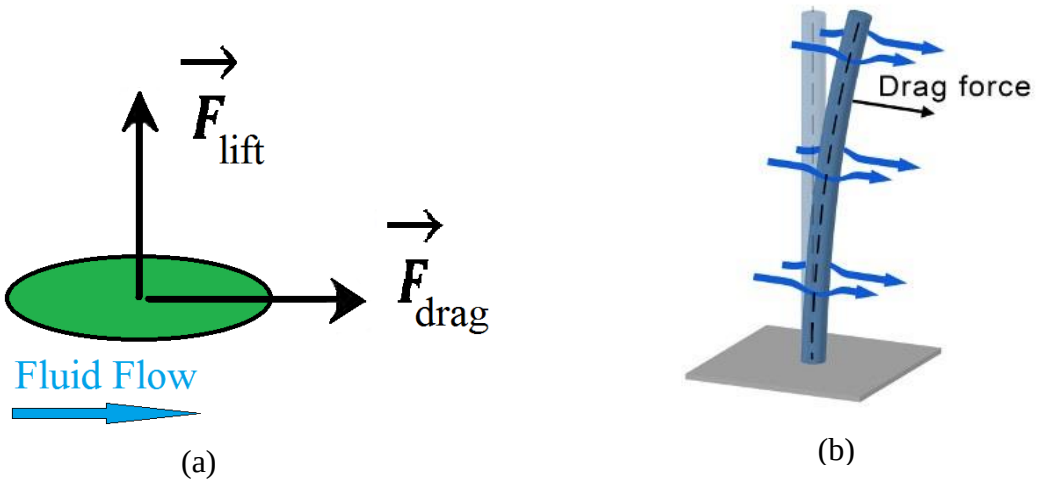

(a) (b)

Figure 2-1: Hydrodynamic forces on the submerged subject (a) drag and uplift forces on the submerged subject, (b) drag forces on the cylindrical subject.

Equivalent static loads can be adopted instead of a dynamic load, to simplify the current methodology, Different standards' techniques, such as EUROCODE, AS5100, ASCE, for the definition of drag load are similar while the difference is raising from the drag coefficient calculations. The equivalent static drag load is determined by the following equation, according to AS5100 (Standards Australian, 2017):

2-6: $\boldsymbol{F_{Drag}=\frac{1}{2}C_d\rho V_f{}^2 A_d}$

where, C_d is the drag coefficient, depending upon different parameters such as pier shape and flow factors, see (Apelt & Issac, 1968; BS, 2005; Parola, Apelt, & Jempson, 2000; Standards Australian, 2017), and ρ and V_f are the fluid density and velocity, respectively. The area of the surface facing the flow is represented as A_d. In addition, the effect of water flow on piers can be calculated as a function of second-degree parabolic velocity distribution multiplied by a constant (AASHTO, 2002). The constant is a function of drag coefficient which is assumed 1.4 for all piers subjected to drift build-up and square-ended piers, 0.7 for circular piers, and 0.5 for angle-ended piers where the angle is 30 degrees or less. Although international standards use a similar method for calculation of the drag force, they have different coefficients. In this study, AS5100 is selected to compare the numerical approach with the equations proposed by standards. The vertical uplift force and the forces resulting from the impacts of debris and logs should also be considered in addition to water pressure.

2.2.1 Fluid Domain Simulation

In this study a numerical simulation has been developed for rectangular and circular cylinders, representing bridge piers, to investigate the pressure distribution on piers and explore the provisions of the current design standards for bridges in AS5100 (2017). In this study, a 3-D finite-volume incompressible Navier-Stokes model is set up for each rectangular and circular cylinder, and analysed using the ANSYS FLUENT software (FLUENT, 2009). This investigation is focused on the water, as running fluid, around the pier, as a solid and non-structural object, to quantify the total pressure on the submerged pier caused by water flow. The set-up conditions for both models of rectangular and circular piers were the same, and a

wide range of fluid velocities of nearly still water to flash flooding was examined to derive the pressure variations. As the behaviour of the structure in this step was not considerable, the piers were modelled as a non-structured model, as a cylindrical cavity, which means the pier's boundaries were assumed to be non-slip walls, as was the channel walls boundary condition. The piers of the bridge case study shown in Figure 2-2 (a) were modelled during these exercises. This is a typical ageing structural configuration in Australia identified as a U-slab structure. The circular cylinder with the same diameter is comparable to a rectangular model.

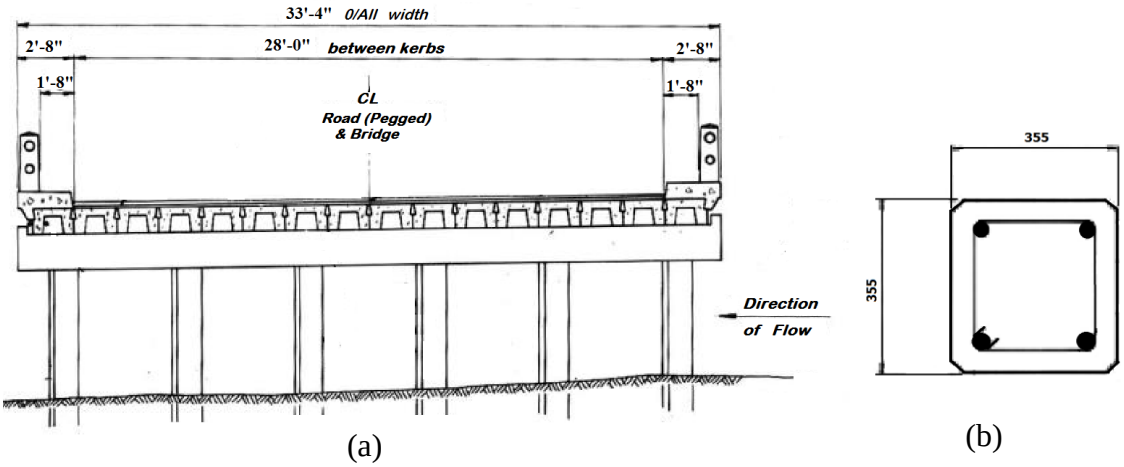

Figure 2-2: (a) A typical U-slab bridge section constructed in Victoria, (b) The U-slab pier cross-section

Previous researchers have recommended the use of a width equal to 14D for cuboids, where D is the width of the object exposed to the fluid. For example, (Zhang, 2017) simulated a cylinder exposed to flow to examine the Reynolds number and noted that 14D width is appropriate Based on the above recommendations, in this research a fluid flow domain confined in a cuboid with the size of 5×7×3.5 (m) in x, y and z directions as shown in Figure 2-3, has been used.

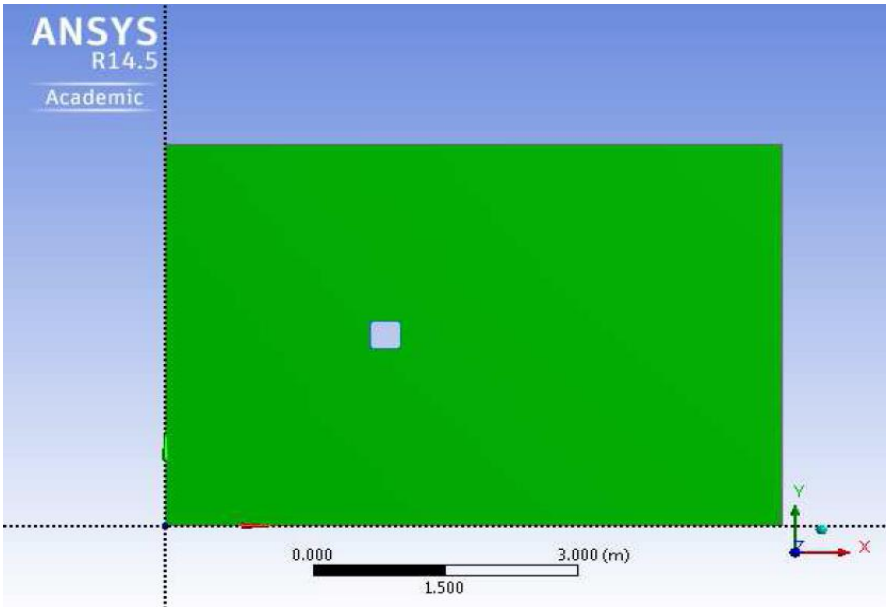

Figure 2-3: Water Flow Domain and Rectangular Cylinder, 5×7×3.5 (m3) X, Y, Z

To design bridge structures, it is recommended to assume the piers which are entirely submerged when considering the critical flood condition (Standards Australian, 2017). In this case, the selected model was a case study of a U-slab bridge pier with a rectangular cross-section (0.355×0.355 m^2) and circular cross-section (0.355 m diameter), and the bridge height was assumed to be 3.5m. As shown in Figure 2-4, the model was developed in FLUENT, and the adaptive mesh was generated in the simulation to save computational time by conducting some mesh sensitivity analysis. A standard k-omega (k-ω) turbulence model was employed to reflect the turbulence boundary conditions. The k-ω model was implemented in the Navier–Stokes flow solver, which was developed for algebraic turbulence models (J. Kok, Boerstoel, Kassies, Spekreijse, 1996) and is usually used for problems of solid/fluid interactions (J. C. Kok, Spekreijse, 2000).

The drag coefficient was selected based on the AS5100:2 (2017) suggestion for rectangular and circular cross-sections varying in the range of 1.3-3.3.

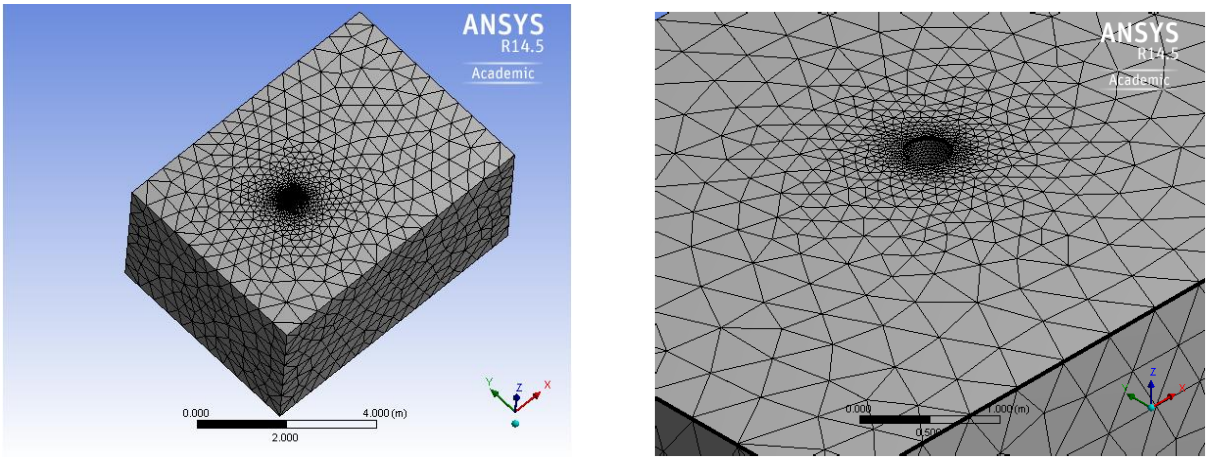

Figure 2-4: Discretised Model in Adaptive Mesh for both Rectangular and Circular Piers

2.3 Results and Discussion

AS5100:2 (2017) proposes full submergence of the bridge as the critical flood height (Fletcher, 1984). Various velocities were applied to the domain in the range of 0.5-10 m/s with 0.5-1 m/s increments. Figure 2-5 shows the flow domain with a pier surrounded by flood domain and depicts the domain velocity streams over the rectangular pier.

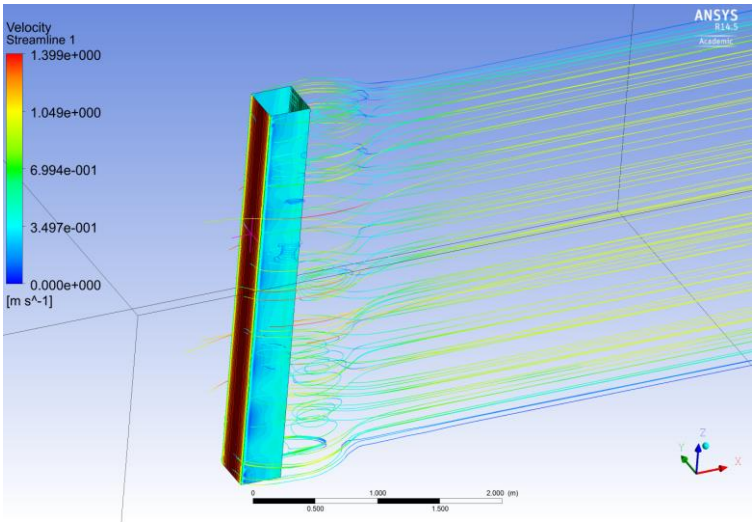

Figure 2-5: Velocity streamlines around a rectangular pier.

Figure 2-6 presents the pressure contours and their distribution on rectangular and circular piers when the water flow velocity is around 5 m/s, and it can be seen that the distribution of the pressure is nearly uniform with minimal depression at the top and bottom of the pier.

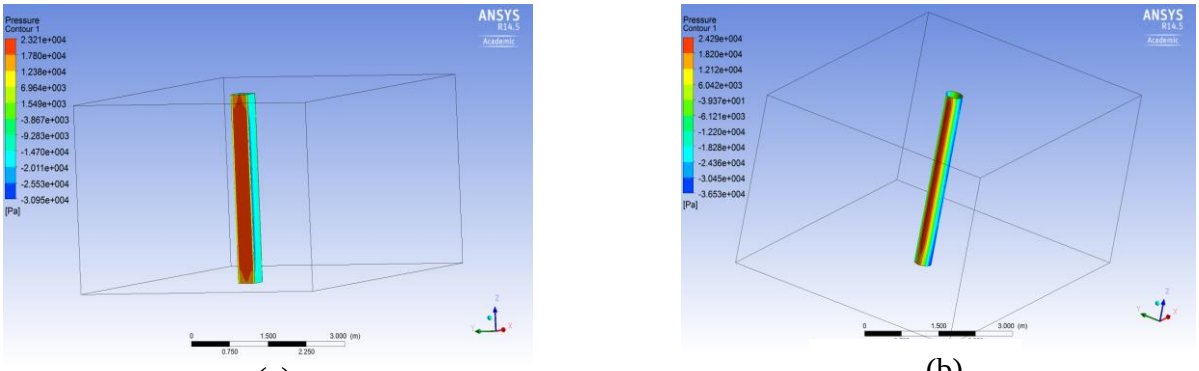

(a) (b)

Figure 2-6: Pressure contours on rectangular (a) and circular (b) pier when inlet velocity is 5 m/s

Figure 2-7 (a) and (b) display the velocity contours and streams on the circular pier and the two imaginary perpendicular plates and the velocity variation around the pier. The responses are compared with the experimental data gathered by (Van Dyke, 1982) in Figure 2-7 (c). The water flow speed increases around the pier's edges, and as expected, it decreases near the domain margin and the non-slip walls.

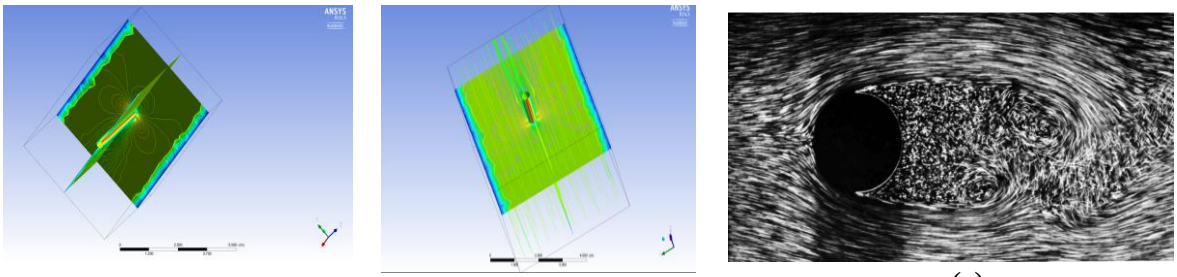

(a) (b) (c)

Figure 2-7: (a) Velocity distribution (b) Streams around circular pier; (c) Experimental study of streams around the cylinder (Van Dyke, 1982)

In order to validate the research methodology, the model's results were compared with the results of (Yuce, Kareem, 2016). The bar charts in Figure 2-8 and Figure 2-9 compare the pressure on the circular and rectangular models for the velocities 1m/s, 1.5 m/s, 2 m/s and 4 m/s. As expected, the values for lower speeds are very close, because the fluid is less turbulent. In contrast, when the water flow velocity increases the difference becomes significant.

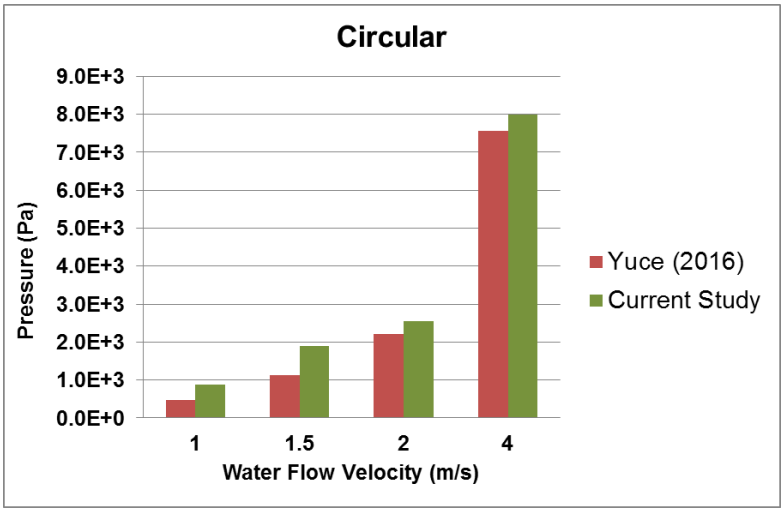

Figure 2-8: Pressure on Circular Model Compared with Yuce and Kareem (2016)

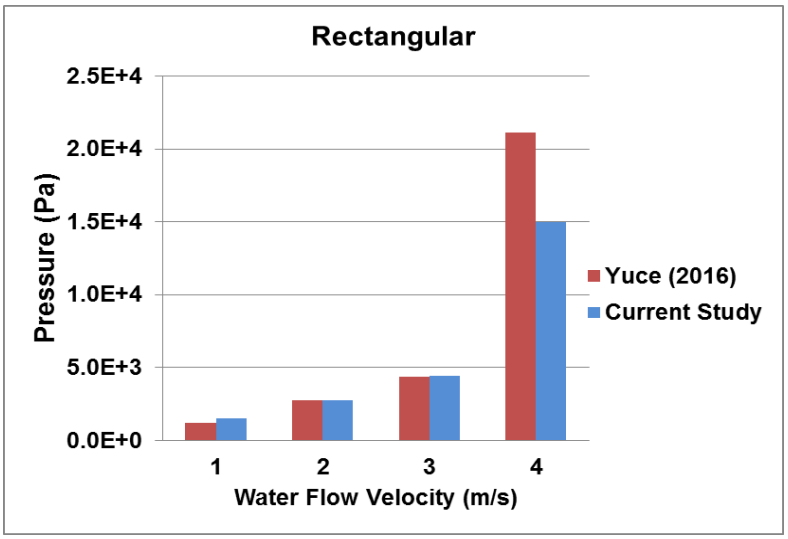

Figure 2-9: Pressure on Rectangular Model Compared with Yuce and Kareem (2016)

Based on these results, the positive and negative pressure distributions along the pier's height are given as the pressure vs pier height. The total pressure in the FLUENT software is

calculated by the summation of hydrodynamics and hydrostatic pressure obtained from water flow around an object. The total maximum pressure derived by CFD analysis for different velocities is demonstrated in Figure 2-10 and

Figure 2-11 2-11. It is noted that with an increase in flood velocity, the pressure increases as expected. However, the distribution of total pressure has a similar pattern for different water flow velocities and is very uniform along with the pier height. McClean and Sumner (2014) reported an experimental exploration of the effect of the aspect ratio and incident angle on the water flow around square prisms. Their research has shown that the water flow pressure along an object's height can be considered as roughly a uniform distribution, regardless of the variation in hydrodynamic parameters. They also showed that the oscillation of the pressure might be accrued because of the generation of vortexes around the cylinder, especially at higher fluid velocities. Almasri and Mogbel (2017) evaluated the drag coefficient around a bridge pier, and their investigation showed fluctuation in the drag force. The fluctuation along the circular pier height can be expressed by the drag coefficient fluctuation based on their study.

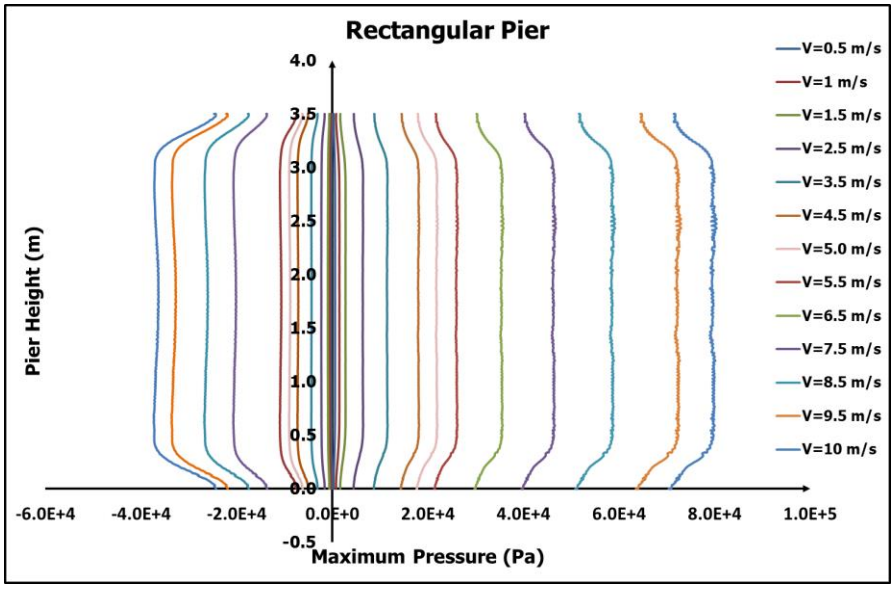

Figure 2-10: Pressure distribution along with Rectangular Pier Height and its Variation by Velocity

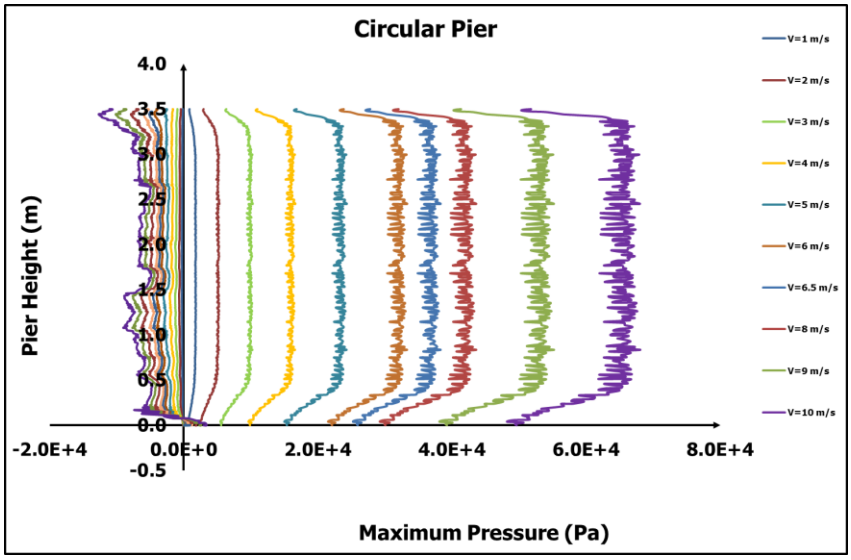

Figure 2-11: Pressure Distribution Along with Circular Pier Height and its Variation by Velocity

The total pressure distribution on the rectangular pier along the pier height shows a smooth curve with a constant value (except for top and bottom) while in the circular pier the pressure distribution fluctuates around a very constant pressure value. The values in the circular pier show the same consistency (except for top and bottom), as do those for the rectangular pier. There is a very significant difference in negative pressure on the other side of the pier. It can be seen that the negative pressure on the rectangular pier at higher velocities is substantial, while the circular pier's negative pressure on the opposite side of the subject is negligible and more irregular; this shows how the shape has a significant influence on the water flow forces.

Figure 2-12 presents a comparison of the negative and positive pressures observed on the rectangular pier for a range of velocities from 0.5 m/s to 10 m/s. These pressures were derived using CFD simulation, and they were compared with the Australian code equation (Equation (2)).

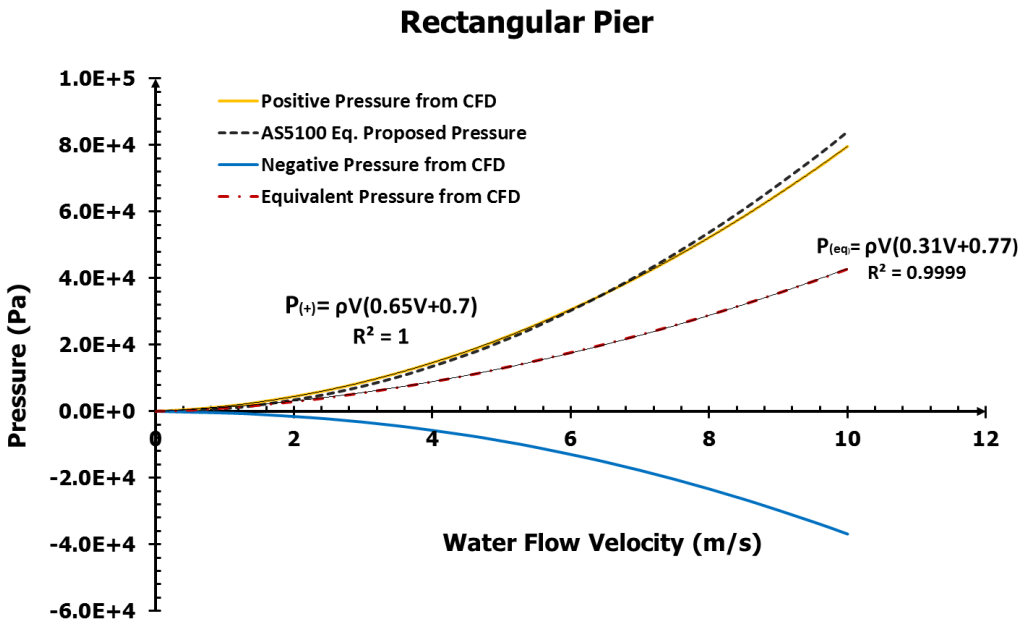

Figure 2-12: Pressure Derived by CFD Method versus Velocity on Rectangular Pier

It is noted that the positive pressure along on the pier is predicted reasonably well using the Australian Standard equation. However, if the positive and negative pressures are combined, the total pressure on the pier is much lower than that given by the code equation. It may be concluded that the AS5100:2 (2017) equation is very conservative for the rectangular pier analysed here using CFD methodology.

Figure 2-13 presents a comparison of the average negative and positive pressures observed on the circular pier at a range of velocities from 0.5 m/s to 10 m/s. These average pressures were derived using CFD simulation. Here the pressures are compared with the code AS5100:2 (2017).

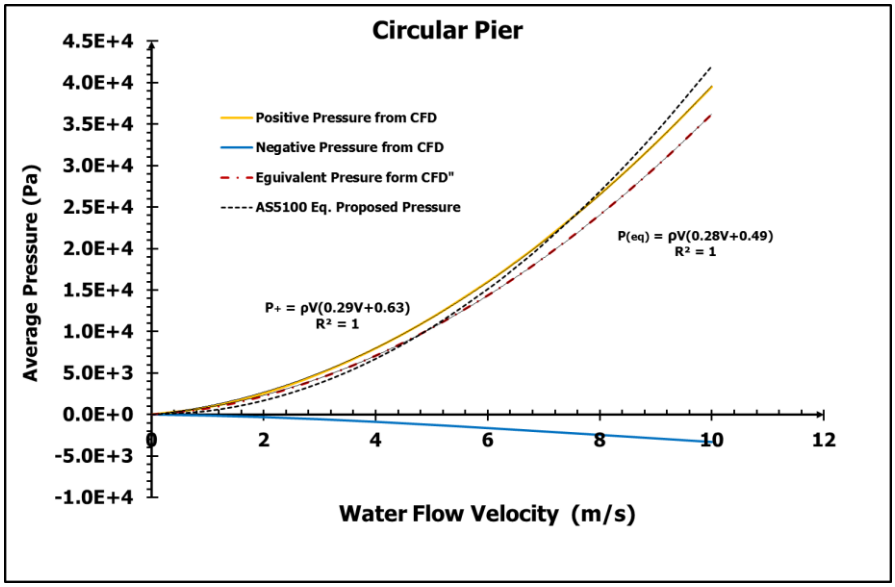

Figure 2-13: Pressure Derived by CFD Method versus Velocity on Circular Pier

It is noted that the positive pressure predicted along the circular pier is very close to the AS5100 equation. However, since the negative pressure on the circular pier is not significant, the combination of the positive and negative pressure, the total pressure, distributed along the pier is very close to the pressure calculated by the code equation and is even slightly under-estimated for velocities less than 5 m/s. It may be concluded that the standard's equation is not conservative for the circular pier analysed here using the CFD calculation method.

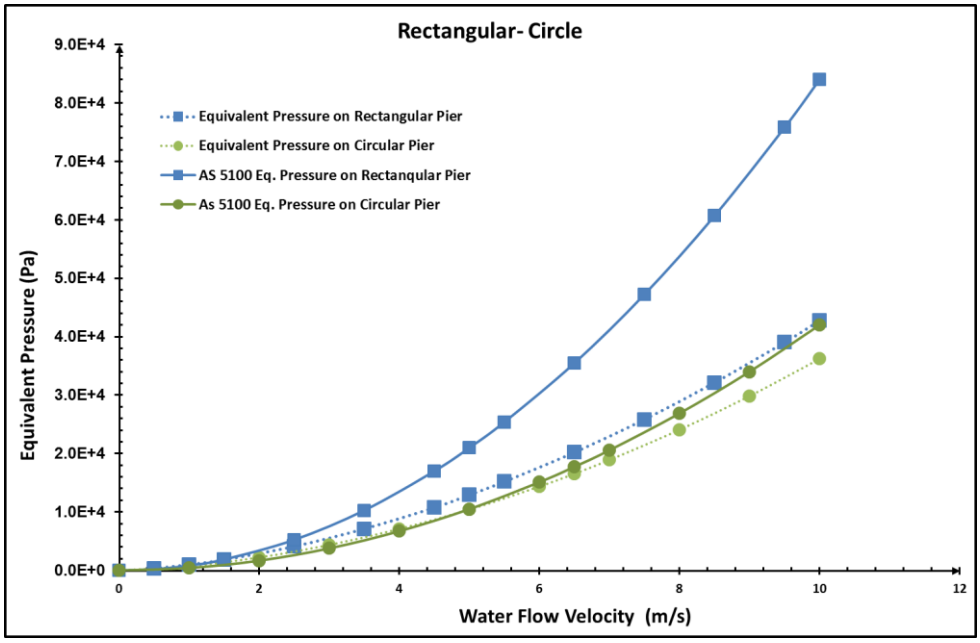

Figure 2-14: Equivalent Pressure Comparison of CFD Method and AS 5100 Equation for Rectangular and Circular piers.

Figure 2-14 presents a comparison of the total pressures calculated using the CFD method on both rectangular and circular piers, and the pressure derived using the AS 5100 equation. Although the pressure proposed by the code is very conservative for the rectangular pier, it is pointed out that the total equivalent pressure on the circular pier is notably smaller than that on the rectangular pier. For design purposes, this may be important since localised failure may require a design for positive pressure, while structural stability may require consideration of the resultant pressure on the piers. It is also noted that the AS5100:2 equations are conservative for the rectangular pier and are not conservative for the circular pier.

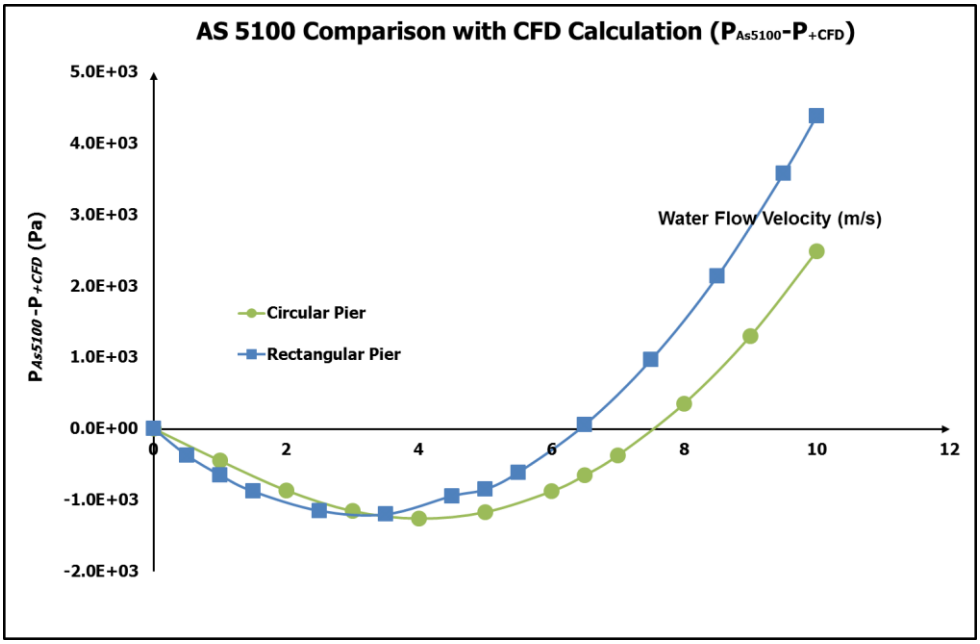

Figure 2-15: Difference between Pressures based on CFD Method Calculation and AS 5100 Equation for Rectangular and Circular Piers.

Figure 2-15 represents the difference between the positive pressure based on the CFD calculation and the AS5100:2 equations for the calculation of drag force for both rectangular and circular piers ($P_{AS\ 5100} - P_{CFD}$). This shows that positive pressure on both piers using the AS 5100 or codes methods is under-estimated for lower velocities in comparison with the present computational method.

Consequently, the graph in Figure 16 provides the normalised pressure differences, ($P_{AS5100} - P^{+}_{CFD}$) and ($P_{AS5100} - P^{t}_{CFD}$), concerning the Australian Standards equation, where P^{+}_{CFD} shows the positive pressures on the piers and P^{t}_{CFD} shows the equivalent total pressures on the piers derived from numerical calculations. The positive pressure on a rectangular pier at higher velocities is very close to the pressure predicted by AS5100. The positive forces are recommended to be considered to determine the pier's damage. Therefore the comparison between the positive pressure applied to the pier and the pressure derived from standard's equation shows the reliability of the Australian code's Equation in determining damage.

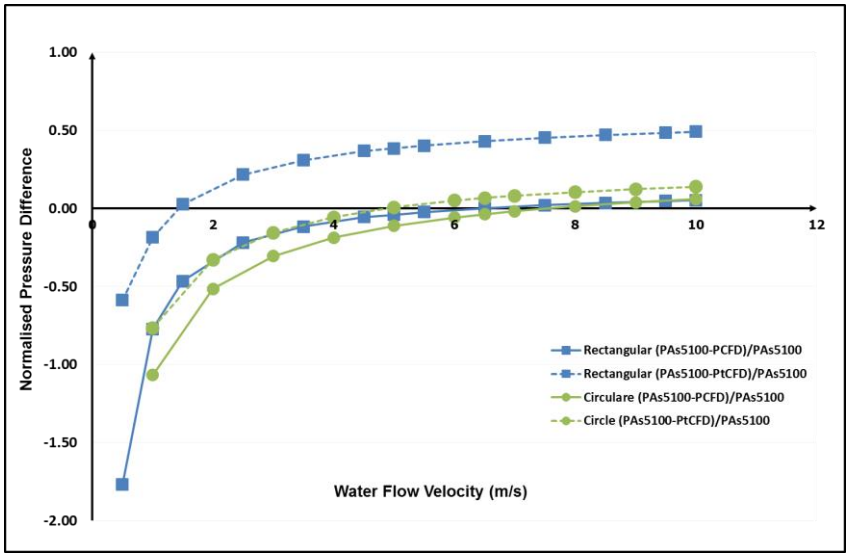

Figure 2-16: Difference between the Pressure Calculated from the CFD Method and AS 5100, Normalized concerning AS5100 Eq.

Consequently, the graph in Figure 2-16 provides the normalised pressure differences, (P_{AS5100}–P^{+}_{CFD}) and (P_{AS5100}–P^{t}_{CFD}), concerning the standard's Equation, where P^{+}_{CFD} shows the positive pressures on the piers and P^{t}_{CFD} show the total pressures on the piers derived from numerical calculations. Although the AS5100:2 equation is conservative for low water flow velocities for both rectangular and circular shape, the graph shows that the results in a higher speed of water flow for the rectangular responses are more close to the standard rather than the circular pier, especially in higher velocities. The difference between total pressure derived from AS5100:2 and CFD method is nearly less than the previous one, but it is conservative for the rectangular model. It can be observed that the difference between positive values of pressure resulting from CFD calculation and standard's equation for the circular pier is minimal and negligible while it is significant on the rectangular pier.

Apart from damage localisation, it is recommended to consider the total pressure, particularly for design and determining the stability of the structure. The graph in

Figure 2-17 shows that the difference between the total equivalent pressure on circular and rectangular piers increases while flow velocity is rising. In addition, the square pier shows more substantial total pressure.

More research in this area is needed to explore the phenomena in more detail, and the relative effects of water flow pressure distribution should be identified. Table 2-1 provides a modified equation for the determination of the pressure on both rectangular and circular piers on a function of the flood velocity, V, and the constant density parameter, ρ. Moreover, the difference between the two specific models is explained in Figure 2-17. The graphs give a simple explanation of how the pressure calculated by the CFD method changes in relation to the water flow velocity. Numerical experiments are required for circular and square piers of different dimensions.

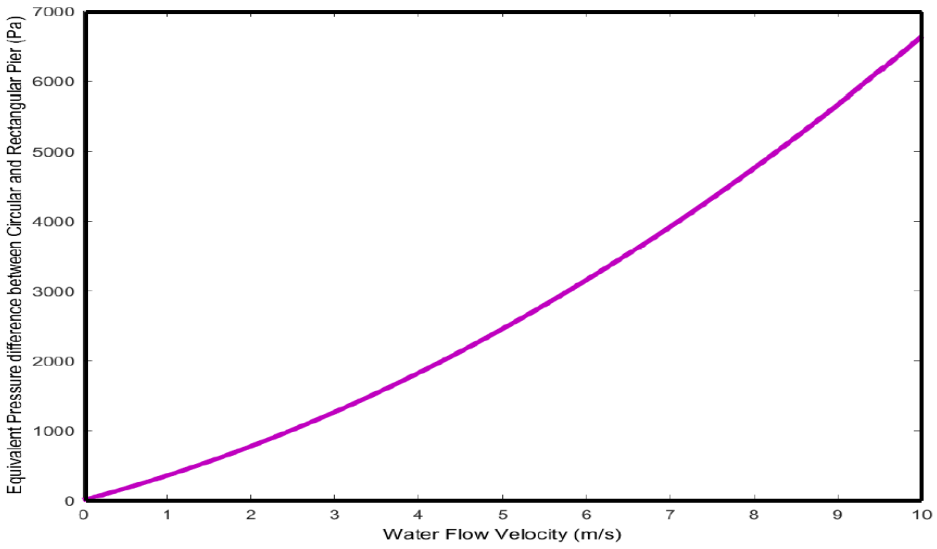

Figure 2-17: Difference between pressures on rectangular and circular piers calculated by CFD method

Table 2-1: Pressures calculated using CFD method for both models and the differences		
Shape	**Total Pressure Derived from CFD Method**	**R^2 (Correlation Parameter)**
Circular	$P_{C(eq)}= 0.28\rho V^2 + 0.49\rho V$	1
Rectangular	$P_{C(eq)} = 0.31\rho V^2 + 0.77\rho V$	0.9999
Pressure Difference	$P_{C(eq)}-P_{R(eq)}= 0.03\rho V^2 + 0.286\rho V$	0.9999

2.4 Conclusions

Resistance to flooding and debris loading are critical parameters affecting the design of bridges under flood loading. Bridges are the most vulnerable elements of the road infrastructure. Therefore, investigations of loads can benefit bridge design codes. This study investigates the water pressure resulting from fluid flow around two different shapes of a single pier to determine how the pressure can be simulated in structural analysis. Two different shapes, rectangular and circular, with the same diameter, were exposed to simulated water flow. To study the water flow behaviour on the structure ignoring the structural response, computational analysis of water flows around a pier was conducted assuming the pier to be a bluff structure, reported here as a non-structured model. Therefore, in this study, the pier's walls were assumed to be non-slip boundary walls located in the water flow domain. Different water flow velocities were examined to determine how they can affect the pier surface exposed to the water flow, using the ANSYS FLUENT software package. The calculation of water flow pressure on bridge piers in various codes for the determination of water flow pressure distribution is very similar (Wang et al., 2015). Therefore, in this paper, the Australian Standard (AS 5100) was selected for investigation in comparison with the computational method. Based on a comparative analysis, the principal results can be summarised as follows:

1. CFD analysis confirms that the pressure distributions on a bridge pier are uniform in both rectangular and circular piers with very slight changes at both top and bottom of piers exposed to water flow.

2. CFD analysis demonstrates that the pressure on a circular pier is under-estimated by the AS5100 equation when comparing total equivalent pressures with the equation provided by AS 5100, at velocities less than 5 m/s.

3. The water flow variations during velocity growth reveal that for a rectangular pier, the AS 5100 equation is very conservative.

4. The possible total pressure on a rectangular pier is close to that predicted using the AS 5100 method or other codes, especially for higher velocities.

5. Positive pressure on both piers using the AS 5100 is under-estimated at lower velocities in comparison with the present computational method when applied in bridge design.

It is observed that the effect of total pressure distributed on the pier is essential in design for structural stability, whereas the positive pressure needs to be considered in the design for localised damage. Further studies of the effect of drag and viscosity on flood forces on bridge piers at high-velocity water flows are recommended.

CHAPTER 3

A Comparative Study of Deflection and Energy-Based Approaches on Damage Estimation of a RC Flexural Element

Statement of Authorship

Journal paper title:	A Comparative Study of Deflection and Energy-Based Approaches on Damage Estimation of an RC Flexural Element
Status:	Manuscript submitted for publication
Reference:	M Nasim, S Setunge, M Mohseni 'A Comparison of the Deflection and Energy Based Approaches on Damage Estimation of the Reinforced Concrete Element', *Manuscript Submitted for publication.*
Name of author:	Maryam Nasim,
Position:	PhD scholar.
Contribution:	Corresponding Author, Collecting and interpreting data, performing analysis, preparing figures and writing the manuscript
Name of author:	Sujeeva Setunge
Position:	Professor, Deputy Dean Research and Innovation School of Engineering, RMIT University
Contribution:	Supervising research, assisting in manuscript preparation and reviewing
Name of author:	Hessam Mohseni,
Position:	Lecturer, School of Engineering, RMIT University
Contribution:	Editing and reviewing the manuscript
Name of author:	Tariq Maqsood,
Position:	Senior Lecturer, School of Engineering, RMIT University
Contribution:	Editing and reviewing the manuscript

3 A Comparison of the Deflection and Energy Based Approaches on Damage Estimation of the Reinforced Concrete Element

Synopsis

Outcomes of the research presented in Chapter 2 indicated that the assumption of a uniformly distributed load is appropriate to represent the effect of the flood on bridge piers. In the next stage, an incremental loading and the resultant damage is explored to understand the vulnerability of bridge piers. Invulnerability modelling of structures, a common approach adopted is depicting damage using a proper damage index which is defined as the ratio between the damage induced at any given level of loading and the complete failure.

Damage indices are commonly used in establishing damages to structures under earthquake loading. In this chapter, a validating numerical model of a concrete structural element is used to compare different damage indices and damage assessment of the structure. An energy-based damage index was proposed and was shown as an improved measure of estimating the level of damage of a concrete column structure under incremental loading.

ABSTRACT: Structural safety and serviceability are vital during extreme environmental loadings such as flood and earthquake. The resilience of critical structures and infrastructures is becoming more vital due to the increase in the intensity of flood loading resulting from global warming over the last decades. This paper presents a comparison of two methodologies to quantify damage and risk of the structural system using finite element analysis. A finite element model developed in ABAQUS software package is used to predict the failure of a concrete element under applied lateral loading. The model is validated using

published experimental work. The validated model is then used to compute the damage indices using two major approaches: a deflection-based approach and an energy-based approach. The change in damage under uniform fluid pressure loading is observed to be similarly represented by the two different methods of estimating damage indices. It is concluded that the energy-based approach is easier to adopt and offers similar levels of accuracy as the widely accepted deflection-based approach.

KEYWORDS**:** Damage Index, Structural Safety and Stability, Finite Element modelling, Nonlinear Analysis, Structural Assessment

3.1 INTRODUCTION

Concrete as a construction material has a significant advantage over other materials. Most of the reported failures of concrete structures occurred during the construction or due to natural hazards (Khan 2014). With the recently reported increases in the frequency of natural disasters, understanding the vulnerability of structures to natural hazards has become extremely important. Most of the current design procedures may not adequately cover the resilience of structures in hazard scenarios. Furthermore, a survey by the US Department of Transportation shows 28% of structures are deficient in the capacity of the structure to carry the design load (Manual 2010). These deficiencies can increase the vulnerability of the structures under disasters.

In general damage, assessment is used to determine the capacity of a structure under given loading scenarios. A wide range of different assessment procedures exist with varying complexity, and the choice of the appropriate method depends highly on the specified requirements of assessment. Structural damage assessment has two main objectives: to confirm the structural safety and serviceability and to minimise the maintenance cost.

To assess the structural damage, various approaches have been adopted. Field assessment methods are used to determine structural health, such as visual inspection, eddy current, magnetic particle, and ultrasonic methods. This method is also called a measurement-based assessment of the serviceability of the structure. An issue of these methods is the applicability of the approach, i.e., both sides of the damage location (crushing and cracking) are needed to be accessible which is not always feasible (Farrar and Jauregui 1998). Another more economical approach to assess the serviceability of the structure is numerical modelling and analyse the mechanisms of the crack formation in concrete structures due to different damage scenarios. Analytical models for crack propagation and damage indicators for concrete have also been presented by various researchers (Ulfkjær et al. 1995; Neild et al. 2003; Hamad et al. 2015). The numerical modelling of concrete failure has been progressed recently using different failure concepts such as fracture energy models, smeared crack models, plasticity models, non-local damage models (Rabczuk et al. 2005; Rabczuk and Belytschko 2007; Bazant and Cedolin 1979; Hillerborg et al. 1976; Rabczuk et al. 2010).

Damage indices (DIs) are required to quantify the local or the global damage of a structure as a function of complete failure. They can be used as an indicator for representing how the damage risk is progressing concerning different parameters. In different studies focussing on structural behaviour under earthquake loading, this concept is comprehensively studied for quantifying the vulnerability of the structures or the fatigue failures under cyclic loading. A damage index (DI), typically defined as a ratio of the current level of damage and the damage corresponding to failure, is used in literature to represent the level of damage a structure undergoes subjected to different levels of loading. Here in this study, damage or failure is defined as the point at which the structure has reached the strength or serviceability threshold defined for the situation. This representation of the level of damage can be used in

practice to measure the level of recovery effort required for structural refurbishment after a disaster. The value of DI can vary from zero to one; a zero value of DI means the structure is safe without any deficiency, whereas, one represents the fully damaged element or failure of the structure.

3.2 RESEARCH SIGNIFICANCE

This section focuses on the measurement of damage levels (DLs) of a representative model for a bridge pier under flood loading, which induces a uniform water flow pressure. It is evident that with an increase in flood velocity, the pressure increases, and the corresponding damage also will increase. A review of damage indices published in literature has been conducted to understand the damage assessment methodologies. An energy-based method, which can be easily adapted using the output from a commercially available software package, is proposed to establish the DI under different scenarios and will be compared to the deflection-based method. The main purpose of this study is to realise the optimum technique for calculation of the concrete structures damage and the economic loss could be determined based on the output of this research.

To enhance the understanding of structural assessment, a reinforced concrete beam element has been modelled using ABAQUS commercial finite element package under incrementally increasing load. The numerical model has been validated using published experimental studies. The modelling methodology has been used to depict the behaviour of a bridge pier under uniform flood loading with various intensities, and the DIs have been calculated utilising the output of ABAQUS modelling (ABAQUS 6.14 2013). The proposed energy-based method is compared with the deflection-based method of calculation of the damage of the system.

3.3 A REVIEW OF DAMAGE INDICATORS

DIs are able to quantify the structural damage level (DL) numerically, and they play a significant role in decision making on structural resilience during disasters or natural hazards. DIs can quantify the local or the global damage of the structure. Generally, damage to the concrete structures can be represented as the failure of the components of the structure. The failure in reinforced concrete is defined as the instance corresponding to concrete crushing. In flexural members, this will happen well after crack initiation in the tensile zone.

Available DIs can be divided into two categories– cumulative and non-cumulative DIs. The theory of cumulative damage assumes that a stress cycle with alternating stress above the durability limit applies measurable permanent damage (Park and Ang 1985). It also states that the total damage caused by some stress cycles is equal to the summation of damages caused by the individual stress cycles (SYSTEMS 2012). In monotonic loadings, the non-cumulative damage models are more appropriate, and the ductility ratio, which can be expressed as the rate of the deformation in the load time-history to the ultimate or the yield deformation of the structure is one of the most straightforward concepts. The non-cumulative DIs which can be used for monotonically increasing load, usually have been used to determine the local damage and may not be useful for the system's general damage (Roufaiel and Meyer 1987). Displacement, stress, strain, stiffness, fatigue and energy dissipation concepts are the common concepts used for DI description. Due to the complexity of the damage and failure concepts and their theories and methodologies, this paper is focused on the comparison between two methods: dissipated energy and displacement concepts.

3.4 THE CONCRETE BEAM MODELLING AND METHODOLOGY

There are several damage detection algorithms used by researchers for modelling concrete cracking, crushing and damage mechanisms. These are provided in the commercial finite element software packages such as ABAQUS (Ioannides et al. 2006; Sinaei et al. 2012; Alsina et al. 2017). Some of the models have the capability of the actual modelling of the damage such as Concrete Damage Plasticity (CDP) with *dt* and *dc* coefficient, and some of them are not able to capture the actual damage of the concrete (i.e., smeared cracking model). In this study, the CDP approach, which has been the most common and widely accepted constitutive modelling method, has been utilised for the concrete modelling method. The model is able to predict the mechanical behaviour of concrete under different loading such as compression and tension, uniaxial, biaxial and triaxial loading by identifying scalar damage variables.

In order to estimate the damage of bridge pier subjected to flood loading, a geometrically similar structure is selected from literature as an experimental example to correlate the methodology of FEM modelling and to estimate the damage using different approaches. The following sections provide a 4-point beam model to validate and generalise the modelling methodology and then the comparison of displacement and energy approaches is conducted to evaluate the damage induced by incrementally increasing the load under uniform pressure with fixed bed boundary condition to simulate approximately a bridge pier condition. In the work presented here, the comparison is made between the energy-based DI and the deflection-based approach to estimate the structural damage. A simple concrete element has been modelled initially to demonstrate the concept of damage estimation under two methods as a precursor to modelling and estimating of the damage of the pier of a U-slab Bridge structure.

3.4.1 CONSTITUTIVE MODEL

The example is a simply supported reinforced concrete beam for which experimental tests were performed by (Hamad et al. 2011). A static non-linear FEM analysis is performed to examine its applicability for damage detection using commercial software ABAQUS 6.14. Damage parameters using the CPD method and the material properties, i.e. modules of elasticity etc. and the stress-strain relationships are in agreement with most of the models (Hanif et al. 2016). The geometry of the model is a rectangular beam with 130×210 mm cross-section and 2700 mm span length. Figure 3-1 describes the model setup and FEM simulation in ABAQUS. The mechanical properties of concrete used in this study are described in Table 3-1 Two types of reinforcement are used for tensile and compressive bars described in Table 3-2. Modulus of elasticity of concrete and 28-days compressive strength is proposed by Martinez and Nilson (1984) in the range of 21-83 MPa.

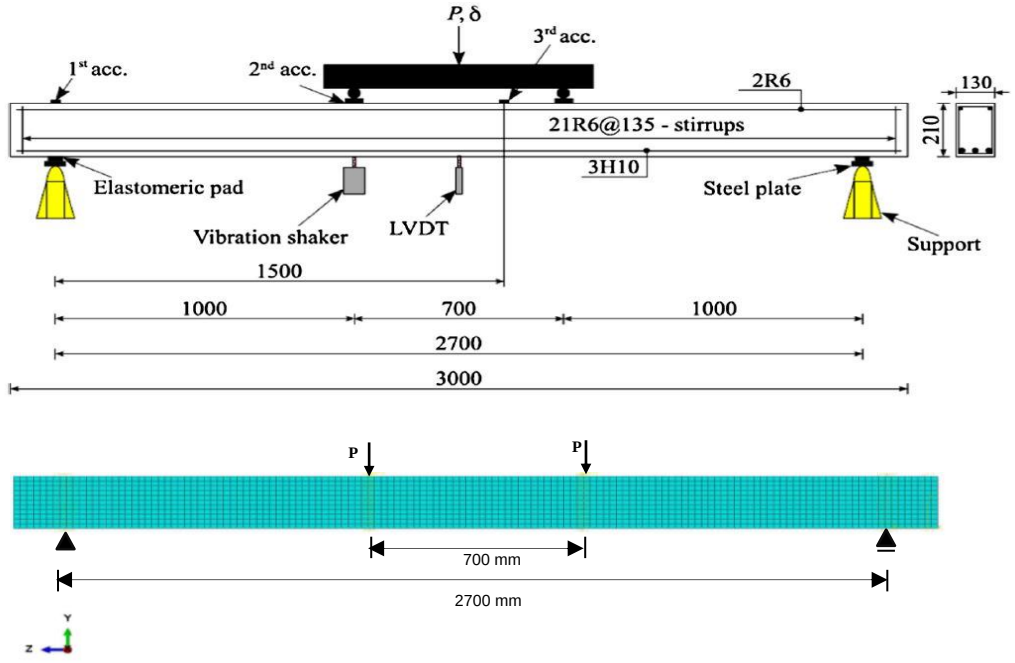

Figure 3-1: (A) Beam setup (Hamad et al. 2011) (B) Beam FEM simulated in ABAQUS and its cross-section

Table 3-1: Mechanical Properties of the Concrete				
Density Ton/mm^3	f_{cu} MPa	f_{ct} MPa	E_c MPa	ν
2.4E-9	36.5	3.65	$Ec = 3320\sqrt{f_c} + 9600 = 26957.85$	0.15

Table 3-2: Mechanical Properties of the Reinforcement						
Bar type	Diameter mm	f_y MPa	E_s MPa	ε_s	ν	ρ Kg/m^3
Plain bars	6	393.6	208,000	0.25	0.3	7850
Main bars	10	540.8	199,200	0.32	0.3	7850

The default values for CDP parameters used in this model are summarised in Table 3-3.

Table 3-3: CDP Parameters				
Dilation Angle	Eccentricity	$\frac{f_{b0}}{f_{c0}}$	K	Viscosity Parameters
35	0.1	1.16	0.667	0

The results of the analysis are used to examine the response of the structure under a monotonic static loading. The structural responses have been evaluated under a 20 KN concentrated load applied on the incremental load.

In order to examine the accuracy of the methodology, the force-displacement relationship of the numerical model has been compared with the experimental response under static loads, and it's been summarised in Figure 3-2. An excellent correlation between the current study and the experimental model's response is observed. The mesh sensitivity is also carried out to ensure the mesh efficiency.

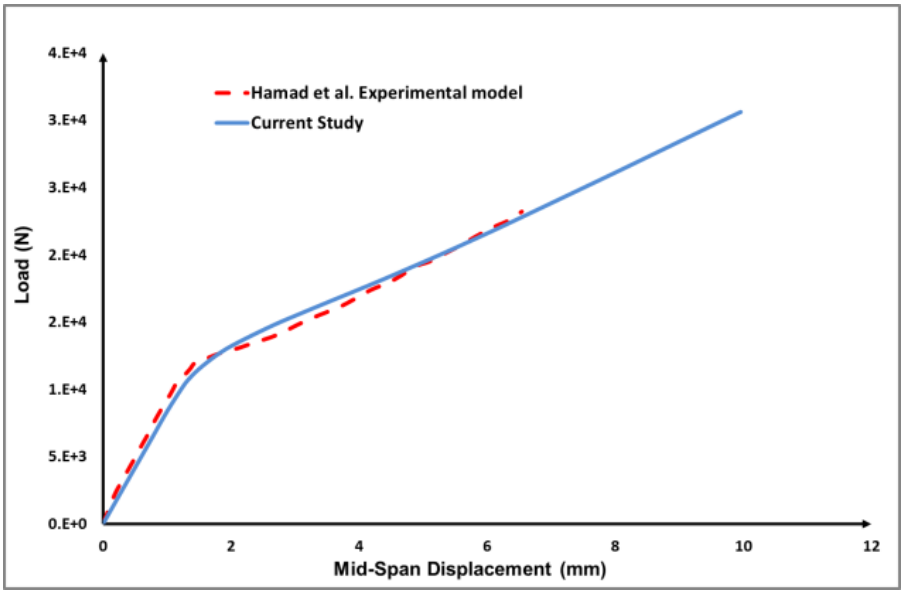

Figure 3-2: Static response in ABAQUS compared with the experimental model (Hamad et al. 2011)

According to the model's response, the load at which cracks appear is approximately 1.5 kN. It is obvious that the cracks must be localised under the concentrated loads and are distributed vertically to the horizontal axes. The crack patterns of the FEM developed flexural model, which is capable of detecting damage through non-linearity, are in a good agreement with the experimental results, (see Figure 3-3). Crack development is investigated to validate the capability of the present study for mixed-mode crack formation.

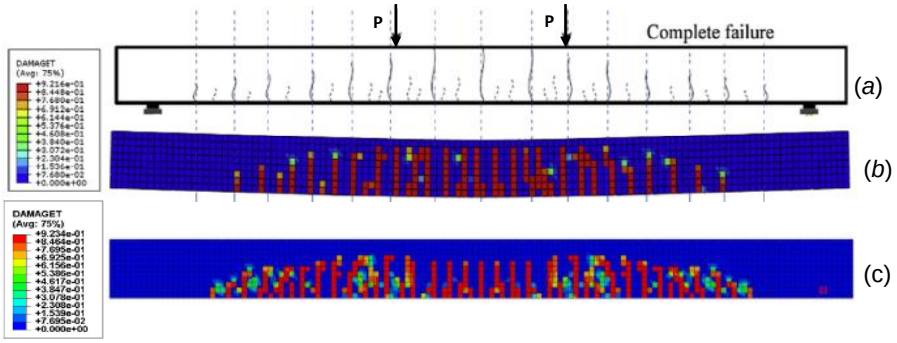

Figure 3-3: Simulated cracking pattern for (a) experiments by Hamad et al. (2011), (b) numerical models by (Hamad et al. 2011, Hanif et al. 2016), (c) current study

3.4.2 ANALYSIS

The model's capacity and behaviour are assessed under 4-point-load by using incremental static analysis in ABAQUS. The model is loaded incrementally as a percentage of damage until the entire failure of the system. Figure 3-4 shows the capacity of the system to be about 45 kN (Hanif et al. 2016). In the current study, 15% of the maximum load is applied to the model to achieve the proper structural response and observe full-plastic behaviour. Crack formation scenarios in different loading levels are set out in Figure 3-4; where it presents the crack formation when the load is increased incrementally. Figure 3-5 presents the load-displacement response at the mid-span of the beam, as a typical structural behaviure to use different works to compare it. The response is presented in three different phases. The initial phase, the blue part of the graph, is when the model has experienced no damage, and the structural response is fully elastic. The very first decrease in the structural stiffness can represent the crack initiation in the critical zone of the structure. Since the flexural moment is maximum between the two concentrated loads, this area has shown more damage and cracks.

Then in the second phase, cracks are initiated and propagated, but still, the behaviour of the structure is linear-inelastic (the green part in Figure 3-5). When the stiffness of the structure is degraded due to increasing load, the first changes on the slope of the curve represent the critical crack initiation load, F1. It represents the maximum load for the safe zone. The nominated value of F2 on the curve is the load which causes the change in the path of the graph, the second critical point when the cracks started to opening and nonlinear-inelastic behaviour is reached. This load is nominated as the maximum load for moderate damage. It is evident that increasing the load causes the beam to crack in the tensile zone, and therefore the tensile stresses are transferred to the reinforcement.

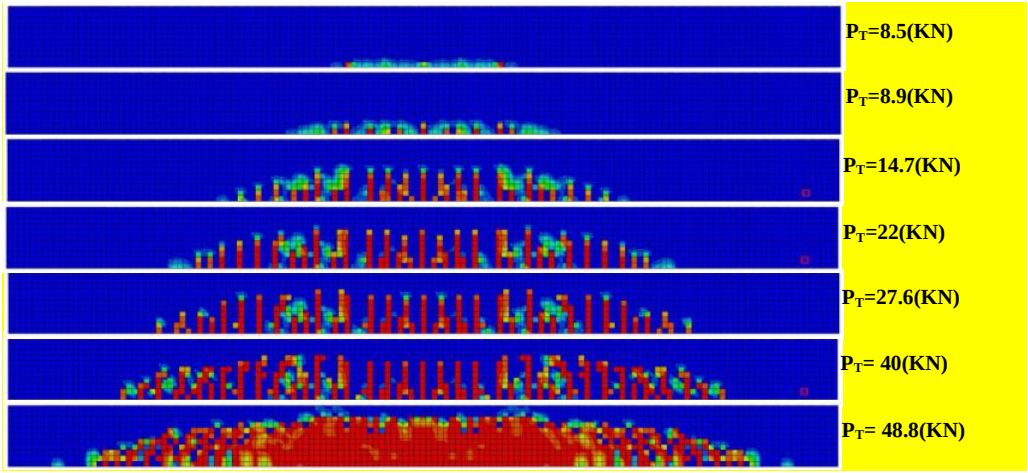

Figure 3-4: Crack formation pattern at different load level in ABAQUS (PT =2P)

With further increasing the load, the third phase of damage initiates when the reinforcement begins to yield, along with nonlinear behaviour of the structure. From this level of damage, the plastic hinge appeared, resulting in the reduction of the stiffness of the structure. Although the appearance of plastic-hinge does not represent the overall instability (failure) of the structure (since it can tolerate more lateral load), the plastic-hinges formation in the system may result in nonrepairable damage. Damage assessment for this structure was assessed through the mid-point deflection of the structure, and the changes in structural stiffness can define different DLs.

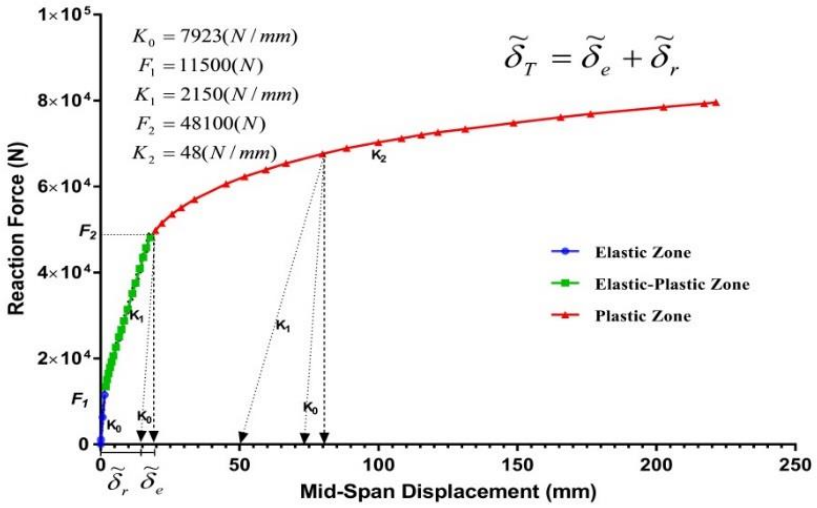

Figure 3-5: Static load-displacement curve for 4-Point load model (envelope curve)

3.4.3 Simulation of a Bridge Pier Subjected to Water Flow Pressure

Adopting the approach in section 3.1, a representative bridge pier is modelled under uniform pressure. Based on a previous study conducted by (Nasim et al. 2015) on the pressure distribution on a bridge pier exposed to water flow, uniform loading seemed to be appropriate to represent the pressure applied on the pier subjected to water flow velocity. In this study, the pressure distribution is assumed 1 MPa as an incremental uniformly distributed load along with the pier model. The uniform pressure is applying to the surface, which is faced with water flow. The weight of the pier, as well as the axial load resulted from the superstructure dead load, is calculated based on the details on drawings (~20t) and are considered in the analysis (see Figure 3-6). The boundary condition for the bottom of the pier is considered as a fix condition. Figure 3-7 represents the load-displacement response for different phases and the load is incrementally increased to show the structural behavioure.

Structural safety and serviceability are factors that will be discussed in following sections. The global factor of safety, which is the ratio of the resistance and the load effect is a common deterministic safety measurement.

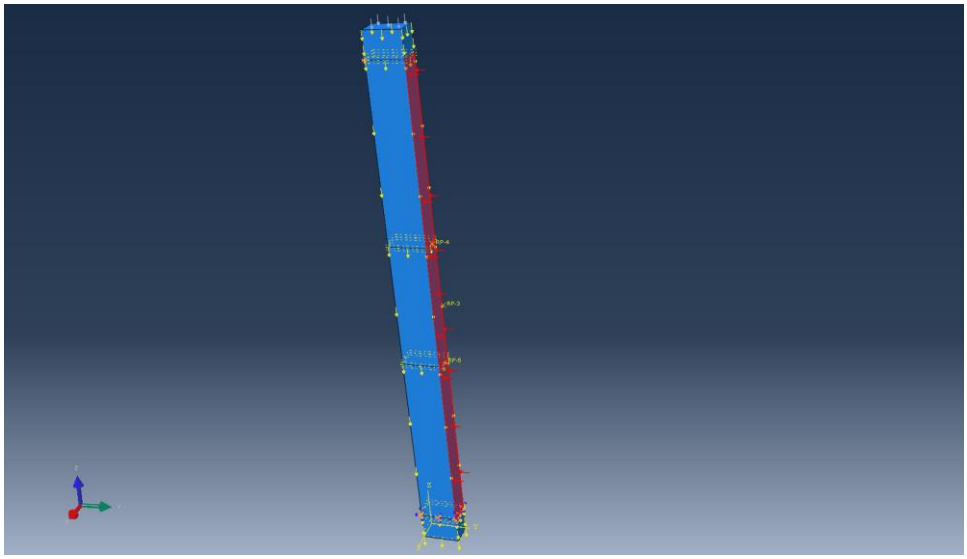

Figure 3-6: Piers simulation in ABAQUS and the water flow pressure applied on the front face.

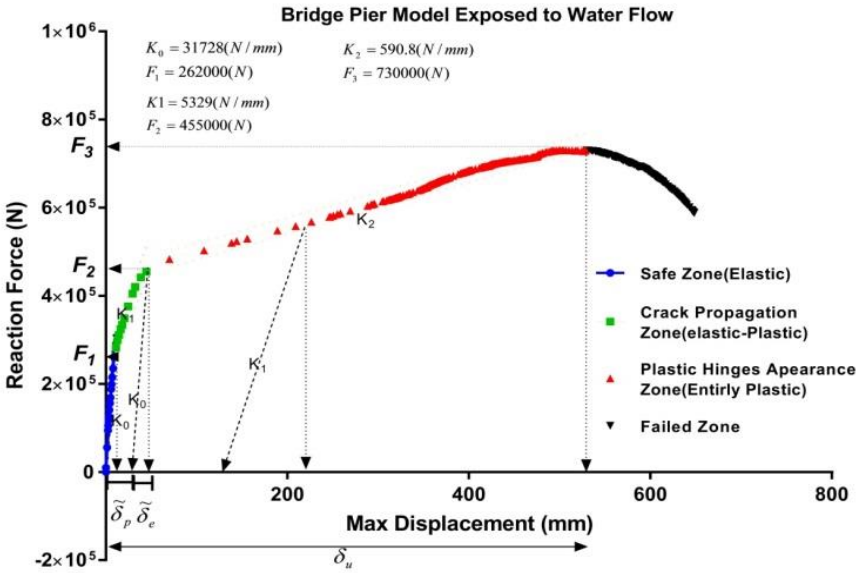

Figure 3-7: Static Load-Displacement Curve for Bridge Pier under Water Flow Pressure (Envelope Curve)

3.4.3.1 Damage to Bridge Piers under Flood Loading

As described above the damage has been categorised in three different levels, the first level is elastic, and this kind of damage assessment is recommended for a susceptible structure with very high-performance requirement (the serviceability limit states). In the first level, no surface cracks in the structure are expected. The limits for this level could be calculated from the structural response to loading. The second level is the damage before the plastic-hinge appearance. The elastic-plastic behaviour of the structure is expected in moderate damage level, and it can be called the ultimate limit. This level can be calculated in the same way as the first level. Finally, the last DL is related to the entire structural failure in which it cannot withstand any more loading. In this section, the total damage caused to the structure for three different DLs is calculated.

3.4.3.1.1 Deflection-based Damage evaluation

Having studied the definition of damage indices, based on the structural displacement using the following equation, (Park et al. 1984), DI for each DL is adopted.

3-1: $$\boldsymbol{DI = \frac{\delta_i}{\delta_{uj}}}$$

where δ_i is the displacement of the mid-span in loading step i and δ_{uj} is the ultimate deformation of the mid-span in each DL, j (j=1,2,3).

To have a perspective on the calculation technique, using the load-deformation response of the structure, presented in Figure 3-7, the ultimate load value, δ_{uj}, and correspondence deflection values are estimated for all of the three DLs. Then to determine damage percentage values for different damage levels the Equation 1 is used. Figure 3-8

compares DI variations with an increase in water flow loading for different DLs in the current study. Comparison of the three different DLs shows a similar trend in different DLs as described with the diagonal dashed lines in Figure 8. Although in the first level of damage, the values of DI change from zero to one due to the increase in the load, no cracks are presented in this stage. The value of DI in the first damage level, L1, shows the structural safety and denotes the system's alignment to the crack appearance. The DI =1 for DL1 is just the initiation of cracks; in other words, since the first crack has been initiated, the structure shows a nonlinear response. When the structure is starting to be cracked in level 1 DI(L1)>1, level 2 damage initiates. The analysis of the outputs and DI values shows that damage in second DL is less than 20% of total damage d2 in Figure 3-8, DI(L2) ≈ 20%DI(L3). The DI=1 for DL2 corresponds to the appearance of the plastic hinges. DI=1 for DL3 is a failure or softening of the structure.

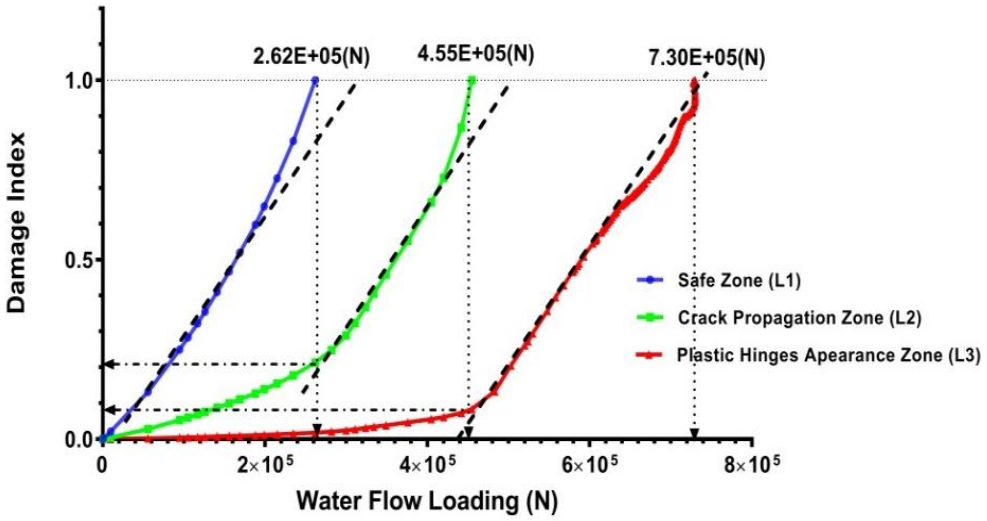

Figure 3-8: Damage index variation during water flow increasing, for the first, second and third DLs

The equivalent equations are defined to describe the damage behaviour of the system considering the displacement concepts by conducting a regression analysis. Structural safety,

when exposed to water flow loading, could be described by the equations provided in Table 3-4. The correlation coefficient, R2, also represent the accuracy of the formulas. However, it is recommended to generalise the methodology for different structures with different characteristics in future studies.

Comparing the three levels of damage calculated so far, it is observed that the ratio of the maximum load required for each level is almost similar. For example, the ratio of the minimum load for DL2 to DL1 is about 1.7, ($\frac{4.55E5}{2.62E5}$), and the ratio of the minimum load is required for DL3 is about 1.6, ($\frac{7.3E5}{4.55E5}$).

The values of all DLs are described in Figure 3-8 and Table 3-4, to explain the results. Another notable observation is that there are very similar trends of the growth in damage or the slopes of all graphs are very close (the nearly paralleled dashed lines in Figure 3-8 are describing this phenomenon).

Table 3-4: Damage index equations, for different damage levels, based on the deflection concepts

Damage Levels	**Equations of Safety**	***R²***	***Damage Load(N)***
(i)	S_i =1 - (1e-22F^4 – 5e-17F^3 + 1e-11F^2 + 2e-06F)	1	2.62e+05
(ii)	S_{ii} = 1 - (2e-23F^4 – 3e-18F^3 + 8e-13F^2 + 5e-07F)	0.9986	4.55e+05
(iii)	S_{iii} = 1 - (-9e-24F^4 + 2e-17F^3 – 6e-12F^2 + 6e-07F)	0.9917	7.30e+05

3.4.3.1.2 Dissipated damage energy-based damage evaluation

Apart from the deflection-based approach, an analysis of dissipated damage energy on the whole system is carried out to quantify the damage of the whole system. The results are compared with predicted scenarios in the previous section of this paper, which carried out based on the deflection concept. In this approach, the time-history trend of the dissipated energy of the whole system is investigated and analysed.

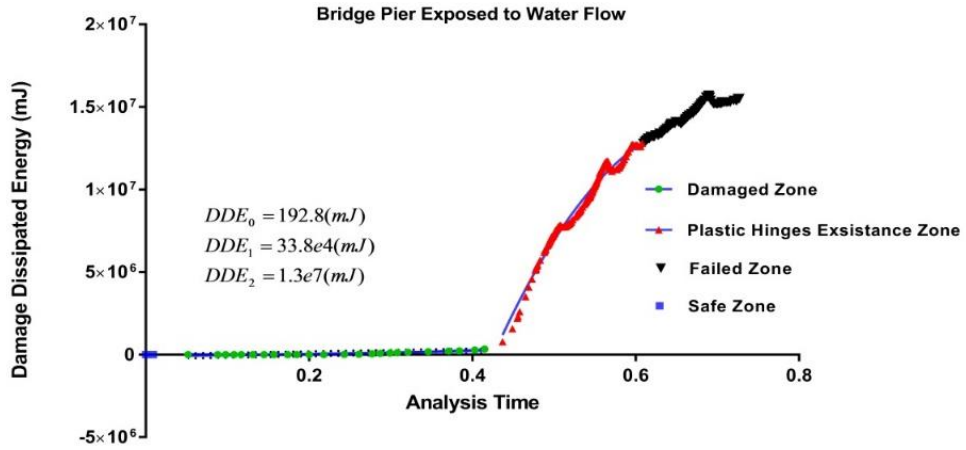

Figure 3-9: Time history of the dissipated damage energy (DDE)

Figure 3-9 shows the time history of the damage dissipated energies (DDE) of the whole system, calculated by the area under the load-deflection curve, which is derived from the output of ABAQUS. The values of DDE for the entire model can be evaluated efficiently using ABAQUS results as the whole model's damage dissipated energy (ALLDMD). It provides the DDE variation while the water flow pressure is increased incrementally. Although the curve's trend is growing during the incremental loading increases, before plastic hinges appearance damage dissipated energy is rising gradually (the second phase of the graph, damaged zone in green, in Figure 3-9), while after this phase, the energy dissipation is developing dramatically (the third phase of the chart, plastic hinges existence zone in red, in Figure 9).

Figure 3-9 demonstrates the different DLs in terms of DDE. All the procedure is carried out via ABAQUS tools itself, and the output is described by ALLDMD parameter, as described above. From the data recorded in Figure 3-9, the thresholds for different levels of damage are calculated. For example, up to crack initiation, 192 (mJ) energy is dissipated in the whole structural system. Comparing Figure 3-9 and Figure 3-7 reveals a similar trend in the displacement and DDE trend during the increase in water flow pressure. Alteration of

dissipated energy versus the increase in water flow pressure is described and plotted in Figure 3-9 and Figure 3-10.

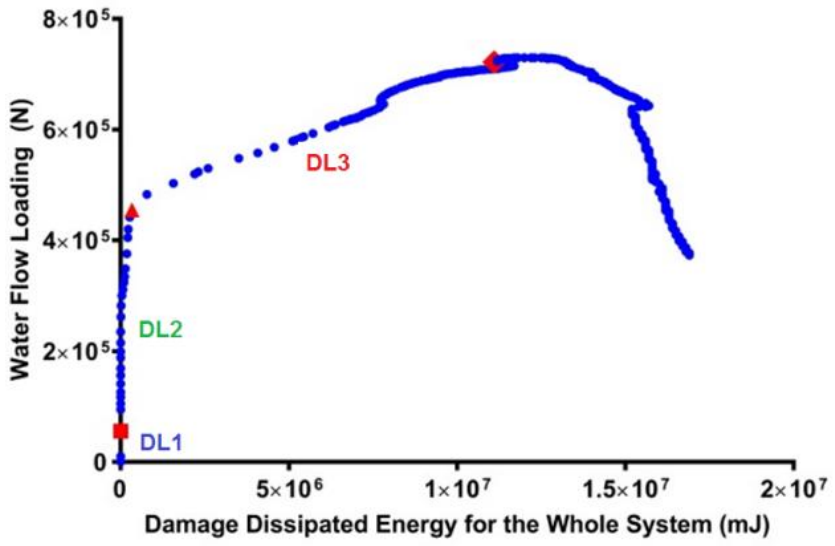

Figure 3-10: Damage dissipated energy (DDE) variation for the whole pier model

Results from above in terms of DDE outcomes for the whole model represent how damage energies are dissipated in different damage modes. For example, for crack initiation in the model, regardless of the damage location, 192.8 (mJ) energy is dissipated; and 338 (mJ) energy is lost when the plastic hinges created, and substantial deflection occurred till the total failure of the structure. In the complete failure phase (failed zone, black zone in Figure 3-9) the structure is unstable, and local damage reduces the structural stiffness. The progressive damage observed in Figure 3-9 can be implicated by the curve in Figure 3-9, and it can give us an applicable DI based on the energy outputs. As explained earlier in the first phase of the structural response, DL1, DDE is zero, while with the increase in the load, the crack inception has occurred gradually. Therefore, here in the energy-based method, the first level's value is zero due to elasticity behaviour of the system, and it shows structural safety zone, therefore in this approach, two levels of damage are investigated. The DI variation during the increase in

water flow has been focused when cracks have appeared in structure, and the energy-based approach is compared with the deflection-based method.

To quantify the DI's based on the dissipated-energy concept, the values of the turning points are highlighted in Figure 11, and the corresponding DDE are evaluated. Then the energy-based DIs presented in this paper are calculated using the following equation:

3-2: $$\boldsymbol{DI} = \frac{\boldsymbol{DDE_i}}{\boldsymbol{DDE_{uj}}}$$

where, DDE_i is the damage dissipated energy in loading step i, and DDE_{uj} shows ultimate damage dissipated-energy.

The first phase, as mentioned earlier, there is no damage recorded in the system due to the elastic behaviour of the system. The second damage level is when the of the cracks appear due to linear plastic behaviour of the system, j=2. The third damage level, j=3, the structure is in the fully nonlinear-plastic zone, and total failure is evident when the $DI_{(L3)} \geq 1$. As discussed, in this phase DL_3, plastic-hinges-appearance-phase, the structure is unstable. Analysing the data indicated that damage in the next level starts when the previous level, DL_2, is entirely completed.

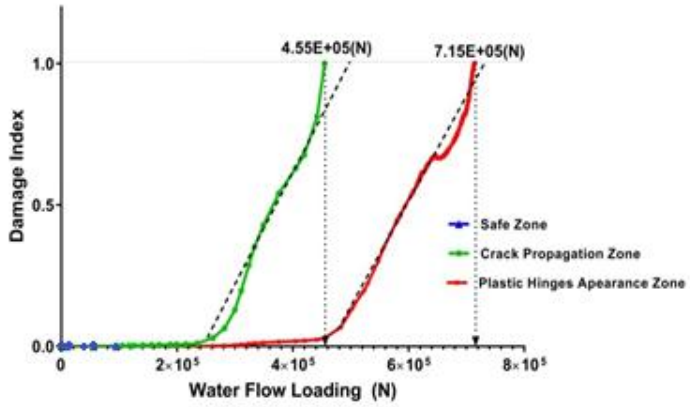

Figure 3-11: Damage Index variation for the elastic-plastic and fully plastic damage mode

To expand the results, the values for different DLs are described in Figure 3-11, and it displays a very similar trend for increasing damage by increasing the load, compared to the deflection-based damage index.

The methods described above shows the application of the energy-based damage index and show that the technique gives similar results to the deflection-based process.

3.4.3.1.3 Correspondent Water flow velocity

In order to understand the effect of the water flow on the bridge pier, a reverse calculation can be conducted to estimate the effective water flow velocity on the case study. The results of water flow loading can be linked to corresponding water flow velocity. The equivalent static drag load is determined by the following equation, according to AS5100 (Standards Australian 2017):

3-3: $$\boldsymbol{F_{Drag}} = \frac{\mathbf{1}}{\mathbf{2}} \boldsymbol{C_d \rho V_f^{\,2} A_d} \Longrightarrow \boldsymbol{V} = \sqrt{\frac{\boldsymbol{2F_{Drag}}}{\boldsymbol{\rho . C_d . A_d}}}$$

where, C_d is the drag coefficient, depending upon different parameters such as pier shape and flow factors, see (Apelt and Issac 1968; Parola et al. 2000; BS 2005; Standards Australian 2017), and ρ and V_f are the fluid density and velocity, respectively. The area of the surface facing the flow is represented as A, here is the rectangle of 130×2700 mm2. Based on the analysis and the related calculation, using Equation 3, the equivalent water flow velocity, could be calculated. Here according to the standards' definition, the drag coefficient of the square element is considered, Cd=1.4, (AS5100-1). The results are shown in Figure 3-12. The graphs show that very high velocity, more than 30 m/s, is needed for the failure of the simulated pier, which is not practical. In the safe zone, DL1, no damage occurred.

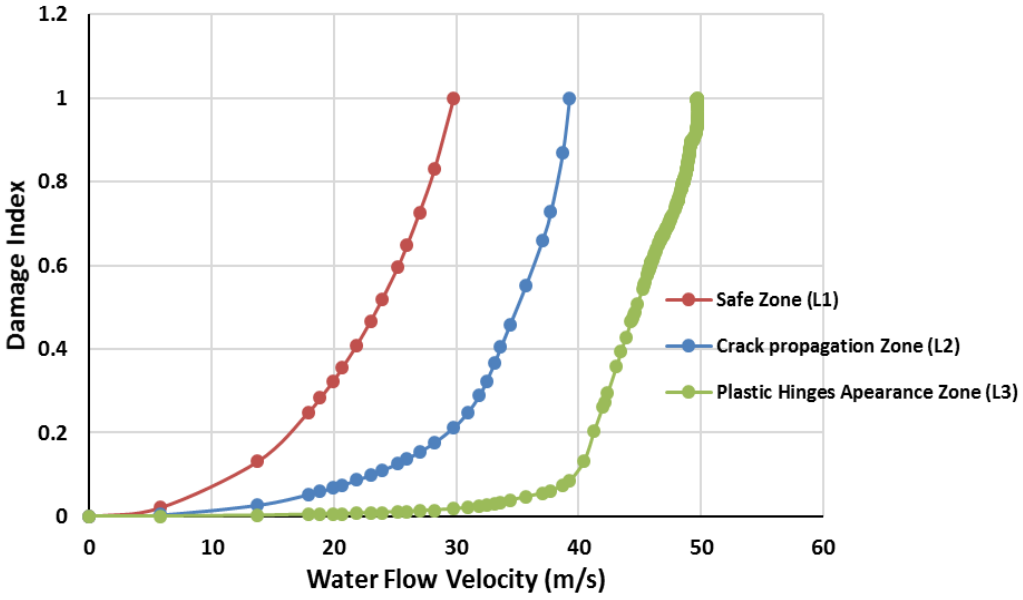

Figure 3-12: Damage Index variation for different damage levels with respect to the water flow velocity

3.4.3.1.4 Comparison of two different concepts of DI

Two approaches for the estimation of risks are compared in this section. According to the description of the evaluation of DI's by two different concepts (Deflection & DDE), in this work, the static non-linear analysis has been carried out for the system under incremental uniform pressure. The DIs have been calculated for each DLs, using the ultimate deflection values, and dissipated energy estimated from the turning points of the discussed curves, (see Figure 3-7, Figure 3-9, Figure 3-10). The quantitative values of the DDE for the whole system (ALLDMD parameter), are derived from ABAQUS outputs. Figure 3-13 provides a comparison between both approaches to evaluate the damage. It must be reminded that the safe zone is zero-damage and are not compared in this section.

The comparison of DIs shows that at a lower amount of loads, they provide exactly similar outputs. While, at the plastic phase, DL3, 6-10% difference in the damage values

between two approaches is observed. This can be interpreted as to the inclusion of damage occurring at different location of the piers in the DDE method.

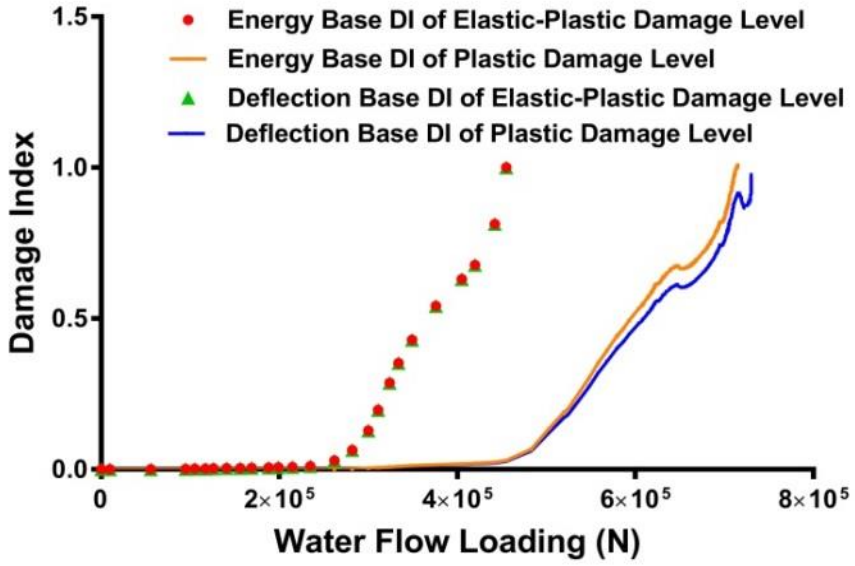

Figure 3-13: Damage Index for both elastic-plastic and fully-plastic-damage-mode and comparing the displacement and energy concept

The result in Figure 3-13 shows that the energy-based damage index can be used for estimation of the damage level of bridge piers under flood loading with a similar level of accuracy as the widely accepted deflection-based method. The advantage of the energy-based method is that the direct output of the ABAQUS model can be used to establish the damage parameters. In establishing the vulnerability of bridge piers under flood loading, the method offers a useful approach to determine the velocity levels which induce significant damage to the structure.

Considering the level 2 damage, it is noted that velocity of at least 10 m/s is needed to induce damage which requires intervention. Also the top connection of the pier is assuming as a pinned connection.

3.5 CONCLUSIONS

This chapter presented a review of DIs presented in literature and noted that there are many different methods to define the DIs. A feasible method for calculating concrete structural damage under increasing static loading using ABAQUS is presented based on CDP modelling, and the validation of the system leads the problem to compare different damage evaluation approaches. A new energy-based approach which can be used for evaluation of the damage of vertical structures such as bridge piers under lateral, flood, loading is presented.

The deflection-based approach and the new energy-based approach have been compared using a case study of a bridge pier. Following conclusions can be drawn from the work presented here.

1. Both the deflection-based DI calculation and the energy-based approaches show similar outcomes for moderate damage.
2. The energy-based DI appears to be more reliable for evaluation of the damage of complex structures when the degree of freedom is increased.
3. The deflection concept could not consider the rotational damages of the fixed boundary condition, while overall damage dissipation energy can address the damage of the whole system.
4. The energy-based approach provides a superior method since it is more straightforward to apply a structural system using finite element analysis results.
5. Structural geometry and degree of indeterminacy have a significant impact on the damage observed and calculated.

CHAPTER 4

Effect of the Mass of a Free-Dropped-Hammer on Dynamic Response of a Reinforced Concrete Beam

Statement of Authorship

Journal paper title:	Parametric Study of the Mass of a Free-Dropped-Hammer on Dynamic Response of a Reinforced Concrete Beam
Status:	Manuscript submitted for publication
Reference:	M Nasim, S Setunge, T Maqsood 'Effect of the Mass of a Free-Dropped-Hammer on Dynamic Response of a Reinforced Concrete Beam', *Manuscript Submitted for publication*.
Name of the author:	Maryam Nasim
Position:	PhD scholar.
Contribution:	Corresponding Author, Collecting and interpreting data, performing analysis, preparing figures and writing the manuscript
Name of the author:	Sujeeva Setunge
Position:	Professor, Deputy Dean Research and Innovation School of Engineering, RMIT University
Contribution:	Supervising research, assisting in manuscript preparation and reviewing
Name of the author:	Tariq Maqsood
Position:	Senior Lecturer, School of Engineering, RMIT University

4 Effect of the Mass of a Free-Dropped-Hammer on Dynamic Response of a Reinforced Concrete Beam

Synopsis

Chapter 3 presented the numerical modelling approach for a bridge pier under flood loading. Further, a new energy-based damage index was proposed as a measurement tool for damage estimation of bridge piers under flood loading.

In chapter 4, the research focused on the impact of floating objects on a bridge pier. A free-dropped-hammer on a concrete beam was modelled to validate the methodology and simulate the impact phenomenon. In this chapter, the effect of the mass of the hammer is investigated on the damage behaviour of a reinforced concrete beam.

Abstract

The dynamic response of reinforced concrete structures when they are exposed to impact loading is essential to understand the practical implication of the collision of an object on the structure. This paper presents a methodology to numerically assess the dynamic response of an RC beam under a dropped hammer with different masses to observe its influence on the structural reaction. A 3-D simulated beam, using ABAQUS, is utilised for calibration. The validated model has been used for further parametric studies on the effect of the mass of the impactor, and the other of impactor such as velocity assumed constant. Peak impact forces,

deflection of mid-span and systems damage levels has been assessed in order to differentiate damage levels. The time history of the impact forces demonstrates that the mass of the impactor has a nonlinear relationship with the structural response. And a linear relationship is observed with the system total energy. An innovative method using the cushioning factor is assisted in predicting damage scenarios when the structure is exposed to different masses of the impactor.

Keywords Finite Element Analysis, Dynamic Response, Impact Loading, Reinforced Concrete Structure, Explicit/Dynamic Analysis

4.1 Introduction

Impact loading is a common phenomenon in reinforced concrete (RC) structures subjected to extreme loading scenario which acts in a very short period of time. Some typical examples are vehicle impact on structures (El-Tawil *et al.* 2005; Zhou *et al.* 2017) and ship collision on marine structures (Dong and Frangopol 2015; Gluver 2017; van Manen and Frandsen 2017). Up to now, Engineers use an equivalent static force to emulate the effects of an impact. The magnitude of the quasi-static force depends on the self-weight of the structure being hit an is considerably small. This necessitates the introduction of impact force to help explain the anomalies (Jankowiak and Łodygowski 2010).

Basically, when a MO hits a given structure, momentum is conserved by a reactionary force that slows down the structure until it comes to a halt. Some of the kinetic energy of the MO is converted to strain energy in the structure that is being hit. As such, it becomes quite difficult to predict the outcome. One of the major problems in the analysis is estimating deformability. Assuming a rigid impact is outrightly out of the question. Rigidity makes us assume an abrupt change of velocities, infinite acceleration and therefore infinite force. In case of structures for which impact occurs regularly, the structure must maintain elasticity, and therefore it is essential to carry out a true dynamic analysis.

The behaviour of RC beams under impact loading has been studied for decades (Cazzani *et al.* 2002), but it is still not well understood. Most design standards allow conversion of an impact load to an equivalent static load for structural design. However, research in this area continues to grow and has been mostly prompted by the recent human-made hazards on vital

structures such as nuclear plants. The understanding of structural response under impact loading is required to establish a new design method to enhance the resilience of structures.

Structural damage under impact loading is categorised into two different reaction phases: i.e. local response and overall response. A local response is originated based on the stress wave that occurs at the point of immediate loading. The overall response results from free vibration of the elastic-plastic deformation of the system and can last over a longer period of time after the impact loading. This study provides an analytical framework for determining the structural dynamic response of concrete elements based on a parametric study on the mass of a drop hammer impact. This paper focuses on assessing the impact forces resulting from a free-dropped-hammer. Numerous research studies (Banthia *et al.* 1989a,b; Kishi *et al.* 2001; Kishi and Mikami 2012; Trivedi and Singh 2013; Kezmane *et al.* 2017; Low *et al.* 2001) report the dynamic behaviour of RC members under impact loading. However, research covering local and global failure modes due to impact loading is scarce.

Pham and Hao (2016) have proposed a new model based on Artificial Neural Networks (ANN) to predict the maximum impact force. Shivakumar *et al.* (1985) analysed an impactor-plate system to configure the impact forces of the system using energy balance and spring-mass approaches and concluded that when the mass of the impactor is greater than 3.5 times the plate mass, the inertial effects of the plate are negligible. Saatci and Vecchio (2009) showed the difference between the static and dynamic response of the specimens by having four groups of drop hammer impact tests on RC beams to study their effect on the shear capacity of the RC beam. They were able to develop a simplified single degree of freedom method. Three approaches are usually adopted to study the impact on structures: empirical (Yao *et al.* 2005;

Kumpyak *et al.* 2013; Chiaia *et al.* 2015), analytical (Yoo *et al.* 2015), and numerical (Kezmane *et al.* 2017).

Drop hammer impact tests on RC beams were conducted to study the shear behaviour of RC beams, covering beams without stirrups, RC beams (Kulkarni and Shah 1998; Kishi *et al.* 2002). Moreover, Banthia et al. (1989) proved that a structure could absorb more energy under impact than under static loading. Previous studies (Kishi *et al.* 2002; Saatci and Vecchio 2009) proved that impact force is significantly higher and quite different from the typical static reaction force in RC beams. However, research covering the dynamic responses of structures under impact loading is quite limited.

In this study, the series of non-linear Dynamic/Explicit analysis has been conducted using the commercial finite element software ABAQUS to understand the mechanism of impact on a structure and the structural nonlinear inelastic response, for instance, maximum impact forces, the energies of the system and beam's deformation. For a selected beam section, the significance of concrete crushing with the increase in impacted mass is evaluated. Furthermore, the damage behaviour of the beam, i.e. deflections and energies under impact loading, is studied. The methodology of modelling is validated using an experimental method from literature.

4.2 Research Significance

In practical situations, concrete structures may be exposed to impact loading. For instance, bridge piers could be subjected to log impact during extreme floods. Understanding the effect of the impact in relation to the mass of the log is essential during the design of the

bridge and retrofit phases. Quasi-static forces calculated from the first principles of momentum and energy are considerably small and therefore cannot explain why log can cause considerable denting. The primary purpose of this research is to address the gap in knowledge by assessing the influence of the mass of an impactor on the damage patterns of an RC beam. Based on the results of the parametric studies, a critical condition between the two failure modes of the structure has been established. The secondary purpose of this paper is to evaluate the effect of the mass of the impactor on the induced impact force, and different types of energies and structural deflection and deformation are assessed. The study gives a perspective on the relationship between different patterns of structural damage and structural responses.

4.3 Test Introduction

4.3.1 Specimen setup and mechanical properties

An experimental model for a simply supported RC beam subjected to a dropped hammer's impact is selected from the literature for this simulation. Fujikake et al. (2009) examined the impact response through an experimental study of four RC girders with a rectangular cross-section. In this study, the selected experimental research is used for validation of the modelling approach. The model's simulation and setup are illustrated in Figure 4-1.

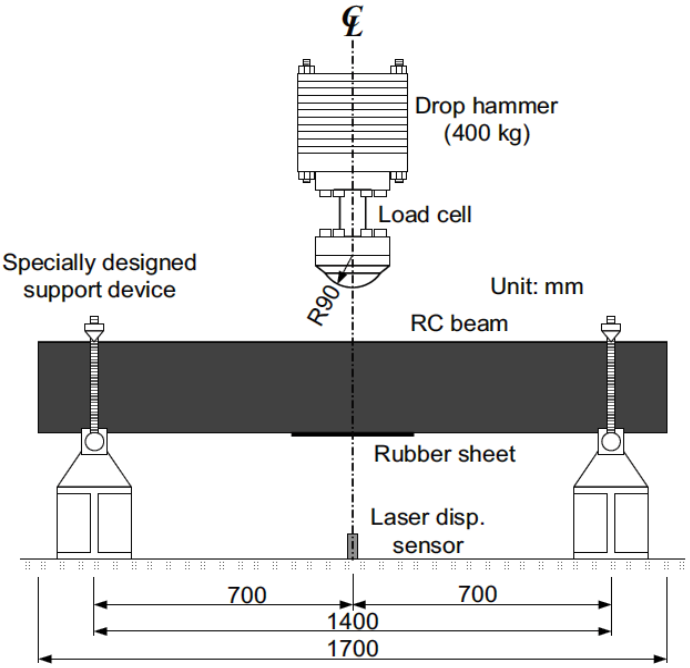

Figure 4-1: Drop Hammer test setup (Fujikake *et al.* 2009)

Figure 4-2 shows the schematic dimensions of the RC beams. The longitudinal reinforcements in both compression and tension sides were 2ØD16 rebar with 426 MPa yield strength. D10 stirrups of 295 MPa yield strength are arranged at 75 mm intervals. The longitudinal tension reinforcement ratio is 1.26% with a cross-sectional diameter of 16mm, and 22 stirrups with 10mm diameter at 75mm intervals are used as shear reinforcement. Table 4-1 provides the details of reinforcement.

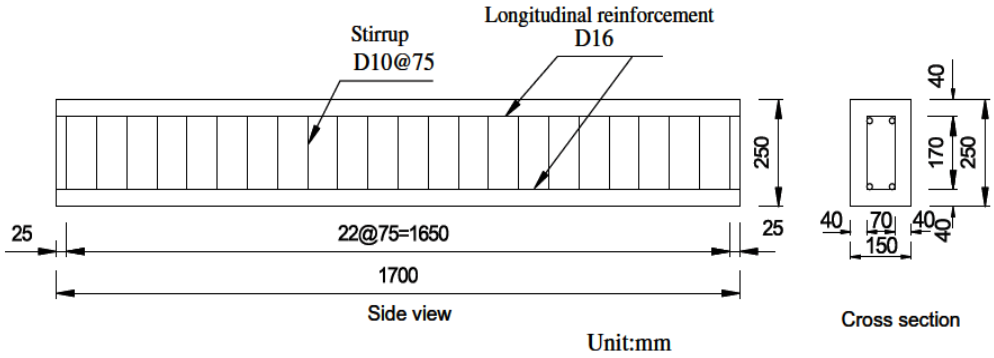

Figure 4-2: Rebar arrangement - side and a cross-sectional view (Fujikake *et al.* 2009)

Table 4-1: Reinforcement details			
Reinforcements	***Numbers***	***F_y (MPa)***	***A_s***
D16	4 (2 tensile + 2 compressive)	426	200.96
D10	22	295	78.5

The hammer's height above the beam is 30 cm. It is positioned to drop on the top surface at mid-span of the beam. The striking head of the drop hammer had a hemispherical tip with a radius of 90 mm. A parametric analysis of the dynamic response of the beam subjected to this drop hammer with different weights is conducted to evaluate the response of the RC beam. Nine different weights of the hammer, 100 kg, 200 kg,300 kg, 400 kg, 500 kg, 600 kg, 700 kg, 800 kg, 1 ton and 1.5 ton are compared for this research. The response of the model with 400 kg weight of impact is used for the validation of the simulation methodology. The concrete compressive strength is 42.0 MPa, and the static analysis gives 33kN of cracking, 108 kN of yielding and 120 kN of ultimate load capacity (Fujikake *et al.* 2009).

An elastic-plastic damage model is adopted to describe the nonlinear behaviour of the RC concrete. Lubliner *et al.* (1989) developed the Concrete Damage Plasticity model (CDP), which is widely accepted and used in the current simulation. It has been assumed that the two main failures are compression crashing and tensile cracking based on the classical continuum

plasticity damage theory (Lubliner *et al.* 1989). The CDP model of concrete is one of the possible constitutive models which can predict the constitutive behaviour of the concrete. This behaviour could be described by identifying scalar damage variables in tension and compression, *dt* and *dc*. By the following equations, the inelastic stress-strain relationship of concrete is determined:

$$\boldsymbol{\sigma_t = (1 - d_t).E_0.(\varepsilon_t - \tilde{\varepsilon}_t^{pl})} \quad (4\text{-}1)$$

$$\boldsymbol{\sigma_c = (1 - d_c).E_0.(\varepsilon_c - \tilde{\varepsilon}_c^{pl})} \quad (4\text{-}2)$$

Figure 4-3 and Figure 4-4 demonstrate the constitutive input and the damage parameters as a function of the compressive and tensile strengths, for 42 MPa compression strength for 71-day concrete. The values are calculated based on the CDP definitions in ABAQUS (ABAQUS 6.14 2013). In this research, a time-dependent impulse function has been used to simulate the interaction between the hammer and concrete (Abrate 2001). Concrete material properties and CDP parameters are presented in Table 4-2.

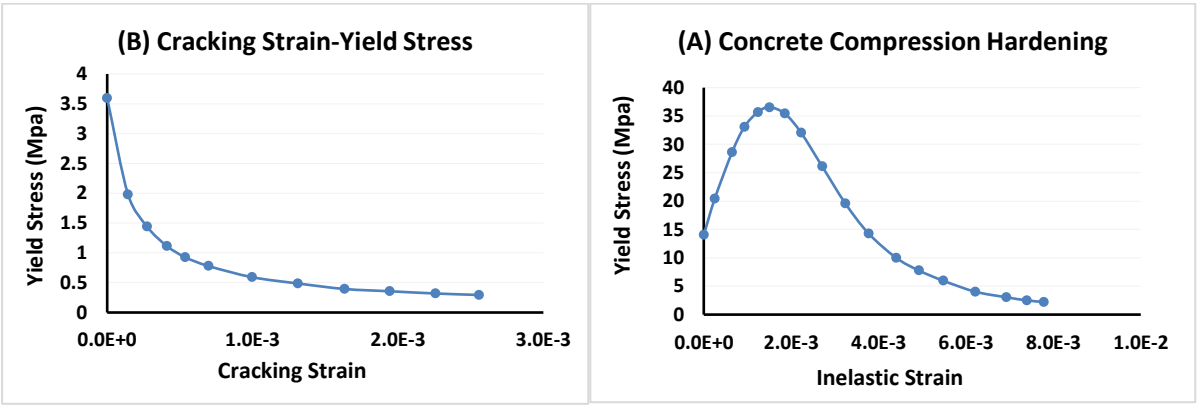

Figure 4-3: Concrete damage parameters in (A) compression and (B) tension

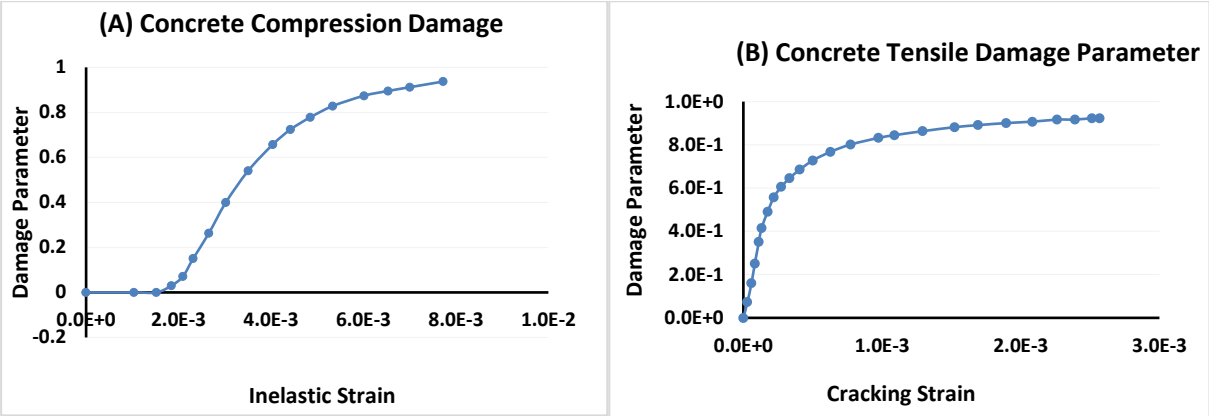

Figure 4-4: Concrete Stress-Strain behaviour in (A) compression and (B) tension

Table 4-2: Concrete CDP properties

Compressive Strength MPa	*Dilation angle*	*Eccentricity*	$\frac{f_{b0}}{f_{c0}}$	*K*	*Viscosity parameter*	*Young's Modulus*	*Poison's Ratio*
42	35	0.1	1.16	0.667	0.01	23,500	0.15

4.3.2 FEM Simulations

A dynamic non-linear explicit integration method of analysis is applied to the simulated model in ABAQUS/Explicit package to solve the equation of motion for the whole system. Forces are propagated as stress waves between neighbouring elements since we are solving for a state of dynamic equilibrium. The explicit solution method is a dynamic procedure originally developed to simulate high-speed impact events in which inertia plays a dominant role in the solution. Since the minimum stable time increment is usually quite small, most problems require a large number of increments (ABAQUS 6.14 2013).

In this study, a parametric study is conducted to investigate the influence of the mass of the impactor as the object in relation to the structural mass as the subject. The simulation is validated at 30 cm drop height above the specimen, and the results are compared with the

experimental study conducted by Fujikake *et al.* (2009). Time sensitivity analysis is also conducted, with 0.025 seconds as the time period. The load is applied via the rigid hammer's cap. The mass of the dropping hammer is applied as an inertia command in ABAQUS. The velocity of the impact is calculated by:

4-3. $$v_{ih} = \sqrt{2gh}$$

where g (m/s^2) is the gravitational acceleration and h (m) is the drop height.

4.3.3 Calibration of the Simulation Technique

Mesh sensitivity analysis is carried out to determine the optimum mesh size of 12.5 mm for the simulation. In this simulation, a 30cm drop height and 400 kg hammer mass is used to compare with the experimental test. The crack propagation after the impact on the simulated RC-beam model is illustrated in Figure 4-5.

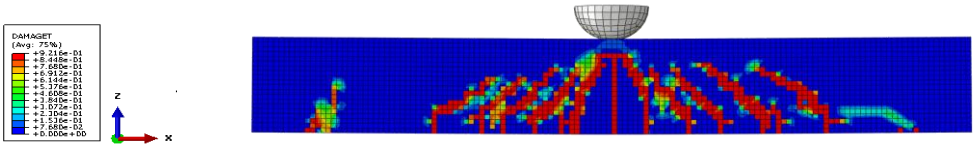

Figure 4-5: Crack propagation in the RC beam with a drop height of 0.3 m, mass of 400 kg

Figure 4-6: Crack propagation in the RC beam for the drop height of 0.3 m, the mass of 400 kg (Fujikake *et al.* 2009)

Figure 4-6 represents the crack pattern from the experimental study with 400 kg hammer mass (Fujikake et al. 2009). A similar crack pattern is seen in the FEM model and the experimental test (Figure 4-5 and Figure 4-6). Figure 4-7 shows the mid-span response of the simulation and the experimental test.

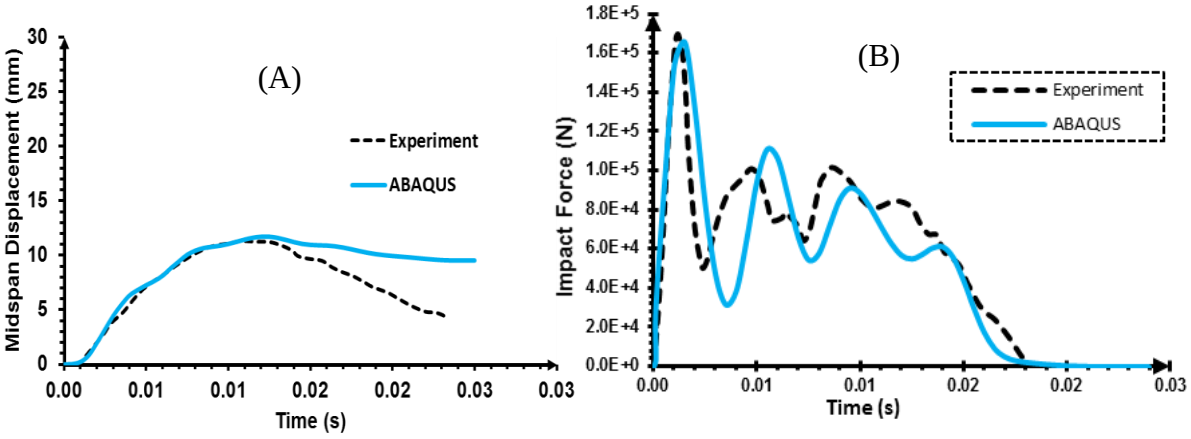

Figure 4-7: (A) Mid-span deflection (B) Impact force for the RC-beam with the drop height of 0.3 m and 400 kg mass of hammer.

The peak values of deflection, impact force and duration of the model's responses are simulated with reasonable accuracy in this study, as shown in Figure 4-7 above. However, there is a slight difference in the post-peak impact forces values. This difference can be attributed to the changes in the velocity, damping and the gravity considerations in the experimental model, which is neglected in the simulated model for the impactor as a rigid body. For example, the speed of the impact in the experimental model would decrease slightly because of the frictional phenomenon, which is neglected in the numerical simulations.

The maximum difference of impact forces between the simulation and the experimental results is about 2.2%, which shows an appropriate correlation. The vibrational behaviour shows both the stress vibration along the length of the model and the free vibrational response of the impact. This difference results from the modelling of hammers in ABAQUS as a rigid-body, which could not absorb energy. However, in the experimental test, a part of the energy of the system is absorbed by the hammer.

4.3.4 The parametric Study and Discussion

In this research, ten different masses of the drop hammer are used to understand the influence of the mass of the hammer on the response of the RC beam and the damage patterns. This study provides a comprehensive overview of the impact response of a simply supported RC beam. Figure 4-8 shows the crack patterns and the deformation of the beam under impact loading for nominated tests. Although the lighter masses of 200 and 400 kg cause critical damage and cracks in the structure, less deformation is visible in the mid-span of the structure. The heavier impactors cause serious damage with more cracks and crushes at the impact point and visible deformation of the structure. The legend shows the value of the tensile damage parameter, which varies from 0 to 1. It also shows the damage severity as the value approaches to 1.

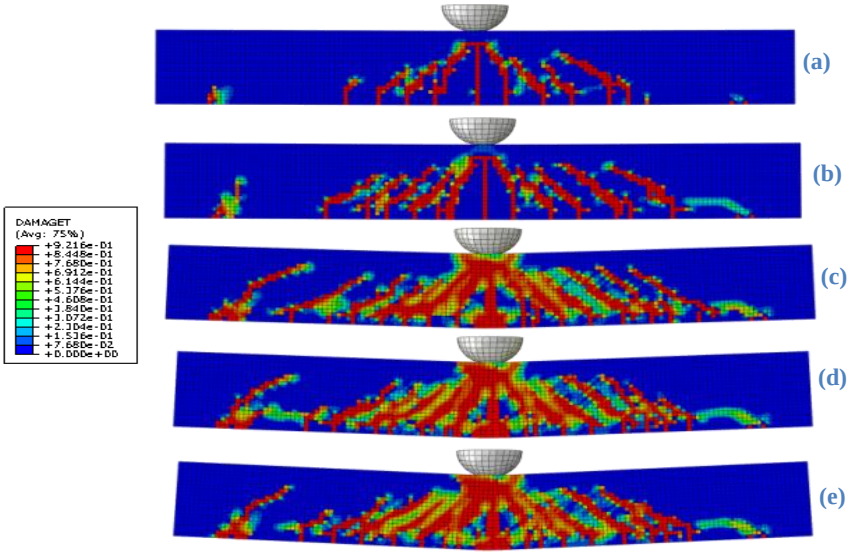

Figure 4-8: Crack pattern in RC beam under impact loading with a mass of (a) 0.1t, (b) 0.4 t, (c) 0.8 t, (d) 1 t and (e) 1.5 t

As can be seen, the severity of the crack does not increase considerably by increasing the mass of the impactor. The added energy of the impactor is used in crushing the concrete around the area of the impact.

4.3.4.1 Impact force

Impact force is one of the significant design considerations for structural resistance. Impact force is defined by the acceleration transferred to the structure under a certain impact load. As expected within the simulation, the impact force is one of the factors which has been affected by changes in the mass of the Hammer. It is obvious that with an increase in the mass of the hammer, the impact force is increased. However, to understand the damage patterns, it is essential to conduct more investigation to distinguish the difference between the failure modes.

One important observation is the distinction between free vibrational behaviour and damping behaviour of the structural system. This is demonstrated in Figure 4-9 by comparing the results from the nominated analysis of the RC beam under impact loading. Lighter impactors (0.2t & 0.4t) cause local damage while massive impactors (0.8t -1.5t) cause severe damage, distinguished by the convex behaviour of the impact force.

The response of the impacts arising from the lighter masses of 200 kg and 400 kg indicate backward reaction of the impactor when the impact forces reduced to zero. The hammer with the mass of 0.4t has the same response after impact, but bouncing back occurs about 0.02 s after contact initiation.

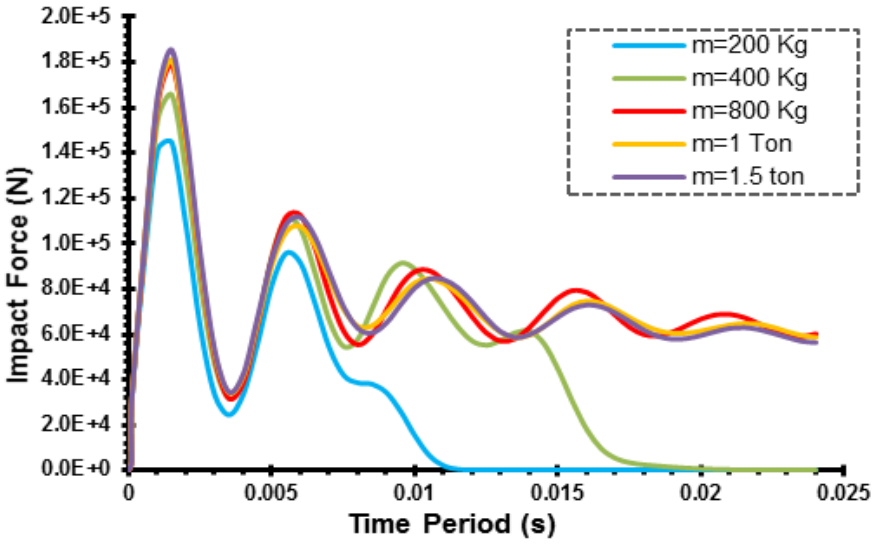

Figure 4-9: Impact force for nominated masses of the hammer during the impact

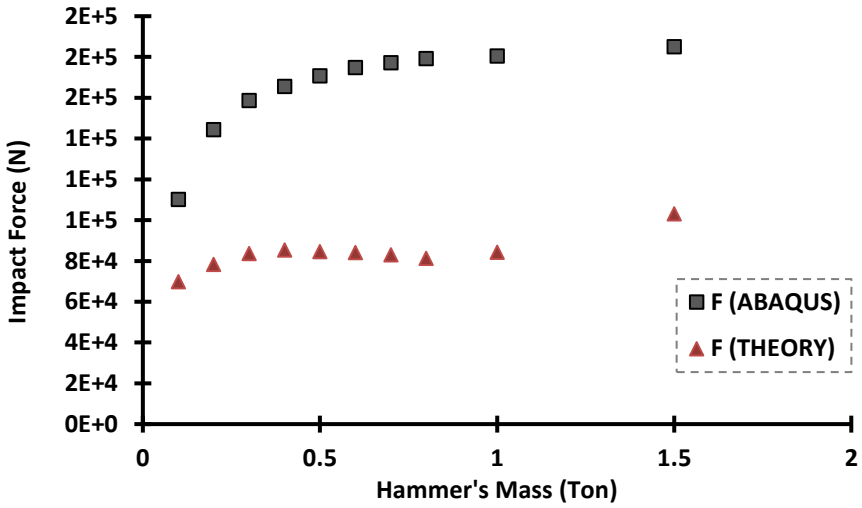

Figure 4-10: Normalised maximum impact force relationship with the normalised mass of the impactor

Figure 4-10 provides the variation of the impact forces derived from the FEM analysis and compares the corresponding values of theoretical impact forces defined by:

4-4: $\boldsymbol{F_{impact}} = \frac{\boldsymbol{mgh}}{\boldsymbol{d}}$

where m is the mass of the dropped object, g is the gravitational acceleration, and d is the displacement value of the hammer. The graph represents the difference between the theoretical values for impact forces are much lower than the real impact force. Using the deformation evaluated from the analysis, this could prove that the nonlinear analysis could perform worse in terms of the definition of the impact force.

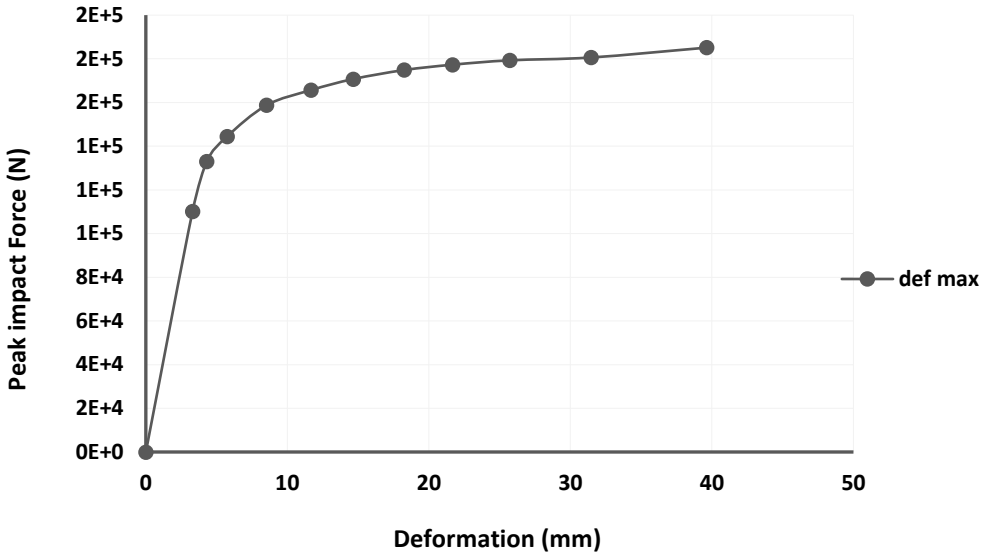

Figure 4-11: The relationship between Peak impact force and the resulted maximum deformation of the mid-span

Structural behaviour under different loading could represent the given criteria for structural damage. Figure 4-11is an example which is describing the relationship between the peak impact force and the correspondence deformation. The graph shows that the mass of 300 kg could represent the ultimate load in which it can cause serious damage and the load more than 400 kg of mass cause significant structural damage which can be interpreted to the structural failure.

4.3.5 Reaction Forces

Figure 4-12 plotted midspan impact-loads and the reactions as a function of time for each test. By theory impact forces induced by colliding the impactor is a coefficient of the acceleration of the impactor. The graphs show that the impact forces are higher than the reaction force. But after peak impact loading, the reaction forces take place. With the increase in the mass of the impactor, the free vibrational response of the beam appears.

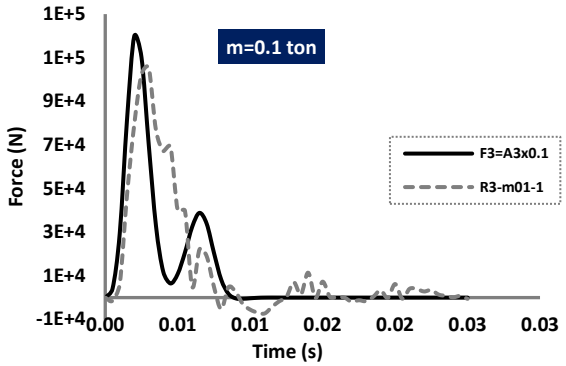
m=0.1 ton
F3=A3x0.1
R3-m01-1
Force (N)
Time (s)

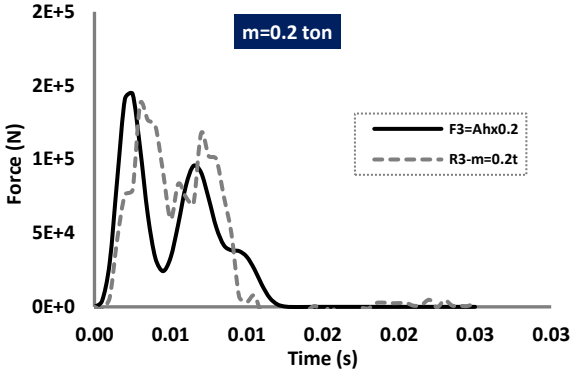
m=0.2 ton
F3=Ahx0.2
R3-m=0.2t
Force (N)
Time (s)

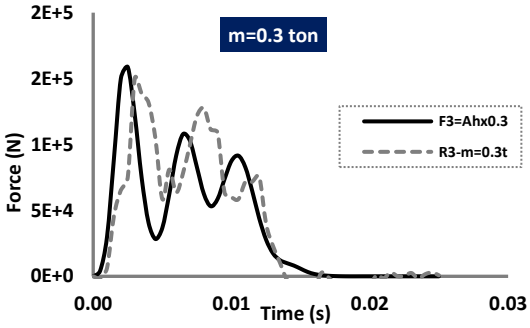
m=0.3 ton
F3=Ahx0.3
R3-m=0.3t
Force (N)
Time (s)

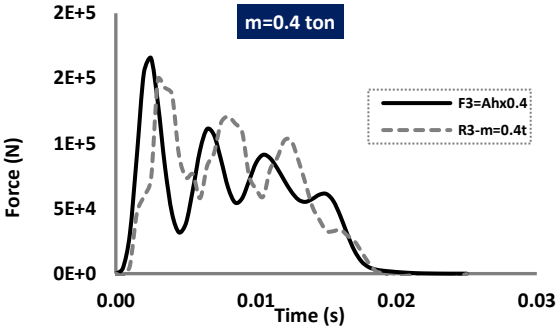
m=0.4 ton
F3=Ahx0.4
R3-m=0.4t
Force (N)
Time (s)

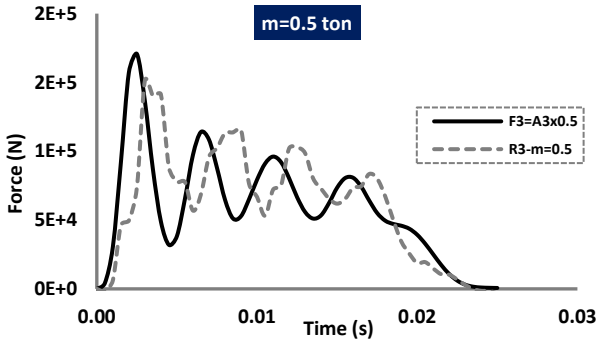
m=0.5 ton
F3=A3x0.5
R3-m=0.5
Force (N)
Time (s)

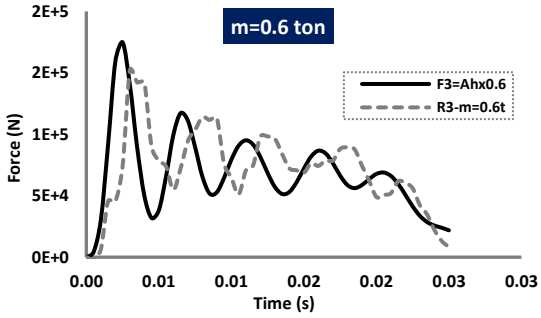
m=0.6 ton
F3=Ahx0.6
R3-m=0.6t
Force (N)
Time (s)

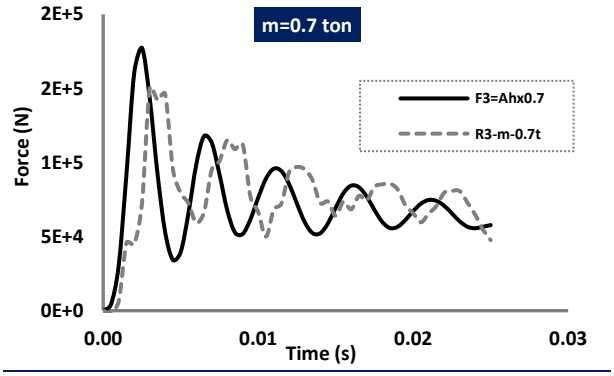
m=0.7 ton
F3=Ahx0.7
R3-m-0.7t
Force (N)
Time (s)

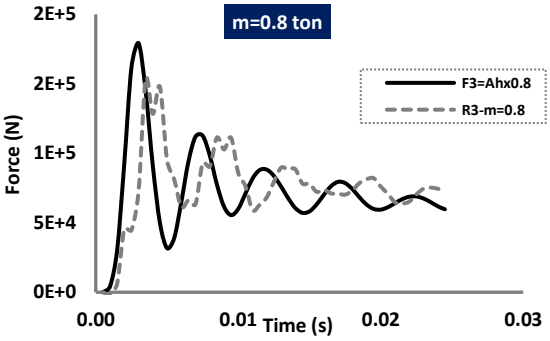
m=0.8 ton
F3=Ahx0.8
R3-m=0.8
Force (N)
Time (s)

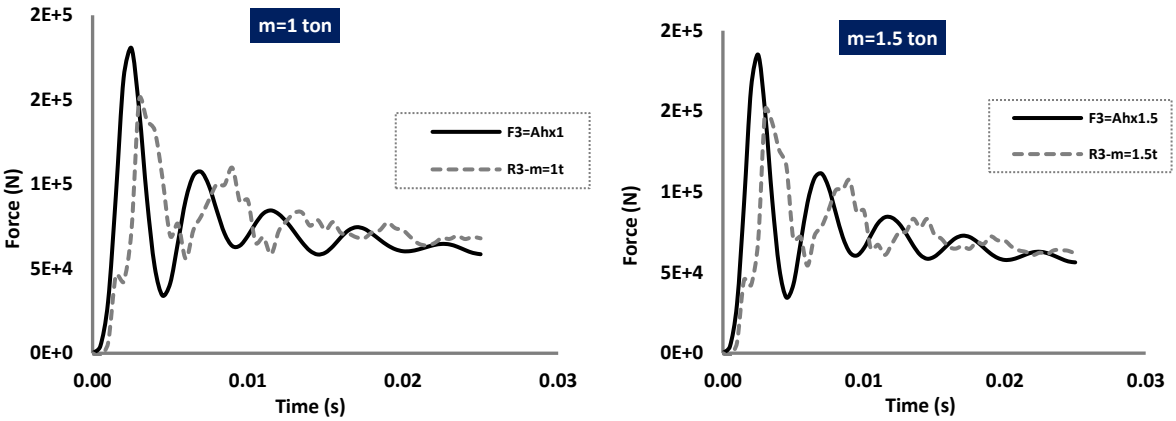

Figure 4-12:Time history of the impact force and reaction forces resulted from the hammer's impact

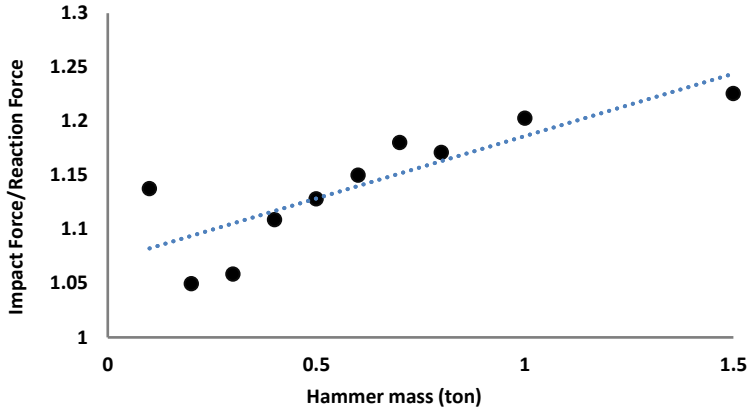

Figure 4-13: The ratio of impact force and reaction force for each simulation

Figure 4-13 also provides a comparison of the impact load and the reaction forces. The analysis shows that the rate of the impact force and reaction force is increasing with a relatively constant coefficient of 0.115 governed from the regression analysis. This shows that the total resulting impact forces are not transferring to the static reaction forces, and the reaction forces could not represent the exact value of the impact force. Structural performance is related to the dynamic impact force, and the failure modes of the impact are predictable, knowing the mass of the impactor using the fitted curve represented in Figure 4-13..

4.3.6 Damping ratio

In the impact simulation, determining the damping of the system and the effect of the mass on this factor can be measured by using the free vibration decay method. The damping ratio can be determined using the following expression:

$$4.\ \xi = \frac{1}{2\pi m} ln \frac{\delta_n}{\delta_{n+m}}$$

where δ_n is the *n*th amplitude of the response curve and *m* is the number of conservative cycles in the response curve.

Damping ratios, in terms of the decay in the structural vibration, for the models with free vibrational responses (0.8t, 1t & 1.5t), are determined by converting the values of the displacement using the above equation. Table 4-3 listed the damping ratios for each model.

Table 4-3: Estimated damping ratios			
Hammer Mass	800 kg	1000 kg	1500 kg
Damping Ratio	5.04 %	5.62 %	5.54 %

The table shows that the damping parameters of the structure could be affected by the impacting force of the hammer onto the beam. The changes in the damping ratios are due to the changes in the stiffness matrix of the structure. However, the changes are not in a regular pattern - the changes vary between 0.05 and 0.056 for these cases.

4.3.7 Impact Acceleration

The variation in the acceleration of the impact is illustrated in Figure 4-14. There is a significant difference between the peak acceleration for the lighter hammer and the heavier

hammer. This variation also represents the distinction between the local and overall damage as the acceleration due to lighter hammers decays to zero rapidly, while for heavier hammers the free vibrational reaction continues.

Figure 4-15 also plotted the peak values of the impactor with respect to the normalised mass of the impactor and the beam. The well-fitted power function presented on the graph (mm/s^2) provides a relatively correlated equation for guessing the resulted acceleration and defining the failure mode of the structure based on the relevant impact forces.

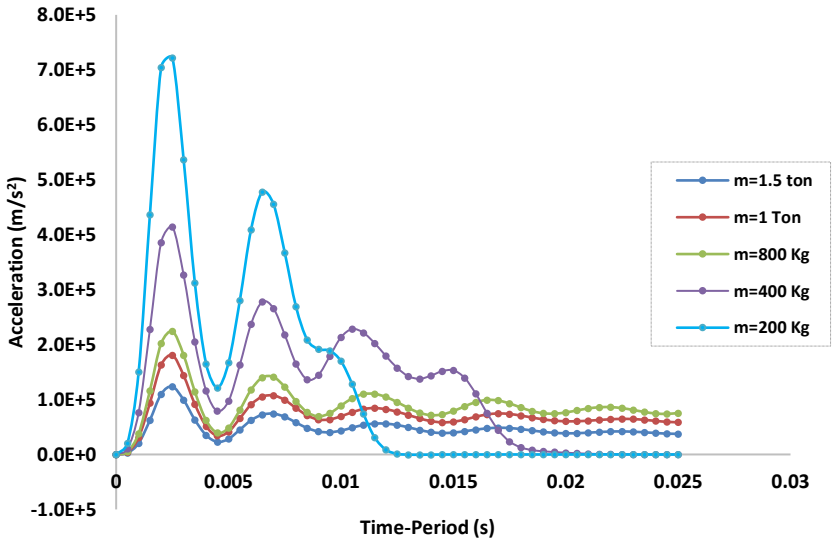

Figure 4-14: Time-history of the acceleration of the impact point

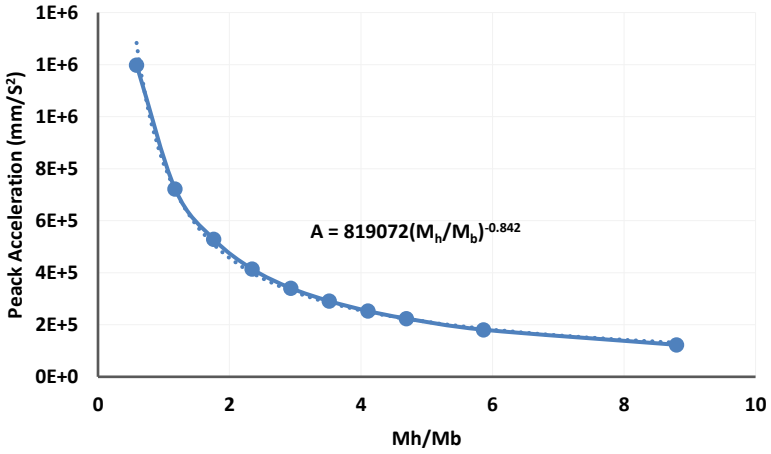

Figure 4-15: Peak Acceleration of the impactor relationship with normalised mass

4.3.8 Energy

The time history behaviour to show the change in the energies (kinetic, internal and total energies) of the system, is evaluated to better understand the energy released during impact loading. Figure 4-16 shows the time history of energies for three nominated models of different masses of the impactor. It is evident that based on momentum theory, the total energy is basically conserved. The conjunction of the kinematic and internal energies is approximately half of the total energy. The maximum internal energy occurs exactly when the kinematic energy is minimum. The changes and relationship between these energies are illustrated, and the graph gives a perspective on how the mass of the hammer can influence the changes in different sorts of energies.

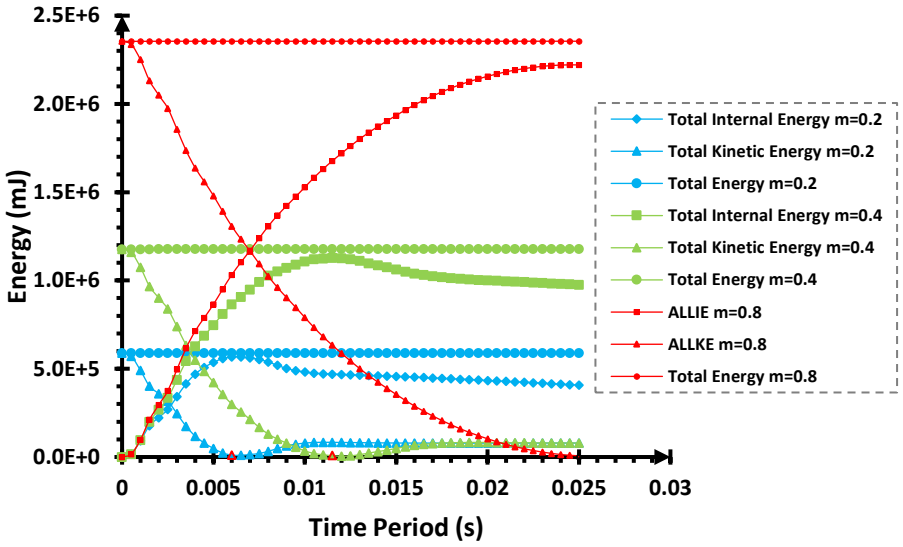

Figure 4-16: Various energies' time-history for the nominated masses of 200 kg, 400 kg, and 800 kg

Figure 4-17 provided the variation of the total energy of the system with respect to the normalised masse with the mass of the beam. A factor of mass, which is the ratio of (Mh/Mb) represent the dimensionless parameter of mass. For all models, the total energies are constant as expected (conservation of energy hypothesis). Regression analysis of the total energy of the system with the factor of mass gives the following equation:

4-5: $\boldsymbol{E_{total} = \beta \varphi_m}$, $(\boldsymbol{\beta = 500.984})$ $(\boldsymbol{J})$, R2=1

The constant coefficient of β in this study represent the formulas slope, and it shows that the factor of mass has a linear relationship with the energy of the system.

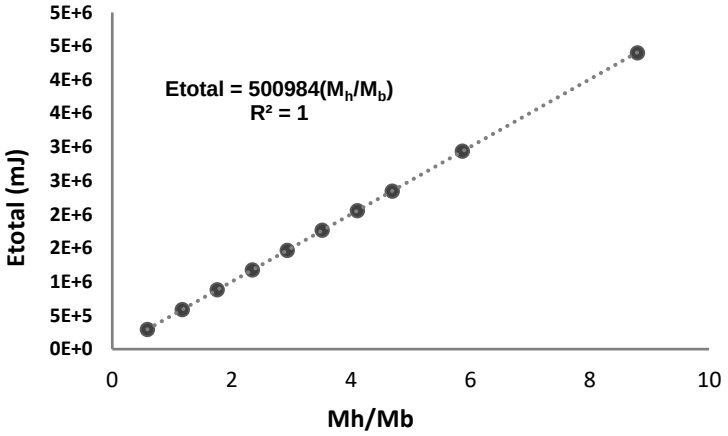

Figure 4-17: Total energies variation with the hammer's mass

On the other hand, energy is a quantitative value which could be translated in force and deformation. The relationship between the total energy and the resultant force from the impact is presented in Figure 4-18, which shows the energy of the systems in the two phases of local and overall damage. A significant difference between local and overall damage mode is observed by comparing the slopes of the two phases of damage. The slope of the curve for overall and local damage modes are differentiated in the graph.

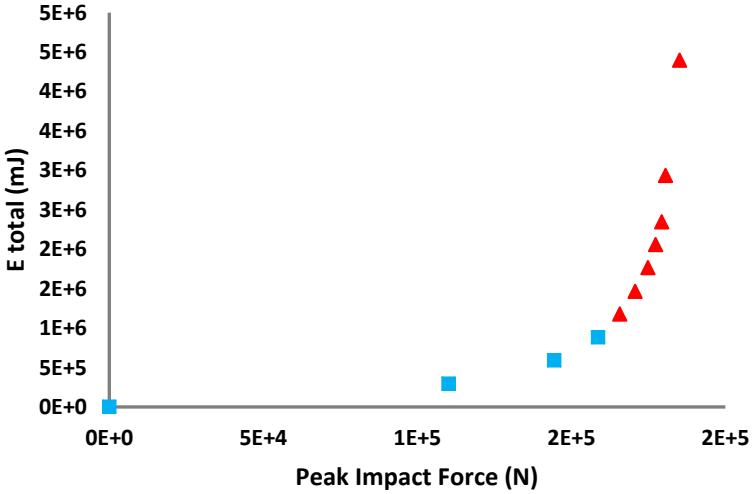

Figure 4-18: The relationship between total energies in the system and the maximum induced forces

The term "ALLDMD" is another important parameter defined by ABAQUS. It represents the damage dissipated energy for the whole system. In theory, the dissipated energy can be calculated using the following equation:

4-6: $\boldsymbol{E_R} = \frac{m_h m_b}{2(m_h+m_b)} v_{ih}^2$

where $m_h$and m_b are the mass of the hammer and beam, respectively.

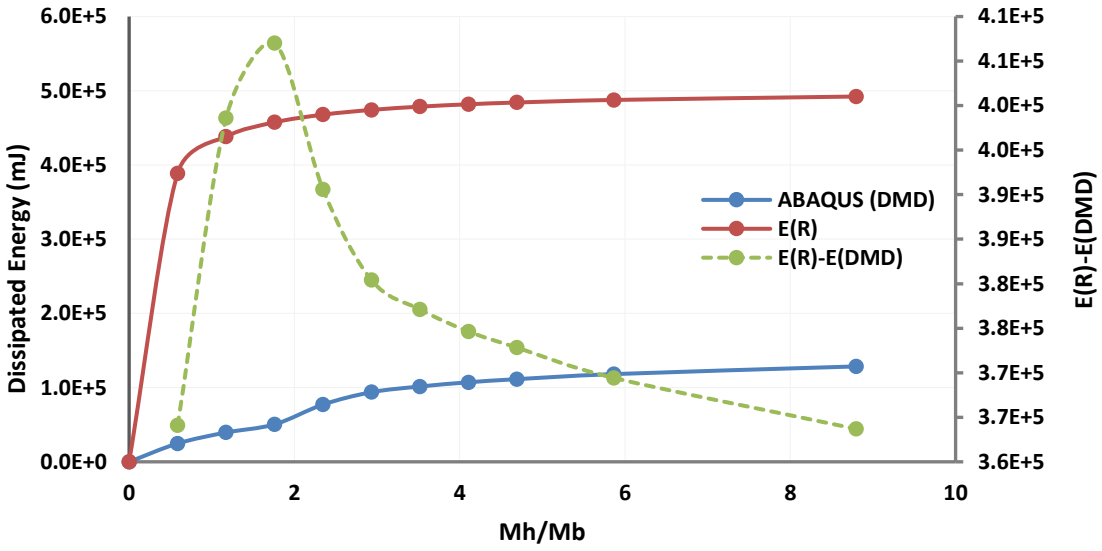

Figure 4-19 Figure 4-19 compares the dissipated damage energies calculated by ABAQUS and the theoretical dissipated energies with respect to the normalised masses and for all models and their differences also are shown by the dashed graph. The graph shows that dissipated damage energy is about 20%-30% of the dissipated energies of the system. On other words,

approximately 20%-30% of the dissipated damage is consumed for the structural damage and as this ratio is increasing structural failure is probable.

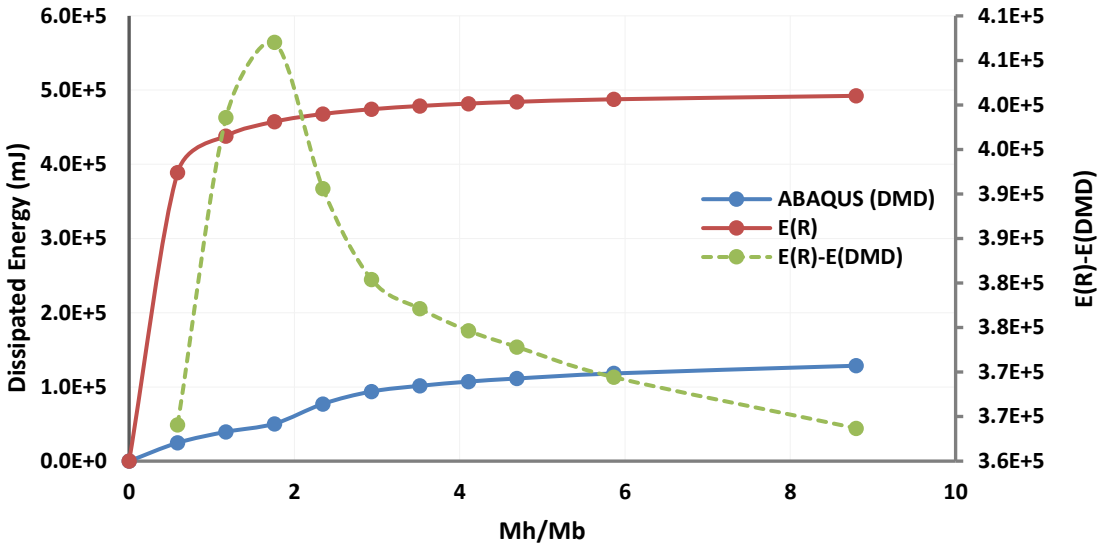

Figure 4-19: Damage dissipated energy for different mass

The difference between dissipated energy and the damage dissipated energies are maximum when the ratio of the mass is about 1.76. According to the current study, these represent 300 kg mass of the hammer.

4.3.8.1 Deformation and Damage

Another aim of this study is to calculate the changes in the section due to the penetration of the hammer in the concrete. The displacements of the top (A) and bottom (B) points are evaluated, and their differences reveal the section variance with time. Figure 4-20 shows the performance of both compressive and tensile surfaces during impact loading for a simulation with a 400 kg and 800 kg hammer with the masses. The figure shows that section shrinks when

the hammer moves back. The backward movement of the lighter hammer is predictable when the displacement starts decreasing. This behaviour is observed for the lighter impactors - the heavier masses behave differently.

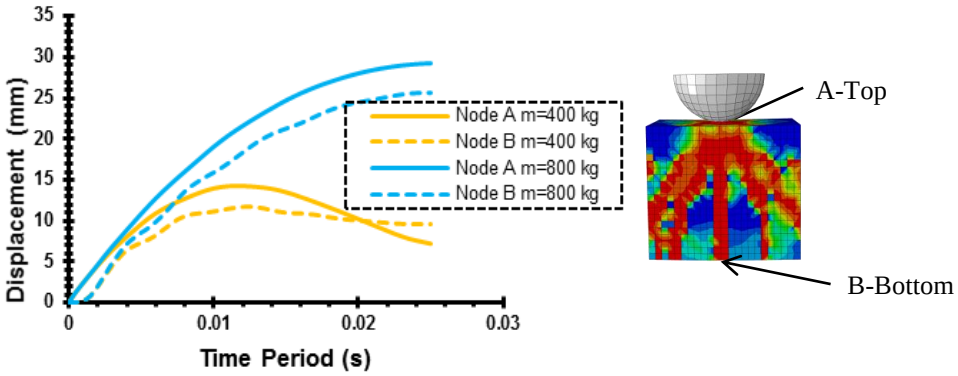

Figure 4-20: Time history displacement of the node A at the top and node B at the surface of the beam section for two models of 400 kg, and 800 kg, mass of the hammer

Figure 4-21 4-21 represents the time history of the section changes. From the graph, it can be identified that the impact has a significant effect on the deformation of the beam section. Moreover, the lighter masses of the hammer – 200 kg and 400 kg – behaved unpredictably. These rather contradictory results may be due to more tensile deformation at the bottom surface rather than compression at the top surface of the beam.

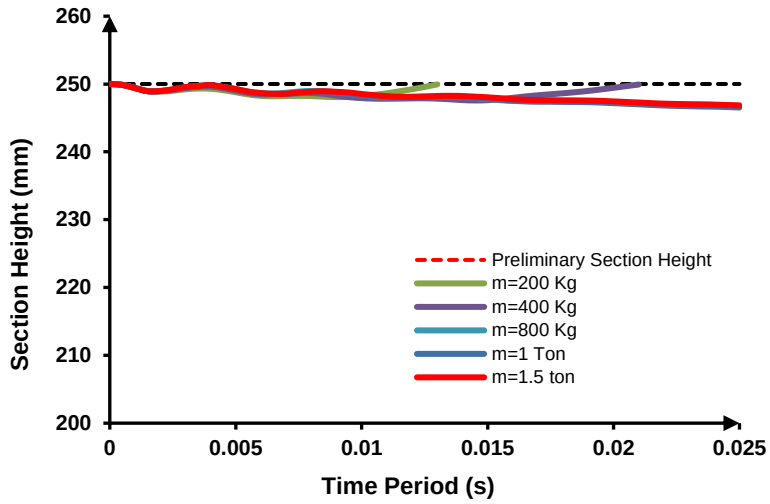

Figure 4-21: Time history of section variation for nominated tests

Consequently, one of the main characteristics of the hammer impact on the structure is bouncing back if the mass is not sufficiently heavy in comparison with the beam's mass. Furthermore, ABAQUS is not capable of considering the gravity for rigid body systems. Therefore, the irregular behaviour observed in the lighter impactors may be due to the exclusion of the gravity influence.

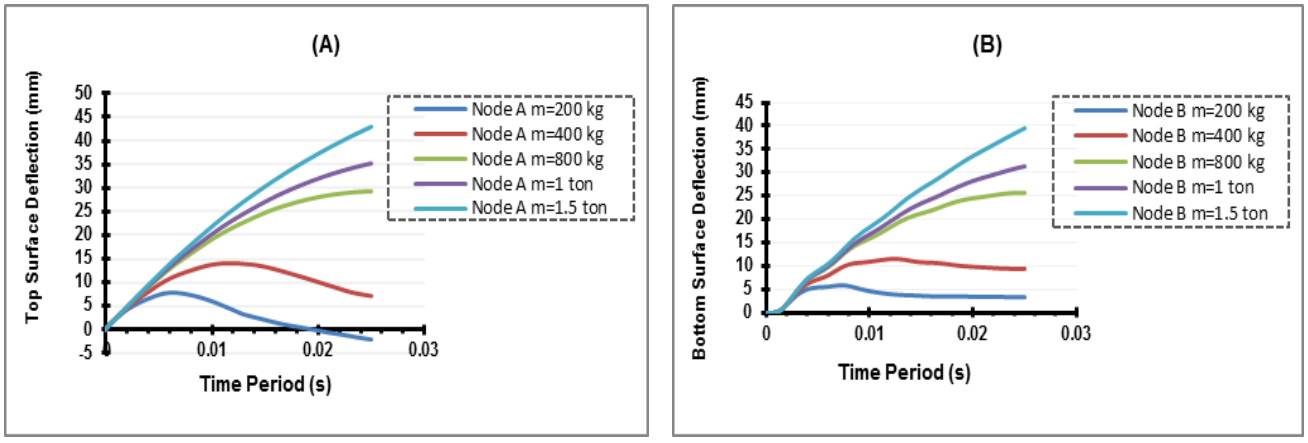

Figure 4-22: Time history of deflection for (A) top surface of the beam (impact point), (B) the bottom surface of the beam

Figure 4-22 provides the time history of the compression surface (Node A) and tensile surface (Node B) of the beam. The structural response observations indicate that, for the lighter hammers, 100 kg to 400 kg, residual displacement at the compression surface is more than the tensile area. However, the more massive impact loads have different performance.

The capability of a structure to absorb the energy can also be defined by the cushioning factor, which is a relationship between stress and energy absorbance of a material. The cushioning factor can be described as:

4-7: $C = (GTb/H)$

where G is the peak acceleration of the impact, T is the beam thickness, and H is the drop height (Wang 2009). The associated paramFeters and their values for each model are described in Table 4-4.

Table 4-4**:** Cushioning factor and associated parameters and maximum and ultimate deformation values

(m_h) Mass of the impactor (ton)	0.1	0.2	0.3	0.4	0.5	0.6	0.7	0.8	1	1.5
(G) Peak Acceleration (m/s^2)	110.2	722.1	529.1	414.2	341.4	291.4	253.3	224.1	180.6	123.4
C=(GT/H) Cushioning Factor (m/s^2)	918	601.8	441	345.2	284.5	242.8	211.1	186.8	150.5	102.8
Maximum deformation of the impact point (mm)	3.3	5.74	8.53	11.67	14.65	17.01	21.3	25.72	31.46	39.63
Ultimate deformation of the impact point (mm)	2.08	3.27	5.8	7.1	13.1	17.01	21.3	25.70	31.46	39.63

Figure 4-23 compares the cushioning factor in relation to the normalised maximum deformation and the ultimate deformations with the. As discussed, the lighter masses have experienced some recoverable deformations while the ultimate deformation in heavier masses is equal to the maximum values. Severe damages can be observed with no recoverable

displacement. On the other hand, the graph shows the values are well correlated with a power equation with different coefficients governed from the regression analysis.

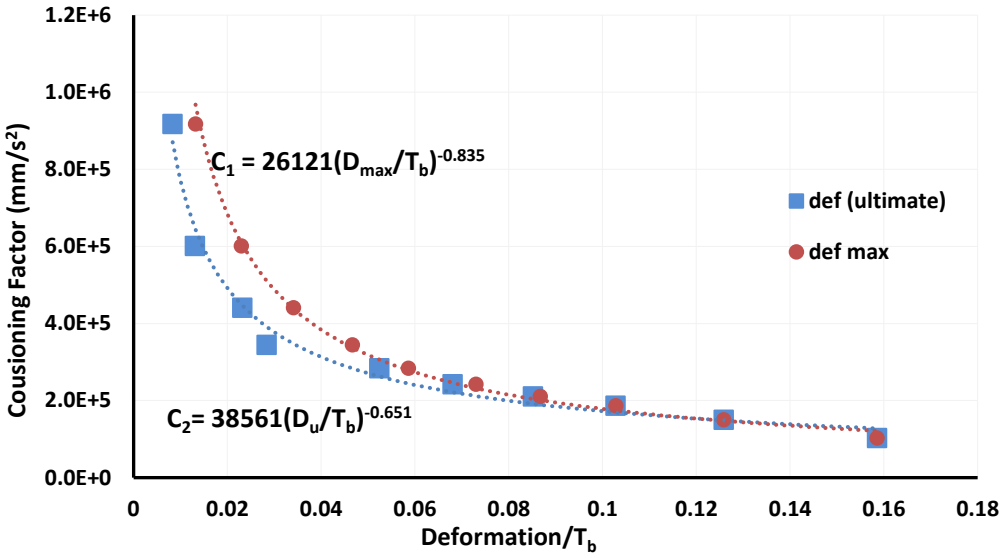

Figure 4-23: Cushioning factor's relationship with the bean deformation

Local damage has experienced a difference between the peak deflection and the ultimate deflection at the end of the analysis. This behaviour is not expected when the beam failure is occurring due to a higher impact. Cushioning factor shows a power relationship between maximum and ultimate deformation of the beam. However, for the 400 kg mass impact, the highest difference between cushioning factors is observed and with the increase in the normalised deformation with the section height, the cushioning factors are decreasing and getting equal when the structure is experiencing total failure.

4.4 Conclusion

Dynamic nonlinear analysis with a parametric study on an RC beam subjected to the impact of a free-drop hammer has been carried out using ABAQUS. The models are exposed to different impact forces resulting from different masses of the hammer. A comprehensive overview of various structural behaviours is implemented and discussed for two different damage scenarios (local and overall damage). Based on the results, the following conclusions can be drawn:

1 Damage modes of the beam have a direct relationship with the mass of hammers. The crack pattern changes with the mass of the hammer.

2 The impact force has a non-linear relationship with the mass of the hammer

3 The mass of the hammer has a linear relationship with total energy.

4 The rate of reduction of the kinetic energies appears to be very similar for different masses of the hammer.

5 The rate of increase of the total damage dissipated energy reduces with the increase in the mass of the hammer.

6 The surface damage caused by the hammer's drop shows a bounce back at low masses of the hammer.

7 The flexural element's height changes are calculated based on the changes on the top and bottom surfaces of the element. Results indicate the crushing of concrete with heavier loads and cracking at lighter loads.

8 The correlation between the simulation and experiments from the literature shows reasonable accuracy of the FE models utilised in this study to assess the maximum impact forces.

9 The cushioning factor is a parameter that can represent the structural response and have a regressive power relationship with the deformation of the structure.

It is acknowledged that the impact response of RC beams is an emerging research area with the high complexity of loading conditions. Therefore, it is recommended that additional experimental investigations be conducted for a broader understanding of the dynamic behaviour of RC structures. For this purpose, a wider range of hammer mass and different structural stiffness can be explored with to obtain comprehensive results.

CHAPTER 5

Log Impact Forces on a U-Slab Bridge Pier: A Parametric Study on Nonlinear/Dynamic Response of a Bridge Pier Exposed to an Object Impact

Statement of Authorship

Journal paper title:	Log Impact Forces on a U-Slab Bridge Pier: A Parametric Study on Nonlinear/Dynamic Response of a Bridge Pier Exposed to an Object Impact
Status:	Manuscript submitted for publication
Reference:	M Nasim, S Setunge, T Maqsood, ‘ A Parametric Study on Nonlinear/Dynamic Response of a Bridge Pier Exposed to an Object Impact ’, *Manuscript Submitted for publication*.
Name of the author:	Maryam Nasim,
Position:	PhD scholar.
Contribution:	Corresponding Author, Collecting and interpreting data, performing analysis, preparing figures and writing the manuscript
Name of the author:	Sujeeva Setunge
Position:	Professor, Deputy Dean Research and Innovation School of Engineering, RMIT University
Contribution:	Supervising research, assisting in manuscript preparation and reviewing
Name of the author:	Tariq Maqsood,
Position:	Senior Lecturer, School of Engineering, RMIT University
Contribution:	Editing and reviewing the manuscript

5 A Parametric Study of Impact Forces and Resilience of Bridge Pier Under Moving Object During Flood Loading

Synopsis

Based on the research findings represented in Chapter 4, log impact on a U-slab bridge pier was simulated in this chapter. Further, the research on the dynamic effect of the mass of the hammer on the reinforced concrete model, Chapter 4 shows a good correlation in the methodology of modelling impact using Explicit/Dynamic analysis.

In Chapter 5, a parametric study is presented on the damage of the bridge pier due to the impact of a floating and moving object. Subsequent to the simulation of the impact of a moving object on the structure using ABAQUS, a parametric study has been conducted to evaluate the effect of the critical parameters of the moving object such as the velocity and the mass of the impactor on the structural response.

The result of these analyses has been compared to Australian and AASHTO Standards. The evidence presented in this chapter shows that standards specifications require further research to arrive at a conservative estimate of the forces induced by the impact of a floating object on the bridge structures under flood loading.

Abstract

Floods may cause structural damage in moderate to extreme load conditions. Log or any other moving object (MO) impact is one of the reasons for damage to over-river bridges during flooding. Log impact-resistant bridge design involves the static application of codes considering some dynamic factors. However, the existing static analysis procedure neglects crucial dynamic aspects of the MO impact. In this research, a parametric study has been conducted to understand the effect of mass and velocity of a moving object on the response of a bridge pier. A new practical equation has been introduced for calculating the maximum impact forces resulted from the impact phenomenon based on selected variables. Moreover, the results of this study, including maximum impact forces, have been compared with the recommended equations of Australian and American standards. The results of this study found that Australian design standards of bridge design load, AS5100, underestimated the impact force significantly.

Keywords

Log Impact, Bridge Structure, Reinforced Concrete Structures, Explicit/Dynamic Analysis, Finite Element Analysis, Bridge Design Codes

5.1 Introduction

Floodwater can pick up and carry objects of all types, from small to large, from light to heavy, including trees, portions of flood-damaged buildings, automobiles, boats, storage tanks, mobile homes, and even entire homes (FEMA, 2014). The failure in reinforced concrete (RC) piers is usually due to the instantaneous loading applied to the structure.

Highway bridges are sufficiently studied under vehicle impact, a load case which is considered in the bridge design procedure. Numerous studies have been carried out to quantify the interaction between bridge structure and vehicle (Zhong et al., 2015, Zhu and Law, 2002, Yang and Papagiannakis, 2010, Green and Cebon, 1997, Kocatürk and Şimşek, 2006, Sawan and Abdel-Rohman, 1986, Zararis and Papadakis, 2001). Cai et al. (2007) studied dynamic impact factor for performance estimation of bridges and researched the effect of wind and bridge approach length on responses of bridge-vehicle interaction (Deng and Cai, 2010, Deng and Cai, 2009, Chen and Wu, 2009, Cai et al., 2007). Numerous studies have been conducted to understand the relationship between the dynamic behaviour of impact and the reinforcement ratio in reinforced concrete structures (Sawan and Abdel-Rohman, 1986, Kishi et al., 2002, Saatci and Vecchio, 2009, Zararis and Papadakis, 2001, Jin et al., 2018, Yoo et al., 2015). Impact loading results from a collision between two bodies during a very small interval of time. Impact loading could occur in RC bridges, walls and slabs if they are struck by vehicles or subjected to a low or high-speed object. Shi et al. (2019) Proposed an elastic-plastic model of the dynamic response of an RC beam when subjected to the impact of a rigid mass. Some research studies are conducted to understand the design and analysis of concrete structures against blast loads (Hao and Hao, 2014; Hao et al., 2016). A simplified means of approximating

dynamic amplification effects and the conservative prediction of the barge impact-resistance bridge design consideration is carried out by (Getter et al., 2011). However, limited studies have been carried out to understand the behaviour and damage mechanism of a bridge pier when subjected to a moving object (MO) impact during flooding.

The objective of this research is to study a U-Slab bridge pier as a case study under impact loading of a relatively rigid MO carried by flooding. The selected bridge type of U-Slab bridge is widely used in Victoria. One of the likely phenomena, causing the failure of the U-Slab bridges, is the impact of a MO to the pier during extreme flooding.

Figure 5-1 provides some examples of damages caused by MO to bridge pier, reported by the Department of Transport Victoria, DOT.

Figure 5-1: Damaged U-Slab Bridge under log impact during flooding, Victoria, 2010

In the present study, the dynamic response of a bridge pier and maximum impact forces resulting from the impact of a relatively rigid MO is studied through a parametric study. The chosen parameters for the study are mass and velocity of a MO. The finite element model of the pier is assumed fixed at the soil-structure connection at bottom and simply supported at the top to simulate the connection of the pier with the bridge headstock. Damage to the MO is not addressed in this study; therefore, cylindrical shape of the MO is assumed as a rigid-body and modelled as a one-degree of freedom with a constant velocity applied to the model to represent the MO impact on the bridge pier. The interaction between bridge pier and the MO is solved using Newmark integration method given in ABAQUS 6.14 (2013).

This study aimed to conduct a parametric study using a series of FE simulations to assess the influence of the mass and velocity of the MO on the peak impact forces on the structure. Provisions in different standards on the design impact forces for the bridge are also reviewed and summarised. These provisions are compared to the outcomes of this parametric study. The results from this study will assist in quantifying the damage to bridge pier under the impact of the MO.

5.2 Provisions of design standards on impact force on the bridge structure

Impact load is an unknown parameter which is most important in designing structures such as bridges. Structural nonlinear finite element analysis can provide a practical approach to understand the impact load transferred from the MO to the structure. An experimental study shows a reduction of 11.4%-15.4% in the reaction forces throughout the energy dissipation in reinforced concrete plates (Iqbal et al., 2019).

In the following section, the guidance on impact forces is reviewed. Three basic approaches are used to estimate the maximum impact force based on the velocity and mass of the MO in different standards. These approaches are:

1) Contact stiffness (AASHTO 1998); requires the effective contact stiffness
2) Impulse-momentum (FEMA, June 2014); requires the stopping time
3) Work energy (NAASRA, 1990); requires the stopping distance

All three approaches are proved to be equivalent. It is observed that stopping distance depends on the effective contact stiffness, the debris mass, and the debris velocity (Haehnel and Daly, 2004).

In a one-degree-of-freedom system, the maximum impact force can be defined using:

$$\mathbf{F_{i,max} = v\sqrt{\hat{k} m_l}} \qquad (5\text{-}1)$$

where v is the object velocity, $\hat{k}$ is effective contact stiffness and m_l is the mass of the object.

5.2.1 AASHTO (1998)

Using the contact-stiffness approach, AASHTO (1998) expressed the impact force on a bridge pier as the maximum collision force based on the dead-weight tonnage of the vessel (DWT) (long tons) and the vessel velocity, v (ft/s). The impact force on the structure can be computed by using the coefficient from an experimental study regardless of the structural geometry, by:

$$\mathbf{F_i(kips) = 8.15v\sqrt{DWT}} \ \ \mathbf{(US\ units)} \qquad (5\text{-}2)$$

This approach requires only the effective contact stiffness of the collision to calculate the maximum impact force of the impactor with known mass and velocity. In AASHTO (2009), the kinetic impact-energy of a floated barge is empirically related to static collision load, which is applied to the bridge in a static analysis procedure. The impact analysis for both vessel and structure has been developed with an analytically derived load prediction model for rounded and flatted surface (Consolazio et al., 2009).

5.2.2 NAASRA (1990)

NAASRA (1990) used the concept of work-energy to evaluate the impact force, assuming the velocity of the object reduces to zero when impacting a structure. Maximum impact force is described by:

$$\mathbf{F_{i,max}} = \frac{\mathbf{mv^2}}{\mathbf{S}} \tag{5-3}$$

where m is the mass of the object, v is the velocity of the object and S is the stopping distance of the object, as the distance the object travels from the point of contact with the target until the moving object is entirely stopped (u = 0) (NAASRA, 1990).

5.2.3 AS5100

AS5100 has a similar suggestion to NAASRA (1990) practising a function of the mass of the object and the velocity of the moving body. The total impact force can be expressed as a work equation of $Work = Force \times distance$.

AS5100 suggested that, where floating logs are a possibility, the design forces (ultimate and serviceability) exerted by the logs directly hitting piers or superstructures shall be calculated on the assumption that a log has a minimum mass of 2-ton (2000 kg) and will be stopped in a distance of:

1) 150 mm for hollow concrete piers

2) 75 mm for solid concrete piers

If fender piles or sheathing are placed upstream from the pier to absorb the energy of the blow, the stopping distance shall be increased. The design forces will be calculated using the mean velocity of water flow at flood level V_S for serviceability, or V_U for ultimate limit states. The forces due to log impact shall not be applied concurrently, but they should be applied with other water flow forces as appropriate. The impact force of a log shall be calculated by:

$$\mathbf{F_{Lu}^{*}} = \frac{\mathbf{0.5mV_u^2}}{\mathbf{s}} \quad (5\text{-}4)$$

Where m is mass of the log and *s* is stopping distance (m) (AS5100, 2017).

In designing against debris forces, the designer should allow for a force equivalent to that exerted by a 2-tonne log, travelling at the stream velocity and detained within distances of 150mm for column type and 75mm for the solid type of concrete piers. “In the UK, 3-tonne logs travelling at 10mph (4.47m/sec) have been reported in upstream areas. If such a log is stopped in 75mm, then the force exerted may be estimated from the kinetic energy (the Highways Agency 1994; Jordan, 2015).

5.3 Research Significance

Little attention has been paid to design considerations of impact loading for bridges in particular flooding. Engineers use an equivalent static force to emulate the impact force influence. And the magnitude of this quasi-static force depends on the impactor's characteristics. Investigation of the influence of the MO characteristics such as mass and velocity will be required to consider impact design load for reducing the damage. Moreover, in recent years, it is observed that the masses of the MO during flooding has changed significantly for the initial estimates in standards which aimed to cover the impact of MO.

The research presented here provides a fundamental understanding of the forces exerted by MO during flooding on bridge piers as a function of the mass of the impactor and the velocity of the flood. A comparison of design loads given in selected standards and numerical results is carried out to better understand the limitation of the current provision.

5.4 Time Sensitivity Analysis of Impact on ABAQUS Explicit/Dynamic

5.4.1 Finite Element Model

With four decades of development of finite element methods (FEM) and the help of high-speed computers, computer simulation based on FEM has been widely and successfully applied in engineering. There are two basic algorithms for time integration within finite element analysis: implicit and explicit formulations. Implicit formulation commonly uses codes for static and vibration analyses of FEM analysis packages, e.g. NASTRAN, ANSYS, and ABAQUS/Standard. On the other hand, the explicit formulation schemes are highly

recommended in impact analysis, for instance; ABAQUS/Explicit. The difference between these two algorithms can be clearly expressed in the governing differential equation of motion which is consist of inertia terms, damping terms and the stiffness terms of the structural response during impact and then the free vibration reaction of the structure (Chopra, 2017; Low et al., 2001).

A prototype RC U-slab bridge which is a common bridge type in Victoria is selected as a case study. The salient features of the simulated pier of the U-Slab bridge and the FE model of impact are depicted in Figure 5-2. The height of the pier is 3m, and the cross-sectional area is 0.355m x 0.355m. Four longitudinal rebars (28mm diameter) are provided with stirrups (6mm diameter) spaced at 100 mm (see Figure 5-2). Boundary conditions are assumed to be fixed at the bottom in connection with the soil and simply supported on top in connection with the headstock as its is suggested in AS5100. The partial axial load from the dead-load of the superstructure is considered and applied for the numerical simulation as a concentrated load on top of the pier (Sharma et al., 2012).

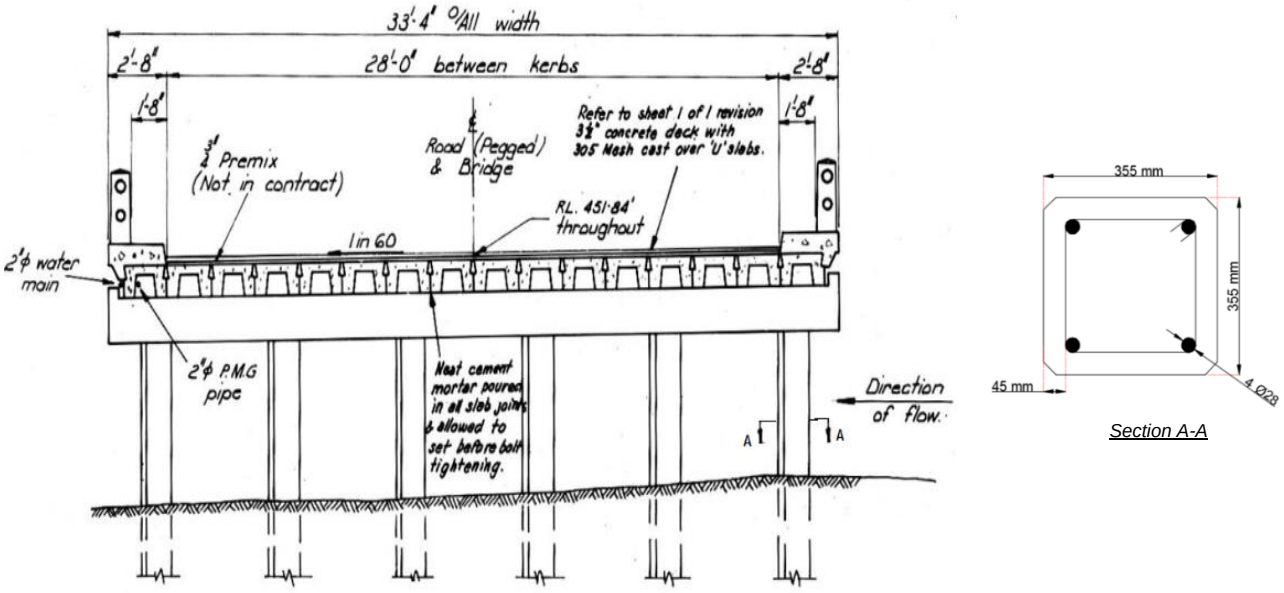

Figure 5-2: The typical case study of a U-slab bridge and the pier cross-section

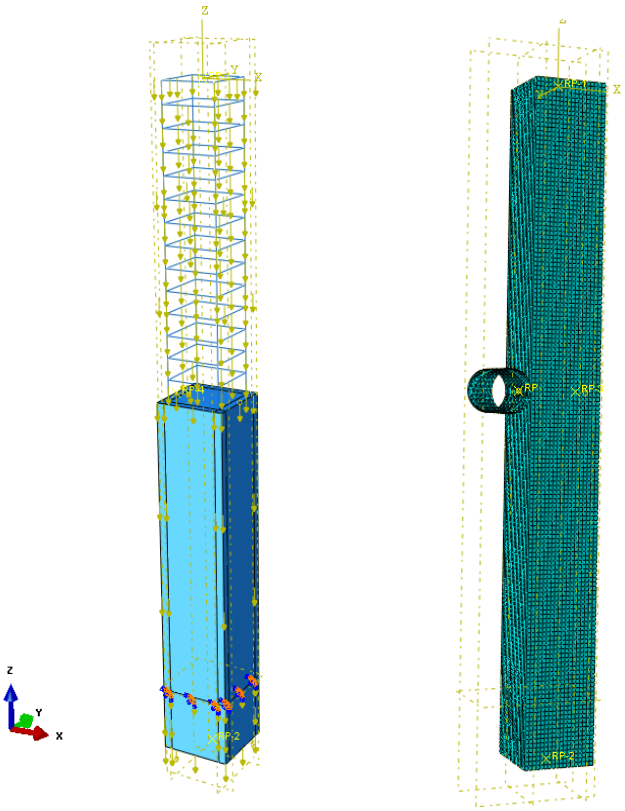

Figure 5-3: FE model of the pier exposed to the impact loading

An elastic-plastic damage model is used to describe the non-linear material properties of concrete. An elastic-plastic model proposed by Mohr et al., (2010) for the dynamic behaviour of the materials is used in this simulation. The Concrete Damage Plasticity model (CDP) developed by Lubliner et al. (1989) with two main failures (compression crashing and tensile cracking) is used for modelling the concrete cracking behaviour in this study. The module of elasticity of the concrete is calculated according to NZS 3106:2006, which is described by:

$$\boldsymbol{E_c = 3320\sqrt{f_c} + 6900} \quad (5\text{-}5)$$

where the compressive concrete strength f_c of the current study is assumed 25 MPa based on the information obtained from the Victorian road authority. Figure 5-4 and Figure 5-5 demonstrate the constitutive input and the damage parameters as a function of the concrete compressive and tensile strengths (25 MPa compression strength). The values are calculated based on the CDP definitions in ABAQUS (ABAQUS 6.14 2013). The detail of material properties and the adopted damage parameters are described Table 5-1. The solid concrete is modelled using the linear hexahedron element type of C3D8R. In addition, the reinforcements are fully embedded using *CONSTRAINT-EMBED option to avoid reinforcement to slid within concrete. Abrate (2001), suggested using time-dependent impulse function to simulate the interaction between the impactor and concrete.

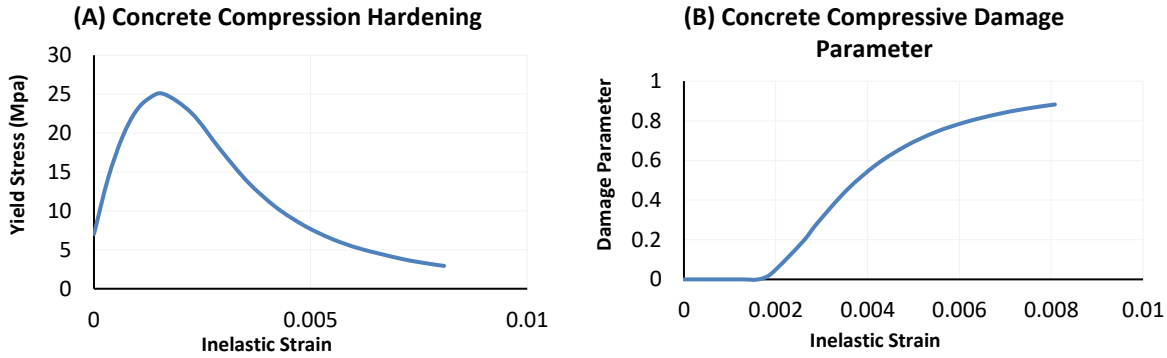

Figure 5-4: (A) Concrete compressive stress-strain relationship (B) and compressive damage parameter

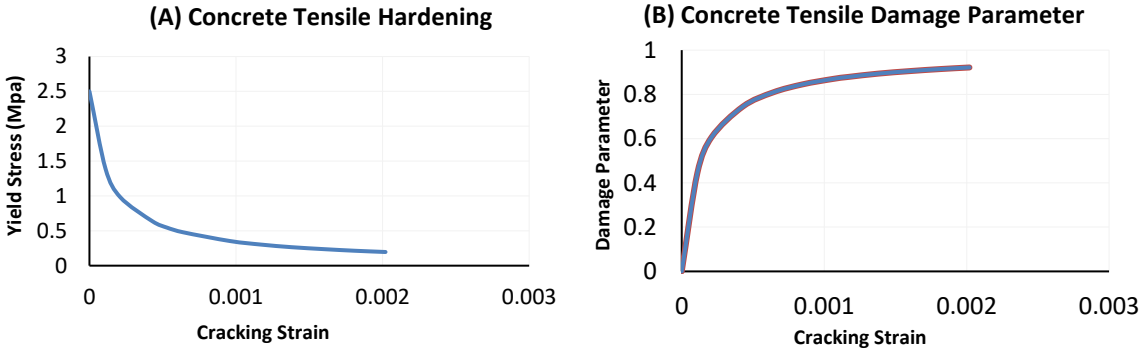

Figure 5-5: (A) Concrete tensile stress-strain relationship (B) and tensile damage parameter

Table 5-1: Concrete CDP properties

Compressive Strength MPa	*Concrete Density (ton/mm^3)*	*Dilation angle*	*Eccentricity*	$\frac{f_{b0}}{f_{c0}}$	*K*	*Viscosity parameter*	*Young's Module*	*Poison's Ratio*
25	2.4E-9	35	0.1	1.16	0.667	0.01	23500	0.15

The impact of MO is simulated with a constant velocity, using *FIELD_VELOCITY and isotropic *POINT_MASS commands in ABAQUS. 100 mm for the diameter of the MO is assumed for this simulation. Since damage to the impactor is not a focus of this research, the MO is considered as a nodal mass of a rigid body.

The methodology of the impact modelling has been calibrated against the experimental study of Fujikake K. et al. (2009). The simply-supported specimen, which is similar to the piers in terms of size and geometry, is exposed to a dropped hammer impact loading. Conducting the mesh convergence analysis of the FE model, the simulation result found to be in good agreement with experimental results when the element size is adopted 12.5 mm. It is observed that further refinement of the elements did not improve the accuracy of the results but reduced the computational efficiency.

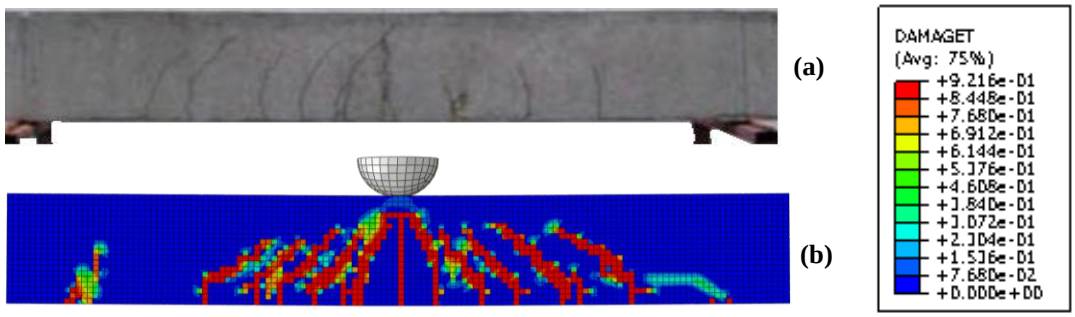

Figure 5-6: 3-D FE model and comparing the crack pattern of the RC beam (a) Fujikake (2009) test, (b) current study

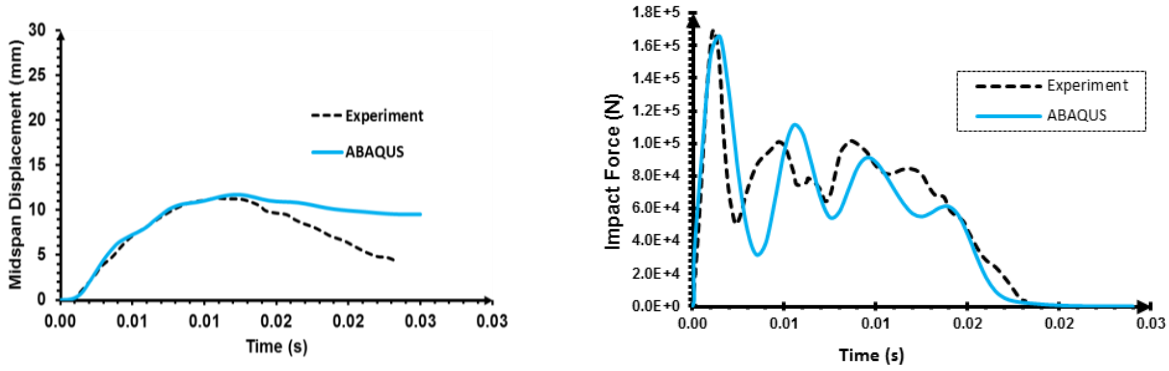

Figure 5-7: Mid-span deflection and time history of the impact force of the RC beam with a drop height of 0.3 m and 400 kg mass of the hammer

Figure 5-6 compares the crack pattern predicted in the 3-D simulated model of the RC beam against the cracks observed in impact test conducted by Fujikake K. et al. (2009). The damage is presented in the form of the damage parameters contours valued from zero to 1.

Figure 5-7 shows the time-history of the mid-span deflection and induced impact force when it is exposed to the impact loading of a free dropped hammer. In particular, the difference in the peak impact force is about 2.2%, and the difference in the maximum deflections is about 2.3% from these observations. From these results, it can be concluded that the simulation technique, RC material model (CDP) and the contact modelling of impact adopted in this FE model study are appropriate to assess the impact load of a MO.

5.5 Results and Discussion

Numerical 3-D simulation of an RC pier has been conducted to understand the structural response against horizontal impact loading due to a MO using ABAQUS/Explicit. A high-speed impact event is a dynamic procedure in which inertia plays a dominant role in which explicit solution method is highly recommended for such solutions. The minimum stable time increment is usually quite small. Therefore most problems require a large number of increments, so using explicit approaches can be more efficient in solution time (ABAQUS 6.14, 2013).

This study explores different responses of a bridge pier when subjected to an impact of a MO with varying mass and velocity. A parametric study has been carried out using dynamic analysis of the typical pier, in order to aid in the development and verification of the characteristics of the MO impact on the bridge pier. The velocity of the impact is varied from

1 m/s to 7 m/s with an increment of 1 m/s. The mass of the MO is taken as 0.2ton, 0.4ton, 0.6ton, 0.8ton, 1 ton, 1.2ton, 1.5ton and 2ton.

The main objective of this parametric study is to understand the influence of the mass and the velocity of a MO on the structural response and comparing the result with the selected design standard. Since water flow with the velocity of less than 7m/s has no significant lateral effect on the pier, the water flow effect is neglected, to simplify the calculation, as suggested by (Nasim et al., 2019).

The analysis shows that a higher velocity of the MO and corresponding water flow velocity can cause severe damage. The plastic behaviour of the structure under high-velocity impact could represent the structural collapse under the impact loading. For instance, the pier behaves unstable with a substantial deformation when exposed to impact at the velocities more than 6 m/s. This study ignores flow velocity of more than 6 m/s since the maximum water flow velocity could rarely reach up to 6 m/s in Australia (Standards Australian, 2017). Moreover, increased cracking and concrete crushing is found at lower velocities of the MO. In fact, higher velocities can influence the characteristics of the structure such as structural response, stiffness or stability of the structure.

An example of damage development of the simulated structures under the impact of MO with different velocities and constant mass is illustrated in Figure 5-8, where the velocity is the primary variable, and the mass of the MO is constant (1 ton). It has been recorded that high-velocity impact loading induces overall structural damage, where most of the energy is

dissipated over a very small area immediately close to the point of impact. This phenomenon is confirmed by (Cantwell and Morton, 1989).

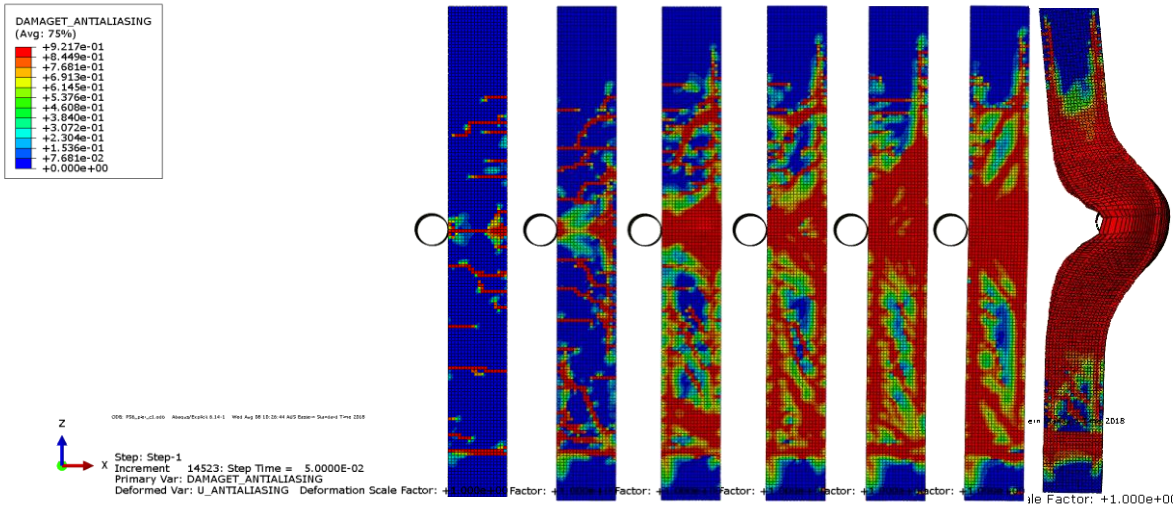

Figure 5-8: Structural response when the velocity of MO varies from 1 m/s to 7 m/s; the constant mass of the MO (1 ton)

From the crack patterns illustrated in Figure 5-8, the fixed support of the boundary condition is a critical area of damage as well as the collision surface. For lower velocities up to 3 m/s, the tensile cracks are more common while at higher velocities concrete crushing is found to be the main failure mechanism.

According to the wave theory, the velocity of wave propagation in concrete is calculating by:

$$v_{\omega} = \sqrt{\frac{E_c}{2\rho(1+\nu)}} \tag{5-6}$$

where E_c is the module of elasticity of concrete, ρ is the concrete density and ν is the poison's ratio. Therefore, the wave propagation length at the peak impact force is calculated by multiplying the velocity of the wave propagation and the time of the peak impact force as following:

$$\boldsymbol{l = v_{\omega} t_p} \tag{5-7}$$

According to this definition, the wave propagation velocity in the current study is 2663.3 m/s and t_p is approximately 0.003 second; for the model with 0.2-ton mass and the velocity of 1 m/s. therefor the wave-length propagation during maximum impact fore is ~7.9 m. This means the entire impact force will be absorbed by the supports and be reflected in impact force calculation from the supports reactions (Pham and Hao, 2016).

Impact force Figure5-9 compares the time history of the impact forces for a series of simulations resulting from the kinetic energy transferred to the structure due to the collision of a selected MO. In this scenario, the responses of the pier for different velocities of the MO with different masses are compared. The graphs show the significant effect of the velocity of the MO on the maximum impact forces transferred to the structure for constant masses. For the design of the structures, it could be suggested to consider the maximum impact force and neglect the post-peak behaviour of the impact loading on the structure. There is a notable difference in the post-peak responses between these series of curves. In higher velocities of MO (3m/s-6m/s), the difference between the maximum impact forces is not considerable.

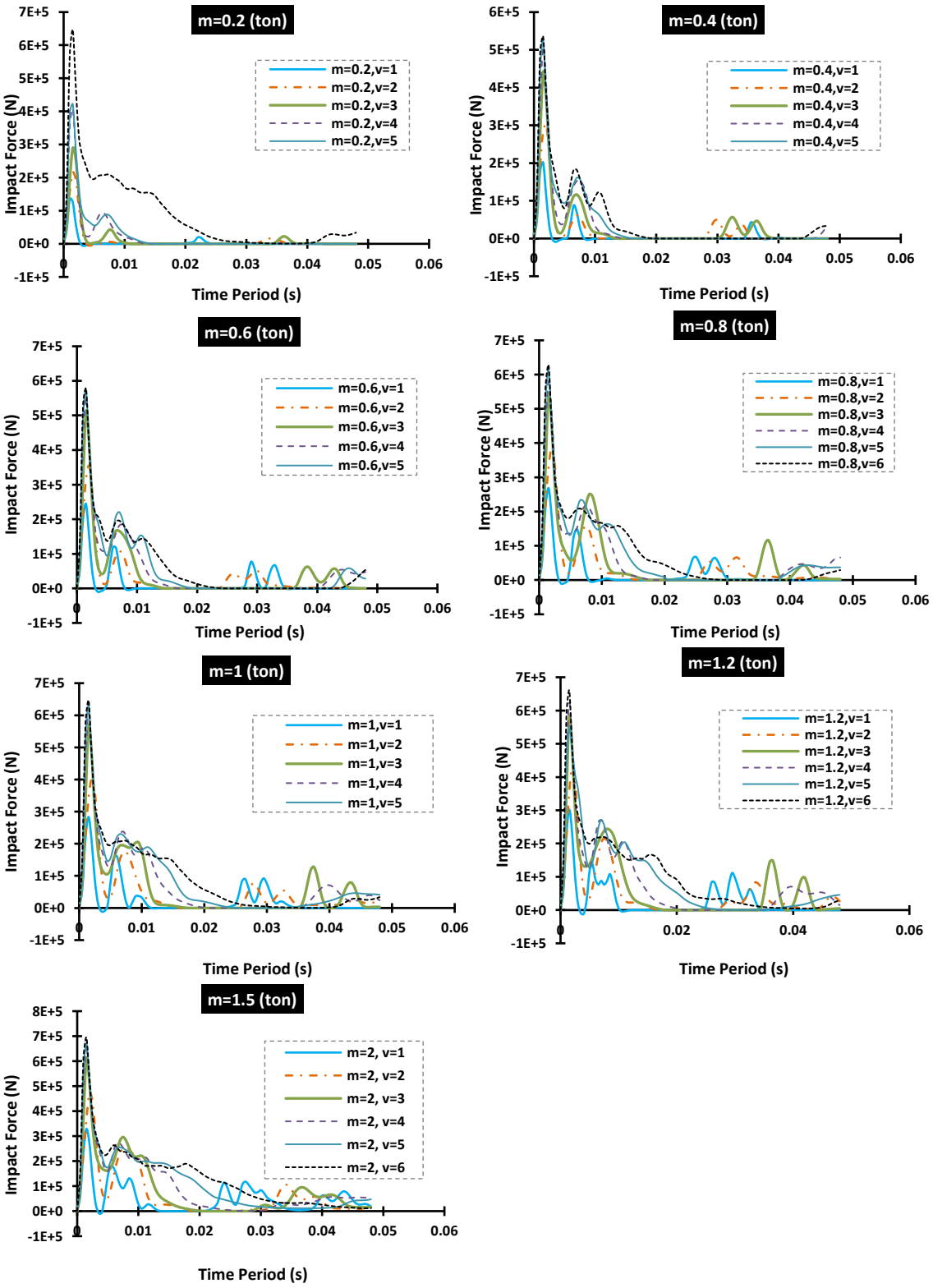

Figure 5-9: Time history of impact load resulted from the collision of the bridge pier with MO with constant masses and different velocities

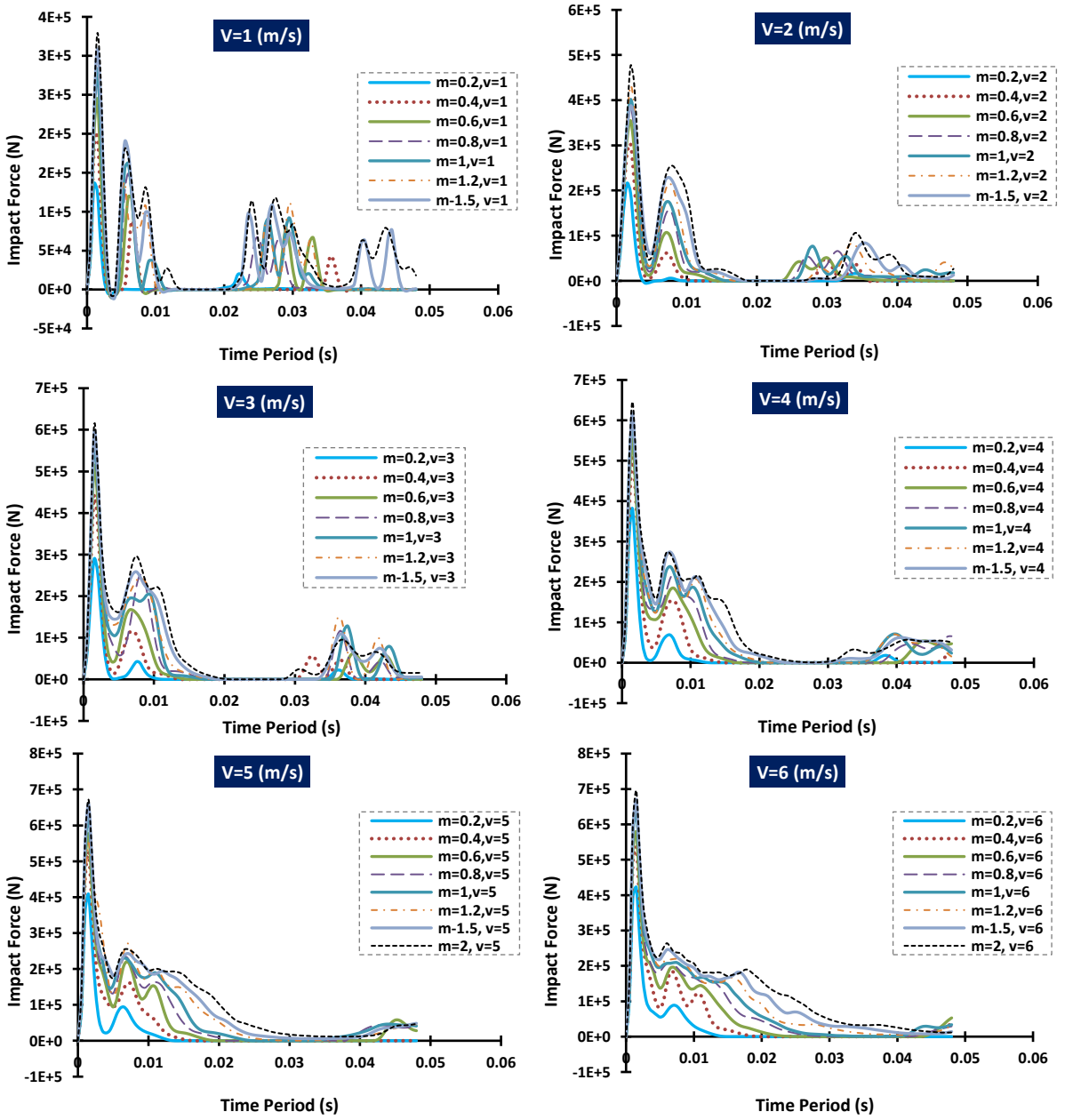

Figure 5-10: Time history of impact load resulted from the crashing of MO with bridge pier with different masses when the velocity of the MO is constant

Figure 5-10 compares the time history of impact loads for a series of simulations with constant velocity and different masses, resulted from the hitting of the MO with the bridge pier. There is a clear difference between the maximum forces when the object is more substantial, but the rate of changes is different compared to the effect of velocity. Here Figure 5-11 provides a series of curves which show the variation of the maximum impact forces. A big difference in the peak impact forces is observed when the velocity of the object or impact loading is increased to 7m/s. This means that the high velocity of impact has an entirely different reaction on the structure, and in other words, the structural stability is significantly affected when the velocity of the impact loading is increased. Although the effect of the higher velocities is severe, in a pragmatic situation, the water flow velocity of more than 5 or 6 m/s is not practical. Therefore in this study, the discussion is focused on the speeds between 1-6 m/s.

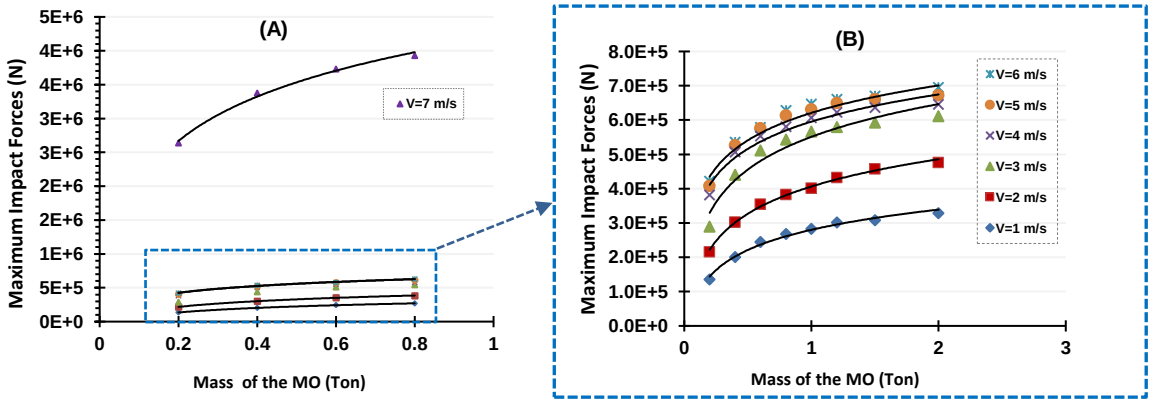

Figure 5-11: Variation of the Maximum impact forces (A) with different velocities 1-7 m/s (B) with different velocities 1 to 6 m/s

Figure 5-12 shows changes in the maximum impact forces versus the squared values of the velocity of the MO for constant masses of the MO. The pattern of increase in peak impact

force with respect to velocity for constant masses is relatively similar. Apparently, the speed of 3 m/s plays a critical role in increasing the peak impact forces in particular for the masses over 400 kg. The velocities lower than 3 m/s, the peak impact force is growing rapidly, while the rate of increase in the peak impact forces for higher speeds (>3 m/s) are slower. In other words, the increase into the resulting impact forces are divided into two scenarios of growth; with a very small increase in impact force correspondent to the velocities more than 3 m/s, the very significant changes of the velocity ranges are predicted.

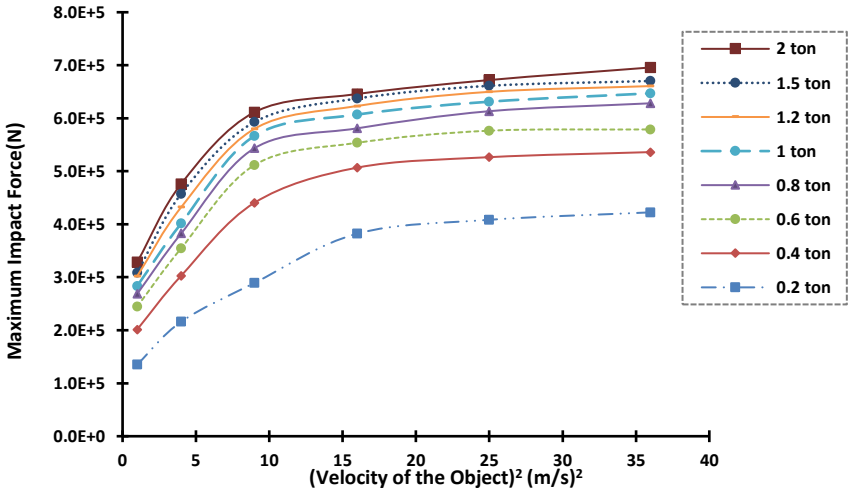

Figure 5-12: Variation of the Maximum impact forces with respect to the increase in velocity for different masses of the MO.

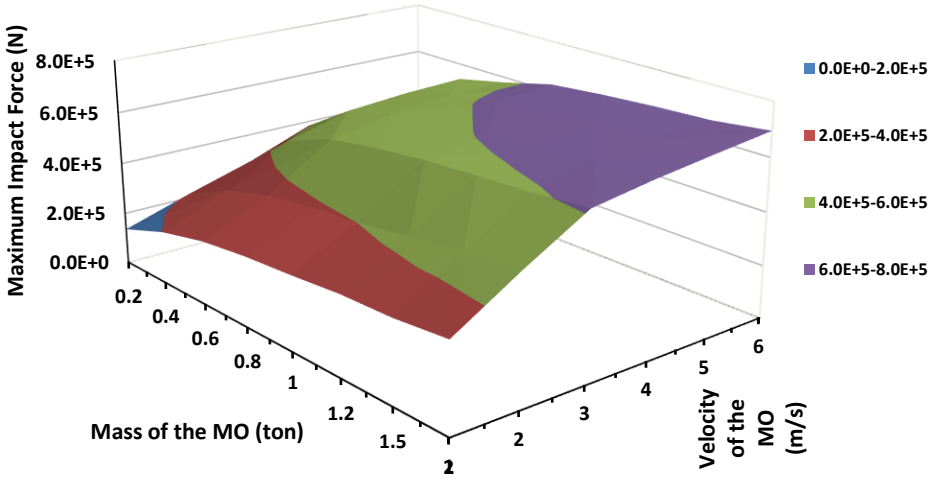

Figure 5-13: Peak Impact Force with respect to the impactor's parameter

Figure 5-13 illustrates the variation of the peak impact force with the increase in velocity and mass of the MO. From the surface presented in

Figure 5-13 5-13, it is observed that the peak values of impact force increase with two different slopes; the velocity of 3 m/s seems to be a critical velocity. The peak values are normalised with the mass and the square value of velocity to obtain a dimensionless factor of the peak impact forces (φ_{pi}) (see Figure 5-14). For higher masses and velocities the coefficient of φ_{pi} is lower which means the velocity and mass of the MO has a reverse relationship with the design impact force. Based on this investigation, it can be recommended to consider a higher coefficient for describing the impact forces when the mass and velocities are less. The peak impact force can be described by the following equation:

$$\boldsymbol{F_{ip} = \varphi_{pi} m v^2} \tag{5-8}$$

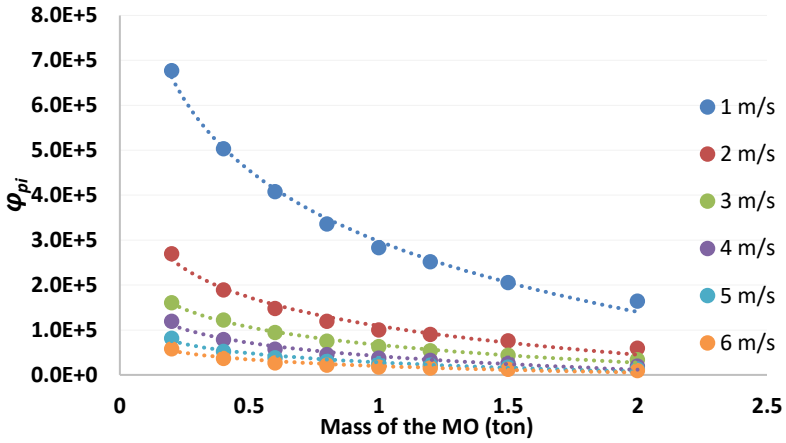

Figure 5-14: Variation of the maximum impact forces coefficient of $\boldsymbol{\varphi_{pi}}$ with increasing velocity and the mass of the MO (Note: SI system of the unit)

The analysis revealed that for constant velocity, with the increase in the values of the mass of MO the values of dimensionless factor of φ_{pi} are decreasing, and the rate of the descending is related to the speed of impact. Under these circumstances, the design load of the impact is critical for the resistance of the structure under undetermined loading. In the following section, the introduced dimensionless factor of φ_{pi} will be compared to the design considerations such as AASHTO and AS5100.

5.5.1 Comparison of the maximum impact loading with Standards

This section presents a comparison between the analytical dynamic peak impact forces and Australian standard (AS5100) and AASHTO's recommended formulas for design loads. Analysis show correlation between sets of qualitative variables from the three approaches and it reveals that the forces based on the Australian standard, AS5100, are significantly underestimated. Considering simplified assumption as a rigid body in the modelling of the MO could justify obtaining comparatively higher values for impact forces resulted from FEM

analysis than given in the AS5100 and AASHTO. Nevertheless, more research is recommended to fully understand the influences of the mass and velocity of the impactor. Figure 5-15 presents a comprehensive comparison of the peak impact forces resulted from the current study for different masses and velocities and are compared to the AS5100 and AASHTO impact load definitions. The results of the present study are close to AASHTO suggested impact load when the speed of the impact loading is increasing depending on the mass of the MO. The results also are far different from AS5100's design impact load. Despite considering the simplified assumption, it appears that AS5100 underestimates the impact forces, and it is suggested to revise the standard design considerations regarding the impact of a MO on the bridge structures.

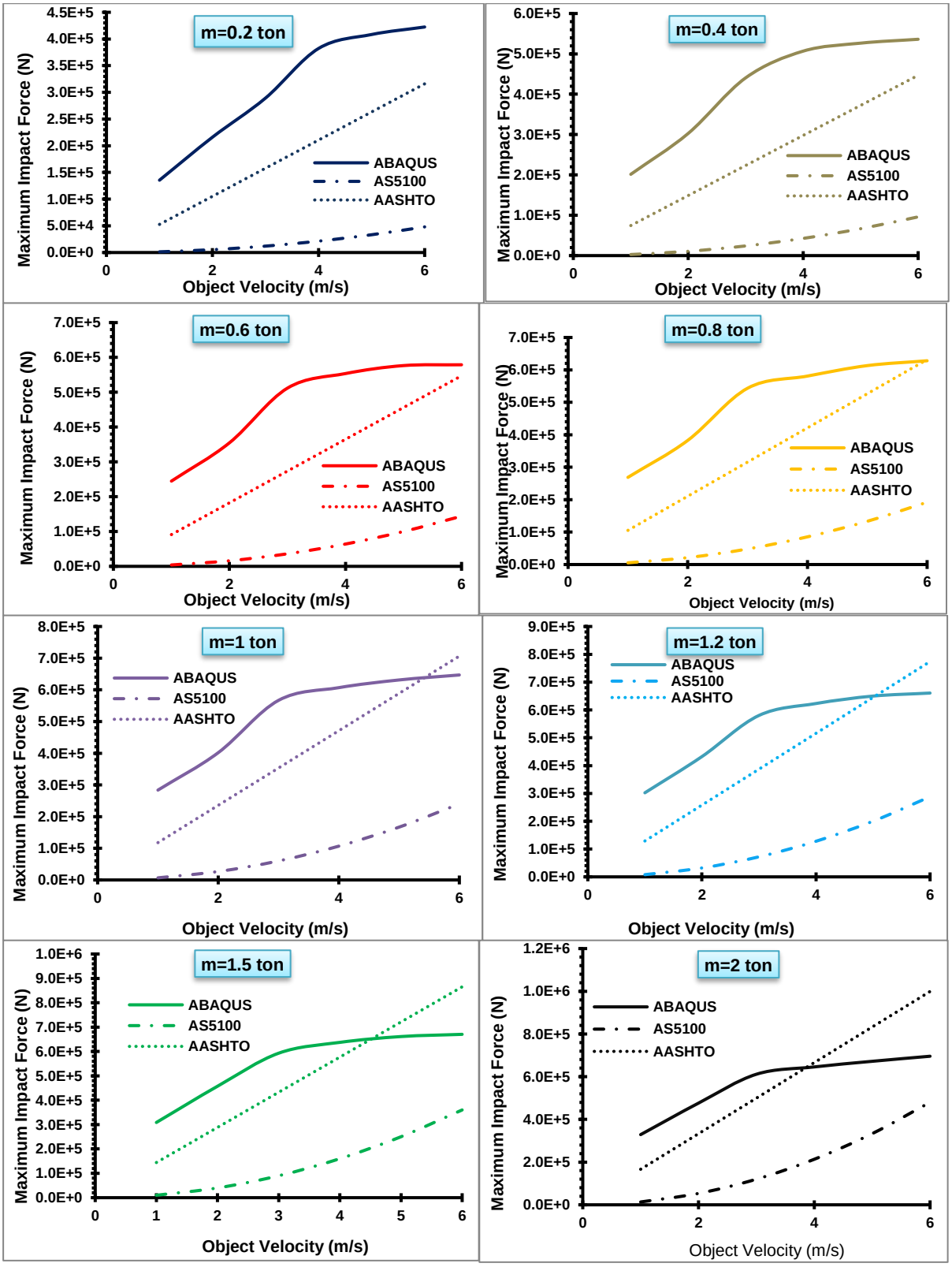

Figure 5-15: Comparing the peak impact forces resulted from the current study and the

equations provided by AS5100 and AASHTO with respect to the velocity of the MO for different weight of the object.

AASHTO-suggested impact load is closer to the numerical results ignoring the structural condition and geometry. This study can give a better understanding of the impact of design force and standard considerations. Consequently, the big difference between AS5100 and the numerical analysis and AASHTO could be addressed by defining a multiplier.

5.5.2 Dynamic Multiplier of Impact Forces

The knowledge of the impact of a MO on bridge pier is essential for the design of the bridges, and the AS5100 has given a quasi-static definition of the maximum MO loading. The dynamic effects of the MO loading have been studied in this section, which is resulted from the vertical movement of a MO followed by flooding. For this study, the dynamic multiplier of impact forces (DMIF) can be defined as the ratio of the design codes suggested impact load to the peak dynamic loads for identical parameters of mass and velocity. The DMIF's for different velocities are compiled in graphs and illustrated in Figure 5-16 and Figure 5-17.

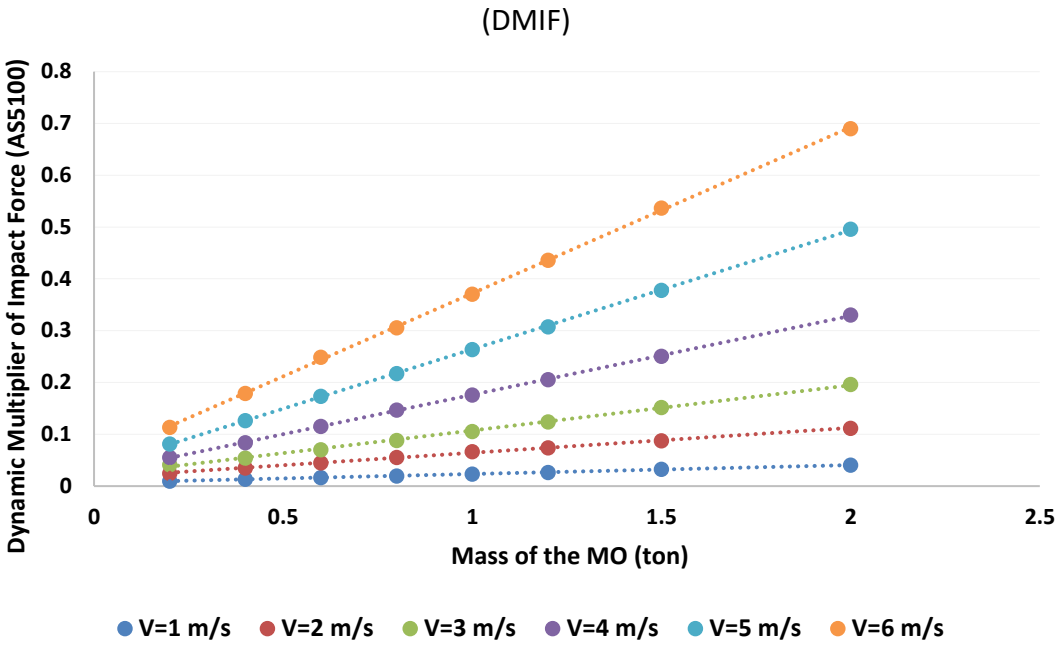

Figure 5-16: Variation of the dynamic impact factor based on the AS5100

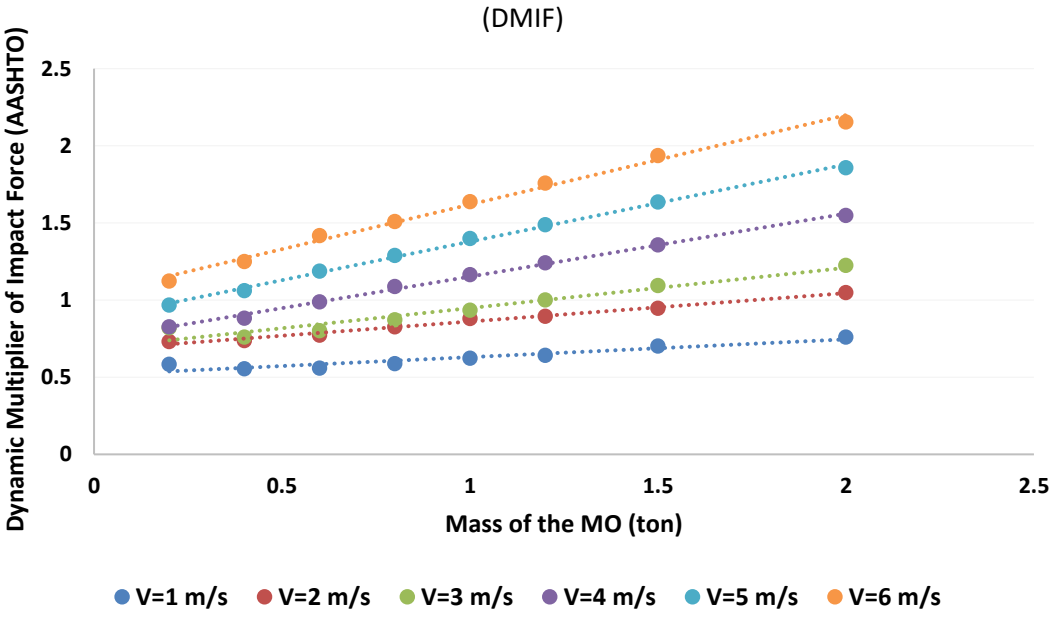

Figure 5-17: Variation of the dynamic impact factor based on the AASHTO

Figure 5-16 shows that the DMIF values with respect to the Australian code (AS5100) are under 70% of the numerically-estimated impact forces for a range of mass and velocity of the MO. DMIF values with respect to the AASHTO design loads varies from 50% to more than 200%. These factors could be helpful in considering the dynamic effects of the impact loading in bridge design procedures. Furthermore, these results provide a better understanding of the dynamic effect of an impact due to a MO for different standards considerations.

5.6 Conclusion

This chapter presented a parametric study on the mass and velocity of a MO when it collided with U-slab RC bridge pier. The pier is simulated employing ABAQUS software assuming a fixed bed boundary condition at the bottom and simply supported condition on the top. An explicit/dynamic analysis has been conducted to express the behaviour of the concrete pier when it is exposed to an impact by a MO. The modelling methodology has been validated using an experiment from literature. The focus of this study is to understand the effect of mass and velocity of a MO when collided with a concrete structure, and the result of this project is compared with the design standards of Australia (AS5100) and USA (AASHTO). From this study, the following conclusion can be drawn.

1. Higher velocities of impact, e.g. greater than 6 m/s, could affect the structural response and at higher speeds > 6m/s, the structure behaves unstable regardless of the mass of the impactor.
2. Mass and velocity of the impactor have a nonlinear relationship with the peak impact force preferred for design procedure.

3. The current study found that Australian design standards of bridge design load, AS5100, underestimates the impact force significantly.
4. AASHTO design considerations underestimate the impact load at low velocity and mass of MO, but when the velocity and the mass of the MO are high, the resulting forces are very close or more than those given by the FE analysis in this study.
5. Given DMIF for both Australian and American standards, introduced in these studies, are useful in improving design impact load.

The outcomes of the numerical study presented here demonstrate that the dynamic behaviours of the pier of bridges under floating object impact are significantly different from those used in the design standards and the changes are nonlinear.

This study is limited to a slender U-Slab bridge pier and will require further work to expand as a generic method.

CHAPTER 6

Conclusion

6 Conclusion

6.1 Introduction

This thesis presents a comprehensive research study conducted to understand the vulnerability modelling of concrete bridge piers under flood loading and impact of an object carried through flood water. Flood loading is a phenomenon which can cause damage to the failure of river-bridges. In order to predict the structural damage during a flood disaster, it is essential to model the behaviour of a bridge via numerical simulation or experimental validation. This study is categorised into different steps, to a better understanding of the structural behaviour. Hence, this chapter presents a summary of the conclusions of the thesis.

6.2 An investigation of water-flow pressure distribution on bridge piers under flood loading

Resistance to flooding and debris loading are critical parameters affecting the design of bridges under flood loading. Basically, bridges are the most vulnerable elements of the road infrastructure and a good understanding of their behaviours in complex scenarios will enable mitigation of potential failure. This study investigates the pressure distribution for two piers types using CFD analysis. For the sake of fair comparison, the area of the cross-section of these two piers is the same while they are shaped in a rectangular and a circle, respectively. Though the cross-section of the piers under investigation is different (one rectangular one circle), with the same diameter were exposed to simulated water flow. To eliminate the water flow behaviour on the structure, ignoring the structural response, computational analysis of water flows around a pier was conducted assuming the pier to be a bluff structure, reported here as a non-structured

model. Therefore, in this study, the pier's walls were assumed to be non-slip boundary walls located in the water flow domain. Different water flow velocities were examined to determine how they can affect the pier surface exposed to the water flow, using the ANSYS FLUENT software package. The calculation of water flow pressure on bridge piers in various codes for the determination of water flow pressure distribution is very similar (Wang et al., 2015). Therefore, in this thesis, the Australian Standard (AS 5100) was selected for investigation in comparison with the computational method. Based on a comparative analysis, the principal results can be summarised as follows:

1. Numerous CFD analysis confirms that the pressure distributions on a bridge pier are uniform in both rectangular and circular piers with very slight changes at both top and bottom of piers exposed to water flow.
2. CFD analysis demonstrates that the pressure on a circular pier is under-estimated by AS5100 equation when comparing total equivalent pressures with the equation provided by AS 5100, at velocities less than 5 m/s.
3. The water flow variations during velocity growth reveal that for a rectangular pier, the AS 5100 equation is very conservative.
4. The possible total pressure on a rectangular pier is close to that predicted using AS5100 method or other codes, especially for higher velocities.
5. Positive pressure on both piers using AS 5100 is under-estimated at lower velocities in comparison with the present computational method when applied in bridge design.

It is observed that the effect of total pressure distributed on the pier is essential in design for structural stability, whereas the positive pressure needs to be considered in the design for

localised damage. Further studies of the effect of drag and viscosity on flood forces on bridge piers at high-velocity water flows are recommended.

6.3 Damage Estimation for the Reinforced-Concrete Model under Uniform Pressure Loading; a comparison on the deflection and energy-based approaches

This part of the study presents a review of DIs presented in the literature that there are many different definitions for structural damage indices of structural elements. A feasible method for calculating concrete structural damage under increasing static loading using ABAQUS is presented using CDP modelling, and the validation of the system leads the problem to compare different damage evaluation approaches. This section proposed a new energy-based approach which can be used for evaluation of the damage of vertical structure such as bridge piers under lateral, flood, loading which monotonically increasing consequent pressure from velocity.

A deflection-based approach and the new energy-based approach have been compared using a case study of a bridge pier. Following conclusions can be drawn from the work presented in the current section.

1. Both the deflection-based DI calculation and the energy-based approaches show similar outcomes for moderate damage.
2. The dissipated energy-based DI is more appropriate for estimating damage of complex structures with more degrees of freedom.

3. The deflection concept could not consider the rotational damages of the fixed boundary condition, while overall damage dissipation energy can address the damage of the whole system.
4. The energy-based approach provides a superior method since it is simply applicable for a structural system using finite element analysis results.
5. Structural geometry and degree of indeterminacy have a major impact on the damage observed and calculated.

6.4 Effect of the Mass of a Free-Dropped-Hammer on Dynamic Response of a Reinforced Concrete Beam

In order to understand the effect of object impact on bridge piers under flood, numerical simulation of an RC beam subjected to the impact of free-drop of a hammer has been carried out using ABAQUS. The model has been exposed to different impact forces resulting from different masses of the hammer. Various aspects of structural response are derived and discussed. The results are analysed and integrated to formulate the influence of the mass of the impactor on the structural damage. Based on the results discussed in this paper, the following conclusions are drawn:

1- Damage modes of a reinforced concrete flexural member have a direct relationship with the mass of hammers. Crack pattern changes with the mass of the hammer.
2- The impact force has a non-linear relationship with the mass of the hammer
3- Mass of the hammer has a linear relationship with total energy with the coefficient of 3E+06 considering SI (mm) system of units.

4- The rate of reduction of the kinetic energies appears to be very similar for different masses of the hammer.
5- The rate of increase of the total damage dissipated energy reduces with the increase in the mass of the hammer.
6- Surface damage caused by the hammer's drop shows a bounce back at low masses of the hammer.
7- The structural member's height changes are calculated based on the changes on the top and bottom surfaces of the element. Results indicate the crushing of concrete with heavier loads and cracking at lighter loads.
8- The correlation between our simulation and experiments from literature validates the accuracy of the FE models utilised to formulate the maximum impact forces

It is noteworthy that the impact response of reinforced concrete beams is a complex issue due to the nonlinearity of the reinforced concrete system itself and the loading conditions. Therefore, additional experimental investigations are still needed for a broad understanding of the dynamic behaviour of reinforced concrete structures. For this purpose, a wider range of hammer mass can be explored as well as different shape and size analysis of the hammer. For example, the influence of the shape of the contacted surface of the hammer is not considered, and in formulating the maximum impact force, it is notable. These issues are considered to calculate the maximum impact force in future work.

6.5 Log Impact Forces on a U-Slab Bridge Pier: A Parametric Study on Nonlinear/Dynamic Response of a Bridge Pier Exposed to an Object Impact

This section presented a parametric study on the mass and velocity of the moving object when it collided to a case study U-slab bridge pier. The pier is a reinforced concrete structure with a fixed bed boundary condition which implies a stiff bed or enough embedded support. An explicit/dynamic analysis has been carried out to express the behaviour of the concrete pier when it is exposed to the log or any moving object impact. The modelling methodology has been validated with an experiment from literature. The main focus of this study is to understand the effect of mass and velocity of a floated MO when collided to a concrete structure.

The result of this part of the thesis is compared with the recommended equation from designing standards of Australia (AS5100) and USA (AASHTO). From this study, the following results can be drawn.

1. At high velocities of impact, e.g. greater than 6 m/s, a ductile behaviour is observed even when the mass of the impactor is low.
2. Combination of the effect of mass and velocity parameters of the MO has been represented by a driven surface function of maximum impact forces resulting from the impact on the structure.
3. Comparing the maximum impact forces resulting from the current study with AS5100 design loads shows that the impact force can be underestimated by the standard even for the higher masses of MO.

4. AASHTO design considerations still underestimate the force, but when the velocity and the mass of the MO are high, the resulting forces predicted are very close to those of the current study.
5. The coefficient introduced in Could be useful to use as a correlated coefficient of designing loads introduced by AS5100.
6. Given DMIF for both Australian and American standards, introduced in these studies, are useful in improving design impact load.

The findings in this thesis reveal that the dynamic analysis of the impact loading is different from the standards considerations. In the present study, the effect of the shape of the impactor or MO, and even the structural geometry has not been taking into account. Therefore, it is recommended to study more in this area. Moreover, the formula should be amended in accordance with future studies on the effect of collided objects.

6.6 The significance of the Findings of the Research Reported in the Thesis

1. The fluid pressure applied on bridge piers under flood loading can be assumed as a uniformly distributed load over the depth of inundation.
2. The shape of the cross-section of the bridge piers impact on the load applied on the piers under flood loading. The pressure on a circular pier can be higher than that predicted using the equations gives in the standard.
3. The energy-based damage index proposed provides a simpler approach for predicting damage of bridge piers under flood loading.
4. Flood velocities less than 10 m/s will not cause significant damage to bridge piers.

5. Impact of floating objects can impose significant damage on concrete bridge piers under flood loading.
6. Even at very low velocities of 1 m/s, a floating object of 1-tonne mass can cause significant damage to the bridge piers.

6.7 Recommendation for Future Works

The future works recommended are listed as below:

1. Further studies of the effect of drag and viscosity on flood forces on bridge piers at high-velocity water flows are recommended
2. A broader range of hammer mass can be explored as well as the impact of different shapes and sizes and additional experimental investigations are still needed to understand the dynamic behaviour of reinforced concrete structures.
3. The effect of non solid object impact on the bridge pier can be recomanded to be investigated for more realistic impact effect.
4. Probability based investigation on impact formulation is recomanded as a viable option for bridge assessment considerations, to estimate the reliability of the structures.

REFERENCES

7 References

AASHTO. (2002). Standard Specifications, *for Highway Bridges*. American Association of State Highway and Transportation Officials: 444 North Capitol Street, N.W., Suite 249, Washington, D.C. 20001.

ABAQUS 6.14, 2013. Analysis User's Guide, Theory Manuals, *Volume 2: Analysis.* Providence, RI, USA: Systèmes, Dassault.

Abrate, S. (2001). Modeling of impacts on composite structures. *Composite Structures*, *51*(2), 129-138. doi:https://doi.org/10.1016/S0263-8223(00)00138-0

Aghaee, Y., & Hakimzadeh, H. (2010). Three dimensional numerical modeling of flow around bridge piers using LES and RANS. *River Flow, Dittrich, Koll, Aberle & Geisenhainer (eds).-2010.-P*, 211-218.

Almasri, A., & Moqbel, S. (2017). Numerical Evaluation of AASHTO Drag Force Coefficients of Water Flow Around Bridge Piers. *Journal of Engineering Materials and Technology*, *139*(2), 021001-021001-021008. doi:10.1115/1.4035253

Alsina, C., Guadarrama, S., Renedo, E., & Trillas, E. (2017). Numerical simulation of RC frame testing with damaged plasticity model. Comparison with simplified models. *Engineering Structures*, *132*, 70-86.

Andreaus, U., Placidi, L., & Rega, G. (2010). Numerical simulation of the soft contact dynamics of an impacting bilinear oscillator. *Communications in Nonlinear Science and Numerical Simulation*, *15*(9), 2603-2616.

Andreaus, U., Placidi, L., & Rega, G. (2011). Soft impact dynamics of a cantilever beam: equivalent SDOF model versus infinite-dimensional system. *Proceedings of the Institution of Mechanical Engineers, Part C: Journal of Mechanical Engineering Science*, *225*(10), 2444-2456.

Apelt, C. J., & Issac, L. (1968). BRIDGE PIERS--HYDRODYNAMIC FORCE COEFFICIENTS. *Journal of the Hydraulics Division*.

Arnold, P., Bea, R., Idriss, I., Reimer, R., Beebe, K., & Marshall, P. (1977). *A study of soil-pile-structure systems in severe earthquakes.* Paper presented at the Offshore Technology Conference.

ASCE. (1994). Minimum Design Loads for Buildings and other Structures *Standards ASCE/SEI 7-10* (Vol. 7): American Society of Civil Engineers.

Ataei, N., & Padgett, J. E. (2015). Influential fluid–structure interaction modelling parameters on the response of bridges vulnerable to coastal storms. *Structure and Infrastructure Engineering, 11*(3), 321-333. doi:10.1080/15732479.2013.879602

Bangash, M. (2001). *Manual of numerical methods in concrete: Modelling and applications validated by experimental and site-monitoring data*: Thomas Telford.

Banon, Irvine, Max, H., Biggs, & M, J. (1981). Seismic damage in reinforced concrete frames. *Journal of the Structural Division, 107*(9), 1713-1729.

Banon, H., & Veneziano, D. (1982). Seismic safety of reinforced concrete members and structures. *Earthquake engineering & structural dynamics, 10*(2), 179-193.

Banthia, N., Mindess, S., & Bentur, A. (1989). Energy balance in instrumented impact tests on plain concrete beams *Fracture of concrete and rock* (pp. 26-36): Springer.

Banthia, N., Mindess, S., Bentur, A., & Pigeon, M. (1989). Impact testing of concrete using a drop-weight impact machine. *Experimental Mechanics, 29*(1), 63-69.

Bazant, Z. P. & Cedolin, L. (1979). Blunt crack band propagation in finite element analysis. *ASCE J Eng Mech Div, 105*(2), 297-315.

Beheshti, A., & Ataie-Ashtiani, B. (2009). Experimental study of three-dimensional flow field around a complex bridge pier. *Journal of Engineering Mechanics, 136*(2), 143-154.

BITRE. (2001b). *Australian Bureau of Statistics (ABS), Summary of Industry Performance,*

Small and Medium Businesses, Retrieved from Cat., Canberra.:

BS. (2005). EN 1991-1-6 *Eurocode 1. Actions on structures. General actions. Actions during execution*. BA 59/94

Burnett, D. S. (1987). *Finite element analysis:: from concepts to applications*.

Cai, C., Shi, X., Araujo, M., & Chen, S. (2007). Effect of approach span condition on vehicle-induced dynamic response of slab-on-girder road bridges. *Engineering Structures, 29*(12), 3210-3226.

Calomino, F., Tafarojnoruz, A., De Marchis, M., Gaudio, R., & Napoli, E. (2015). Experimental and numerical study on the flow field and friction factor in a pressurized corrugated pipe. *Journal of Hydraulic Engineering, 141*(11), 04015027.

Cao, M., Liu, Z., & Meng, J. (2009). Statistical analysis and reflections on bridge deficiencies and disasters in the United States. *Highway, 7*(7), 162-167.

Cao, Van, V., Ronagh, H., Ashraf, M., & Baji, H. (2011). A new damage index for reinforced concrete structures subjected to seismic loads. *structure, 1*(1), 1.

Cao, V. V., Ronagh, H. R., Ashraf, M., & Baji, H. (2014). A new damage index for reinforced concrete structures. *Earthquake and Structures, 6*(6), 581-609.

Carpinteri, A., Chiaia, B., & Cornetti, P. (2004). A mesoscopic theory of damage and fracture in heterogeneous materials. *Theoretical and Applied Fracture Mechanics, 41*(1-3), 43-50.

Catalano, P., Wang, M., Iaccarino, G., & Moin, P. (2003). Numerical simulation of the flow around a circular cylinder at high Reynolds numbers. *International Journal of Heat and Fluid Flow, 24*(4), 463-469.

Cazzani, A., Mongiovı, L., & Frenez, T. (2002). Dynamic finite element analysis of interceptive devices for falling rocks. *International Journal of Rock Mechanics and Mining Sciences, 39*(3), 303-321.

Chen, C., Liu, H., & Beardsley, R. C. (2003). An unstructured grid, finite-volume, three-dimensional, primitive equations ocean model: application to coastal ocean and estuaries. *Journal of atmospheric and oceanic technology, 20*(1), 159-186.

Chen, S., & Wu, J. (2009). Dynamic performance simulation of long-span bridge under combined loads of stochastic traffic and wind. *Journal of Bridge Engineering, 15*(3), 219-230.

Chiaia, B., Kumpyak, O., Placidi, L., & Maksimov, V. (2015). Experimental analysis and modeling of two-way reinforced concrete slabs over different kinds of yielding supports under short-term dynamic loading. *Engineering Structures, 96*, 88-99.

Chopra, A. K. a. (2017). *Dynamics of structures: theory and applications to earthquake engineering* (Fifth edition. ed.). Hoboken, NJ: Pearson.

Chung, C. H., Lee, J., & Gil, J. H. (2014). Structural performance evaluation of a precast prefabricated bridge column under vehicle impact loading. *Structure and Infrastructure Engineering, 10*(6), 777-791.

CONSOLAZIO, G. R., COOK, R. A., MCVAY, M. C., COWAN, D., BIGGS, A. & BUI, L. 2006. *Barge impact testing of the St. George Island causeway bridge*, Department of Civil and Coastal Engineering, University of Florida.

Coulbourne, W. L. (2011). *ASCE 7-10 Changes to Flood Load Provisions.* Paper presented at the Structures Congress 2011.

Deloitte Access Economics, (2017). Building resilience to natural disasters in our states and territories. Retrieved from Sydney:

Deng, L., & Cai, C. (2009). Identification of parameters of vehicles moving on bridges. *Engineering Structures, 31*(10), 2474-2485.

Deng, L., & Cai, C. (2010). Development of dynamic impact factor for performance evaluation of existing multi-girder concrete bridges. *Engineering Structures, 32*(1), 21-31.

Doebling, S. W., Farrar, C. R., Prime, M. B., & Shevitz, D. W. (1996). *Damage identification and health monitoring of structural and mechanical systems from changes in their vibration characteristics: a literature review*. Retrieved from

Dong, Y., & Frangopol, D. M. (2015). Probabilistic ship collision risk and sustainability assessment considering risk attitudes. *Structural Safety, 53*, 75-84.

Ebrahimi, M., Kripakaran, P., Djordjevic, S., Tabor, G., Kahraman, R., Prodanović, D., & Arthur, S. (2016). Hydrodynamic Effects of Debris Blockage and Scour on Masonry Bridges: Towards Experimental Modelling.

Edalat-Behbahani, A., Barros, J. A. O., & Ventura-Gouveia, A. (2017). Three dimensional plastic-damage multidirectional fixed smeared crack approach for modelling concrete structures. *International Journal of Solids and Structures, 115-116*, 104-125. doi:https://doi.org/10.1016/j.ijsolstr.2017.03.006

Einstein, H. A., & El-Samni, E.-S. A. (1949). Hydrodynamic forces on a rough wall. *Reviews of modern physics, 21*(3), 520.

El-Tawil, S., Severino, E., & Fonseca, P. (2005). Vehicle collision with bridge piers. *Journal of Bridge Engineering, 10*(3), 345-353.

Farrar, C. R., & Jauregui, D. A. (1998). Comparative study of damage identification algorithms applied to a bridge: I. Experiment. *Smart materials and structures, 7*(5), 704.

Farrar, C. R., & Worden, K. (2007). An introduction to structural health monitoring. *Philosophical Transactions of the Royal Society A: Mathematical, Physical and Engineering Sciences, 365*(1851), 303-315. doi:10.1098/rsta.2006.1928

FEMA. (June 2014). Homeowner's Guide to Retrofitting Six Ways to Protect Your Home From Flooding *Federal Emergency Management Agency*, (Vol. 3rd Edition). Washington, D.C.: P-312.

Ferraro, D., Tafarojnoruz, A., Gaudio, R., & Cardoso, A. H. (2013). Effects of pile cap thickness on the maximum scour depth at a complex pier. *Journal of Hydraulic Engineering, 139*(5), 482-491.

Fletcher, C. A. (1984). Computational galerkin methods *Computational Galerkin Methods* (pp. 72-85): Springer.

FLUENT. (2009). *ANSYS FLUENT 12.0 User's Guide*.

Fujikake, K., Li, B., & Soeun, S. (2009). Impact response of reinforced concrete beam and its analytical evaluation. *Journal of Structural Engineering, 135*(8), 938-950.

Gao, X.-K., & Zhu, X. (2006). Hydrodynamic effect on seismic response of bridge pier in deep water. *Beijing Jiaotong Daxue Xuebao(Journal of Beijing Jiaotong University), 30*(1), 55-58.

Gaudio, R., Tafarojnoruz, A., & Calomino, F. (2012). Combined flow-altering countermeasures against bridge pier scour. *Journal of Hydraulic Research, 50*(1), 35-43.

CANTWELL, W. J. & MORTON, J., 1989. Comparison of the low and high-velocity impact response of CFRP.*Composites*, 20**,** 545-551.

GETTER, D. J., CONSOLAZIO, G. R. & DAVIDSON, M. T., 2011. Equivalent static analysis method for barge impact-resistant bridge design. *Journal of Bridge Engineering*, 16**,** 718-727.

Ghobarah, A., Abou-Elfath, H., & Biddah, A. (1999). Response-based damage assessment of structures. *Earthquake engineering & structural dynamics, 28*(1), 79-104.

Ghodsi, H., & Beheshti, A. A. (2018). Evaluation of Harmony Search Optimization to Predict Local Scour Depth around Complex Bridge Piers. *Civil Engineering Journal, 4*(2), 402-412.

Gholipour, G., Zhang, C., & Li, M. (2018). Effects of soil–pile interaction on the response of bridge pier to barge collision using energy distribution method. *Structure and Infrastructure Engineering*, 1-15.

Gluver, H. (2017). *Ship Collision Analysis: Proceedings of the international symposium on advances in ship collision analysis, Copenhagen, Denmark, 10-13 May 1998*: Routledge.

Goldsmith, W. (1960). Impact: The Physical Theory and Behaviour of Colliding Solids. *London: Edward Arnold Ltd*.

Green, M., & Cebon, D. (1997). Dynamic interaction between heavy vehicles and highway bridges. *Computers & Structures, 62*(2), 253-264.

Haehnel, R. B., & Daly, S. F. (2004). Maximum impact force of woody debris on floodplain structures. *Journal of Hydraulic Engineering, 130*(2), 112-120.

Hamad, W., Owen, J., & Hussein, M. (2015). Modelling the degradation of vibration characteristics of reinforced concrete beams due to flexural damage. *Structural Control and Health Monitoring, 22*(6), 939-967.

Hamad, W. I., Owen, J. S., & Hussein, M. F. M. (2011). A flexural crack model for damage detection in reinforced concrete structures. *Journal of Physics: Conference Series, 305*(1), 012037. Retrieved from http://stacks.iop.org/1742-6596/305/i=1/a=012037

Hamed, A., Vega, J., Liu, B., & Chamorro, L. (2017). Flow around a semicircular cylinder with passive flow control mechanisms. *Experiments in Fluids, 58*(3), 22.

Hanif, M. U., Ibrahim, Z., Jameel, M., Ghaedi, K., & Aslam, M. (2016). A new approach to estimate damage in concrete beams using non-linearity. *Construction and Building Materials, 124*, 1081-1089. doi:http://dx.doi.org/10.1016/j.conbuildmat.2016.08.139

Hao, H., Hao, Y., Li, J., & Chen, W. (2016). Review of the current practices in blast-resistant analysis and design of concrete structures. *Advances in Structural Engineering, 19*(8), 1193-1223.

Hao, Y., & Hao, H. (2014). Influence of the concrete DIF model on the numerical predictions of RC wall responses to blast loadings. *Engineering Structures, 73*, 24-38. doi:https://doi.org/10.1016/j.engstruct.2014.04.042

Hillerborg, A., Modéer, M., & Petersson, P.-E. (1976). Analysis of crack formation and crack growth in concrete by means of fracture mechanics and finite elements. *Cement and concrete research, 6*(6), 773-781.

Hirt, C., Amsden, A. A., & Cook, J. (1974). An arbitrary Lagrangian-Eulerian computing method for all flow speeds. *Journal of Computational Physics, 14*(3), 227-253.

Hognestad, E. (1951). *Study of combined bending and axial load in reinforced concrete members*. Retrieved from

Hung, C.-C., & Yau, W.-G. (2014). Behavior of scoured bridge piers subjected to flood-induced loads. *Engineering Structures, 80*, 241-250. DOI:10.1016/j.engstruct.2014.09.009

Hung, T., & Wang, M. (1987). Nonlinear Hydrodynamic Pressure on Rigid Dam Motion. *Journal of Engineering Mechanics, 113*(4), 482-499. DOI:10.1061/(ASCE)0733-9399(1987)113:4(482)

Ioannides, A. M., Peng, J., & Swindler Jr, J. R. (2006). ABAQUS model for PCC slab cracking. *International Journal of Pavement Engineering, 7*(4), 311-321.

Iqbal, M. A., Kumar, V., & Mittal, A. K. (2019). Experimental and numerical studies on the drop impact resistance of prestressed concrete plates. *International Journal of Impact Engineering, 123*, 98-117. doi:https://doi.org/10.1016/j.ijimpeng.2018.09.013

Jempson, M. (2000). *Flood and debris loads on bridges.* (PhD), University of Queensland.

Jin, L., Zhang, R., Dou, G., Xu, J., & Du, X. (2017). Experimental and numerical study of reinforced concrete beams with steel fibers subjected to impact loading. *International Journal of Damage Mechanics, 27*(7), 1058-1083. DOI:10.1177/1056789517721616

Jin, L., Zhang, R., Dou, G., Xu, J., & Du, X. (2018). Experimental and numerical study of reinforced concrete beams with steel fibers subjected to impact loading. *International Journal of Damage Mechanics, 27*(7), 1058-1083. DOI:10.1177/1056789517721616

Jirasek, M. (1993). *Modeling of fracture and damage in quasi-brittle materials.* Northwestern University, Chicago, IL (United States).

Jordan, B. (2015). Analysis of bridges subjected to flood loadings based on different design standards.

Kalendher, F. (2017). *Synthetic damage curves for concrete girder bridge decks under flood hazard.* (PhD degree), RMIT University, Melbourne.

Kalla, P., Misra, A., Gupta, R. C., Csetenyi, L., Gahlot, V., & Arora, A. (2013). Mechanical and durability studies on concrete containing wollastonite–fly ash combination. *Construction and Building Materials, 40*, 1142-1150.

Kalla, P., Rana, A., Chad, Y. B., Misra, A., & Csetenyi, L. (2015). Durability studies on concrete containing wollastonite. *Journal of Cleaner Production, 87*, 726-734.

Kerenyi, K., Sofu, T., & Guo, J. (2009). *Hydrodynamic forces on inundated bridge decks*. Retrieved from

Kezmane, A., Chiaia, B., Kumpyak, O., Maksimov, V., & Placidi, L. (2017). 3D modelling of reinforced concrete slab with yielding supports subject to impact load. *European Journal of Environmental and Civil Engineering, 21*(7-8), 988-1025. DOI:10.1080/19648189.2016.1194330

Khan, M. A. (2014). *Accelerated Bridge Construction: Best Practices and Techniques*: Elsevier.

Kishi, N., Ikeda, K., Mikami, H., & Yamaguchi, E. (2001). *Dynamic behavior of RC beams under steel weight impact loading. Effects of nose-shape of steel weight.* Paper presented at the CONSEC'01: Third International Conference on Concrete Under Severe Conditions.

Kishi, N., & Mikami, H. (2012). Empirical formulas for designing reinforced concrete beams under impact loading. *ACI Structural Journal, 109(4), 509-519.*

Kishi, N., Mikami, H., Matsuoka, K., & Ando, T. (2002). Impact behavior of shear-failure-type RC beams without shear rebar. *International Journal of Impact Engineering, 27*(9), 955-968. Retrieved from https://ac.els-cdn.com/S0734743X0100149X/1-s2.0-S0734743X0100149X-main.pdf?_tid=59b80b6f-c422-4ef2-af03-62b13ad0c805&acdnat=1542584012_bccfe32707758f7605f02aac7b85879d

Kmiecik, P., & KamiŃSki, M. (2011). Modelling of reinforced concrete structures and composite structures with concrete strength degradation taken into consideration. *Archives of civil and mechanical engineering, 11*(3), 623-636. doi:https://doi.org/10.1016/S1644-9665(12)60105-8

Kocaman, S., Seckin, G., & Erduran, K. S. (2010). 3D model for prediction of flow profiles around bridges. *Journal of Hydraulic Research, 48*(4), 521-525. DOI:10.1080/00221686.2010.507340

Kocatürk, T., & Şimşek, M. (2006). Vibration of viscoelastic beams subjected to an eccentric compressive force and a concentrated moving harmonic force. *Journal of Sound and Vibration, 291*(1-2), 302-322.

Kok, J., Boerstoel, J., Kassies, A., & Spekreijse, S. (1996). *A robust multi-block Navier-Stokes flow solver for industrial applications.* Paper presented at the ECCOMAS computational fluid dynamics conference.

Kok, J. C., & Spekreijse, S. P. (2000). *Efficient and accurate implementation of the k-omega turbulence model in the NLR multi-block Navier-Stokes system*: Nationaal Lucht-en Ruimtevaartlaboratorium.

Kulkarni, S. M., & Shah, S. P. (1998). Response of reinforced concrete beams at high strain rates. *Structural Journal, 95*(6), 705-715.

Kumpyak, O., Galiautdinov, Z., & Kokorin, D. (2013). Experimental and theoretical studies of reinforced concrete beams on yielding supports along the oblique sections under seismic and other dynamic loading. *Seismic Construction, Safety of Structures*, 40-45.

Kuroda, M., Tamura, T., & Suzuki, M. (2007). Applicability of LES to the turbulent wake of a rectangular cylinder—Comparison with PIV data. *Journal of Wind Engineering and Industrial Aerodynamics, 95*(9), 1242-1258.

Lebbe, M. F. K., Lokuge, W., Setunge, S., & Zhang, K. (2014). *Failure mechanisms of bridge infrastructure in an extreme flood event.* Paper presented at the Proceedings of the 1st International Conference on Infrastructure Failures and Consequences (ICFC 2014).

Lee, G. C., & Sternberg, E. (2008). A new system for preventing bridge collapses — i*ssues in Science and Technology, 24*(3), 31.

Li, F., Chen, G., & Wang, Z. (2008). Seismic responses of single-column pier considering the effects of hydrodynamic pressure. *Journal of Earthquake Engineering and Engineering Vibration, 28*(2), 114-121.

Li, Y.-c. (1990). *Wave action on maritime structures*: Dalian University of Technology.

LIU, X.-m., XIONG, L., LIU, J.-h., & ZHAO, M.-h. (2011). Slacking mechanism of red sandstone based on energy dissipation principle. *Journal of Central South University (Science and Technology), 10*, 043.

Low, K. H., Yang, A., Hoon, K. H., Zhang, X., Lim, J. K. T., & Lim, K. L. (2001). Initial study on the drop-impact behavior of mini Hi-Fi audio products. *Advances in Engineering Software, 32*(9), 683-693. doi:https://doi.org/10.1016/S0965-9978(01)00024-2

Lubliner, J., Oliver, J., Oller, S., & Onate, E. (1989). A plastic-damage model for concrete. *International Journal of Solids and Structures, 25*(3), 299-326.

Malizia, F., Montazeri, H., Hespel, P., & Blocken, B. (2016). Numerical simulation of flow around a circular cylinder: comparison of LES and URANS turbulence models.

Manual, H. F. (2010). US Department of Transportation. *Federal Highway Administration Office of Highway Policy Information*.

Massumi, A., & Moshtagh, E. (2013). A new damage index for RC buildings based on variations of nonlinear fundamental period. *The Structural Design of Tall and Special Buildings, 22*(1), 50-61.

Mattiussi, C. (1997). An Analysis of Finite Volume, Finite Element, and Finite Difference Methods Using Some Concepts from Algebraic Topology. *Journal of Computational Physics, 133*(2), 289-309. doi:http://dx.doi.org/10.1006/jcph.1997.5656

Mattiussi, C. (2000). The finite volume, finite element, and finite difference methods as numerical methods for physical field problems. *Advances in Imaging and electron physics, 113*, 1-146.

McClean, J. F., & Sumner, D. (2014). An Experimental Investigation of Aspect Ratio and Incidence Angle Effects for the Flow Around Surface-Mounted Finite-Height Square Prisms. *Journal of Fluids Engineering, 136*(8), 081206-081206-081210. DOI:10.1115/1.4027138

Melbourne, & Water. (2005). *Flood Management and Drainage Strategy*. Retrieved from Victoria:

Miettinen, A., & Siikonen, T. (2015). Application of pressure-and density-based methods for different flow speeds. *International Journal for Numerical Methods in Fluids, 79*(5), 243-267.

Mohr, D., Gary, G., & Lundberg, B. (2010). Evaluation of stress–strain curve estimates in dynamic experiments. *International Journal of Impact Engineering, 37*(2), 161-169. doi:https://doi.org/10.1016/j.ijimpeng.2009.09.007

Montalvao, D., Maia, N. M. M., & Ribeiro, A. M. R. (2006). A review of vibration-based structural health monitoring with special emphasis on composite materials. *Shock and vibration digest, 38*(4), 295-324.

NAASRA, N. (1990). Highway Bridge Design Specification. *Sydney, Australia*.

Nasim, M., Setunge, S., Mohseni, H., & Zhou, S. (2018). An investigation of water-flow pressure distribution on bridge piers under flood loading. *Structure and Infrastructure Engineering*. DOI:10.1080/15732479.2018.1545792

Nasim M., Mohseni H., Setunge S., Zhou S., & Dissanayake A.P. (2015). *A Comparison of the Effect of Pier Shape on Flood Loading on Bridges*. Paper presented at the ABC2015 Conference Melbourne.

Neild, S., Williams, M., & McFadden, P. (2003). Nonlinear vibration characteristics of damaged concrete beams. *Journal of Structural Engineering, 129*(2), 260-268.

Oh, E., Deshmukh, A., & Hastak, M. (2010). Vulnerability Assessment of Critical Infrastructure, Associated Industries, and Communities during Extreme Events *Construction Research Congress 2010* (pp. 449-469): American Society of Civil Engineers.

Olsson, R. (2001). Analytical prediction of large mass impact damage in composite laminates. *Composites Part A: Applied Science and Manufacturing, 32*(9), 1207-1215.

Ou Zhiliang. (2007). *Numerical Simulation Of Flow Around Vertical Cylinders.* (Doctor of Philosophy), University of Western Australia.

Park, Y.-J., & Ang, A. H.-S. (1985). Mechanistic seismic damage model for reinforced concrete. *Journal of Structural Engineering, 111*(4), 722-739.

Parola, A. C., Apelt, C. J., & Jempson, M. A. (2000). *Debris forces on highway bridges*: Transportation Research Board.

Patankar, S. (1980). *Numerical heat transfer and fluid flow*: CRC press.

Pham, T. M., & Hao, H. (2016). Prediction of the impact force on reinforced concrete beams from a drop weight. *Advances in Structural Engineering, 19*(11), 1710-1722.

Prasad Gautham Ganesh. (2011). *Analysis of Bridge Performance under the Combined Effect of Earthquake and Flood-Induced Scour.* (Master of Science, Master of Science), The Pennsylvania State University.

Pulliam, T. H., & Steger, J. L. (1980). Implicit finite-difference simulations of three-dimensional compressible flow. *AIAA Journal, 18*(2), 159-167.

Rabczuk, T., Akkermann, J., & Eibl, J. (2005). A numerical model for reinforced concrete structures. *International Journal of Solids and Structures, 42*(5), 1327-1354. doi:https://doi.org/10.1016/j.ijsolstr.2004.07.019

Rafiei, S., Hossain, K., Lachemi, M., Behdinan, K., & Anwar, M. (2013). Finite element modeling of double skin profiled composite shear wall system under in-plane loadings. *Engineering Structures, 56*, 46-57.

Rashid, Y. (1968). Ultimate strength analysis of prestressed concrete pressure vessels. *Nuclear Engineering and Design, 7*(4), 334-344.

Rezaeiha, A., Kalkman, I., Montazeri, H., & Blocken, B. (2017). Effect of the shaft on the aerodynamic performance of urban vertical axis wind turbines. *Energy Conversion and Management, 149*, 616-630.

Rhie, C., & Chow, W. (1983). Numerical study of the turbulent flow past an airfoil with trailing edge separation. *AIAA Journal, 21*(11), 1525-1532.

Rittel, D., & Dorogoy, A. (2008). A methodology to assess the rate and pressure sensitivity of polymers over a wide range of strain rates. *Journal of the Mechanics and Physics of Solids, 56*(11), 3191-3205.

Roufaiel, M. S., & Meyer, C. (1987). Reliability of concrete frames damaged by earthquakes. *Journal of Structural Engineering, 113*(3), 445-457.

Saatci, S., & Vecchio, F. J. (2009). *Effects of shear mechanisms on impact behavior of reinforced concrete beams*.

Saleemuddin, M. Z. M., & Sangle, K. K. (2017). Seismic damage assessment of reinforced concrete structure using non-linear static analyses. *KSCE Journal of Civil Engineering, 21*(4), 1319-1330.

Sawan, J., & Abdel-Rohman, M. (1986). Impact effect on RC slabs: experimental approach. *Journal of Structural Engineering, 112*(9), 2057-2065.

SHARMA, H., HURLEBAUS, S. & GARDONI, P. 2012. Performance-based response evaluation of reinforced concrete columns subject to vehicle impact. *International Journal of Impact Engineering,* 43**,** 52-62.

Shi, S., Zhu, L., & Yu, T. X. (2019). Dynamic modelling of elastic-plastic beams under impact. *International Journal of Impact Engineering, 126*, 1-10. doi:https://doi.org/10.1016/j.ijimpeng.2018.11.017

Shivakumar, K., Elber, W., & Illg, W. (1985). Prediction of impact force and duration due to low-velocity impact on circular composite laminates. *Journal of Applied Mechanics, 52*(3), 674-680.

Sinaei, H., Shariati, M., Abna, A. H., Aghaei, M., & Shariati, A. (2012). Evaluation of reinforced concrete beam behaviour using finite element analysis by ABAQUS. *Scientific Research and Essays, 7*(21), 2002-2009.

Sousa, J., & Bastos, L. (2013). Multi-temporal SAR interferometry reveals acceleration of bridge sinking before collapse. *Natural Hazards and Earth System Sciences, 13*(3), 659.

Standards Australian. (2017). AS 5100.2, Bridge Design - Part 2: Design Loads: Australian Standards.

Stephen, J., & Yao, J. (1987). P. Damage assessment using response measurement [J]. *Journal of Structural Engineering, ASCE, 113*(4), 787-801.

Storey, Chris, Delatte, & Norbert. (2003). Lessons from the collapse of the schoharie creek bridge. *Forensic Engineering*, 158-167.

SYSTEMS, D. (Producer). (2012). SOLIDWORKS Help: Theory of Cumulative Damage.

Tahmasebinia, F. (2008). Finite element simulation of reinforced concrete structures under impact accident. *Structural Survey, 26*(5), 445-454.

Tripathi, B., Misra, A., & Chaudhary, S. (2012). Strength and abrasion characteristics of ISF slag concrete. *Journal of Materials in Civil Engineering, 25*(11), 1611-1618.

Trivedi, N., & Singh, R. (2013). Prediction of impact induced failure modes in reinforced concrete slabs through nonlinear transient dynamic finite element simulation. *Annals of Nuclear Energy, 56*, 109-121.

Tubaldi, E., Macorini, L., Izzuddin, B. A., Manes, C., & Laio, F. (2017). A framework for probabilistic assessment of clear-water scour around bridge piers. *Structural Safety, 69*, 11-22. doi:https://doi.org/10.1016/j.strusafe.2017.07.001

Ulfkjær, J. P., Krenk, S., & Brincker, R. (1995). Analytical model for fictitious crack propagation in concrete beams. *Journal of Engineering Mechanics, 121*(1), 7-15.

Van Dyke, M. (1982). An album of fluid motion.

van Manen, S. E., & Frandsen, A. G. (2017). Ship collision with bridges, review of accidents *Ship Collision Analysis* (pp. 3-12): Routledge.

Wang, Y.-h., Zou, Y.-s., Xu, L.-q., & Luo, Z. (2015). Analysis of Water Flow Pressure on Bridge Piers considering the Impact Effect. *Mathematical Problems in Engineering, 2015*, 1-8. DOI:10.1155/2015/687535

Wei, Z., & Huhe, A. (2006). Large-Eddy simulation of three-dimensional turbulent flow around a circular pier. *Journal of Hydrodynamics, Ser. B, 18*(6), 765-772.

White, F. M. (2011). *Fluid mechanics* (7th ed. ed.). New York, N.Y.: McGraw Hill.

Williams, M. S., & Sexsmith, R. G. (1995). Seismic damage indices for concrete structures: a state-of-the-art review. *Earthquake Spectra, 11*(2), 319-349.

Xiao, H., Huang, W., & Chen, Q. (2010). Effects of submersion depth on wave uplift force acting on Biloxi Bay Bridge decks during Hurricane Katrina. *Computers & Fluids, 39*(8), 1390-1400.

Xie, H., Ju, Y., & Li, L. (2005). Criteria for strength and structural failure of rocks based on energy dissipation and energy release principles. *Chinese Journal of Rock Mechanics and Engineering, 24*(17), 3003-3010.

Xue-kui, G., Xi, Z., & Hui, L. (2006). Seismic Response Analysis of Bridge Pier in Deep Water Excited by Near-fault Earthquakes [J]. *Earthquake Resistant Engineering and Retrofitting, 3*, 016.

Yang, M., & Papagiannakis, A. (2010). A coupled honeycomb composite sandwich bridge-vehicle interaction model. *Journal of Mechanics of Materials and Structures, 5*(4), 617-635.

Yang, Z. (2015). Large-eddy simulation: Past, present and the future. *Chinese Journal of Aeronautics, 28*(1), 11-24.

Yao, J., Teng, J., & Chen, J. (2005). Experimental study on FRP-to-concrete bonded joints. *Composites Part B: Engineering, 36*(2), 99-113.

Yoo, D.-Y., Banthia, N., Kim, S.-W., & Yoon, Y.-S. (2015). Response of ultra-high-performance fiber-reinforced concrete beams with continuous steel reinforcement subjected to low-velocity impact loading. *Composite Structures, 126*, 233-245. doi:https://doi.org/10.1016/j.compstruct.2015.02.058

Yoshihiro, T., & Robert, T. (1988). Restoring forces on vertical circular cylinders forced by earthquakes. *Earthquake Engineering and Structural Dynamics, 16*(5), 98-102.

Yuce, M. I., & Kareem, D. A. (2016). A numerical analysis of fluid flow around circular and square cylinders. *JOURNAL AWWA, 108*, 10.

Zararis, P. D., & Papadakis, G. C. (2001). Diagonal shear failure and size effect in RC beams without web reinforcement. *Journal of Structural Engineering, 127*(7), 733-742.

Zhang, L. (2017). *Numerical Simulation of Flows past a Circular and a Square Cylinder at High Reynolds Number, and a Curved Plate in Transitional Flow.* (Master of Science), Washington University in St. Louis.

Zhong, H., Yang, M., & Gao, Z. (2015). Dynamic responses of prestressed bridge and vehicle through bridge–vehicle interaction analysis. *Engineering Structures, 87*, 116-125. doi:https://doi.org/10.1016/j.engstruct.2015.01.019

Zhou, D., Li, R., Wang, J., & Guo, C. (2017). Study on Impact Behavior and Impact Force of Bridge Pier Subjected to Vehicle Collision. *Shock and Vibration, 2017*, 12. DOI:10.1155/2017/7085392

Zhu, X., & Law, S. (2002). Dynamic load on continuous multi-lane bridge deck from moving vehicles. *Journal of Sound and Vibration, 251*(4), 697-716.

APPENDIX

A. Superstructure Vulnerability under Flood

Grillage analysis is a very simple method of calculation and analysis of the slabs (Shreedhar & Kharde), and in this case study, the model of one span of the bridge has been generated by Space Gass software. Figure A-1 shows the 2D model for grillage analysis.

Loading

$F_d = 0.5 C_d V^2 A_d$ (Drag Forces)

$F_l = 0.5 C_l V^2 A_l$ (Uplift forces)

$F_B = g\rho V = 0.3421\ (KN)$ (Buoyancy forces)

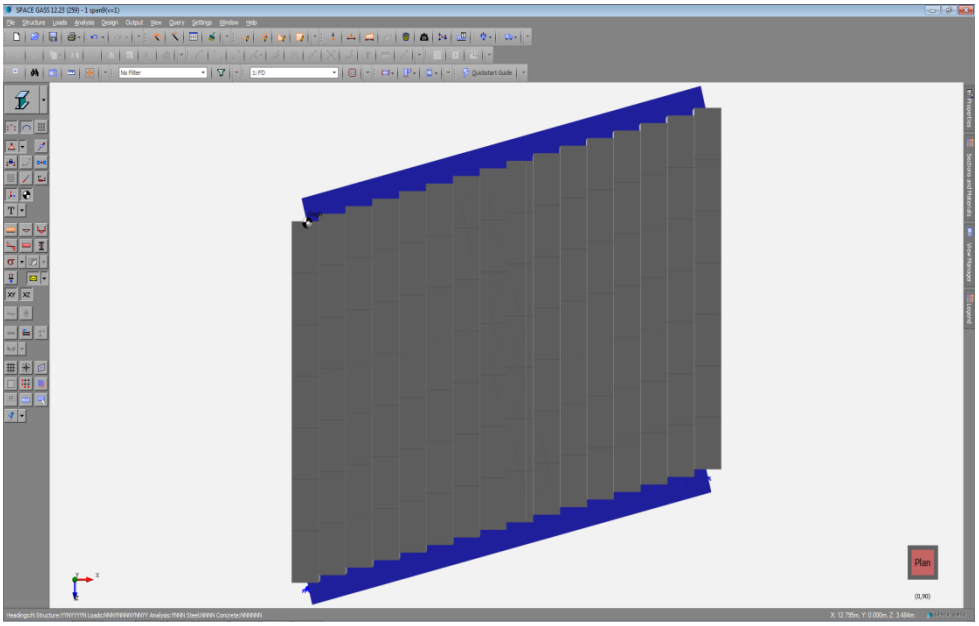

Figure A- 1: Grillage Analysis of the U-Slab Bridge Simulated by Space Gass

Damage index of the superstructure can be determined by the following,

$DI = (M^*/M_{zu}) \leq 1$

The model is exposed to the different water flow velocities and the drag and uplift forces inclined with buoyancy and the deck self-weight.

In order to configure the relationship between (M*) moment generated by flood and the flood velocity, the software has been run for various values of flood velocities. The moment capacity of the U beams has been calculated as recommended in the AS 3600 concrete structure codes. U beam section geometry is described in Figure A-2.

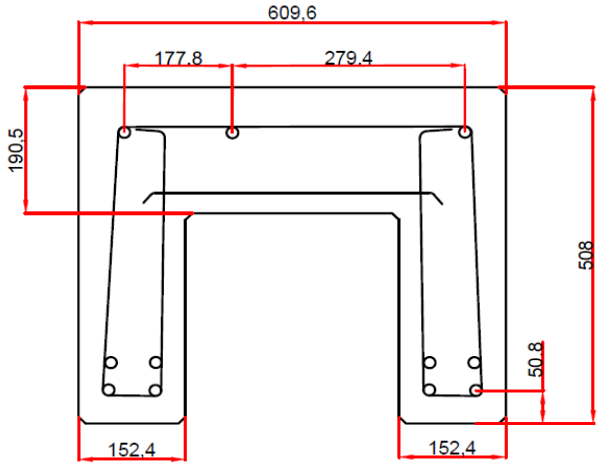

Figure A- 2: Typical U- Beam section

From the calculation of the moment capacity of the beam section considering φ=0.8, according to the AS 3600 concrete structure codes, moment capacity of the U beam has been derived:

$$M_{zu} = 319.2 \text{ (KN.m)}$$

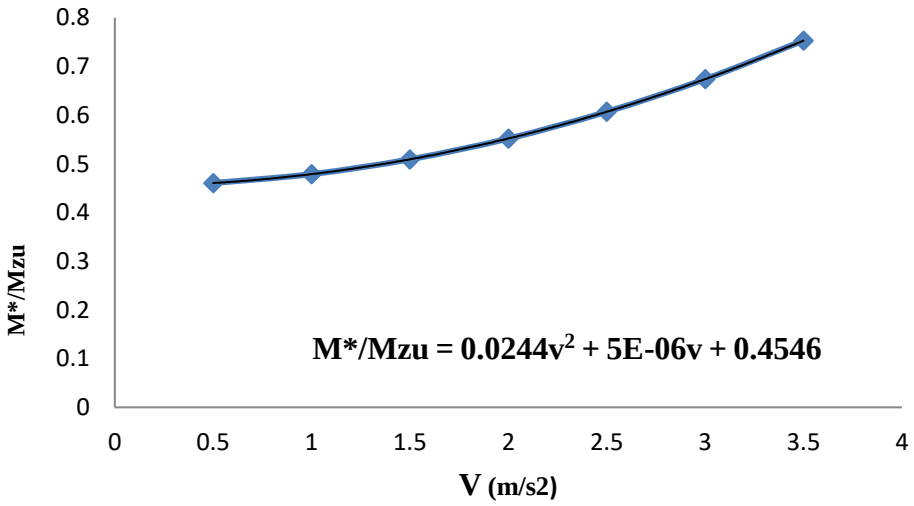

Figure A-3: Vulnerability Curve for Bridge Deck during Extreme Flood

$$(M^*/M_{zu}) = 0.0244V^2 + 5E\text{-}06V + 0.4546$$

Figure A-3 describes the vulnerability of the superstructure during the extreme flood and the formula derived by Excel software can represent the relation of the velocity changes and the damage index variations. From the equation derived by the graph, critical velocity has been derived:

Vcritical=4.73 (m/s)

Which means under the common velocities of the flood, the damage fo the deck should not have happened as the lateral stiffness of the deck is significantly high. But we expected to have a severe condition when the flood velocity is increasing.

B. A REVIEW OF DAMAGE INDICATORS

DIs are capable of quantifying the structural damage level (DL) numerically, and they play a crucial role in decision making on structural resilience during disasters or natural hazards. DIs can quantify the local or the global damage of the structure. Generally, damage to the concrete structures can be represented as the failure of the components of the structure. The failure in reinforced concrete is defined as the instance corresponding to concrete crushing. In flexural members, this will happen well after crack initiation in the tensile zone.

Available DIs can be divided into two categories – cumulative and non-cumulative DIs (Cao *et al.* 2014). The theory of cumulative damage assumes that a stress cycle with alternating stress above the durability limit applies measurable permanent damage. It also states that the total damage caused by some stress cycles is equal to the summation of damages caused by the individual stress cycles (SYSTEMS 2012).

Researchers have developed different DIs based on various concepts. The development of the damage model related to the empirical damage definition goes back to the development of firs damage model which was based on the ductility concept, the most straightforward possible damage index (Banon *et al.* 1981, Williams and Sexsmith 1995). Displacement, stress and strain, stiffness and fatigue, and energy dissipation concepts are the common concepts used for DI description. However, due to the complexity of the damage and failure concepts and their theories and methodologies, in this paper, we will focus on the contrast between two methods, dissipated energy and displacement concepts. The two methods are compared in the context of practical application.

A-1 CUMULATIVE DAMAGE INDICES

Cumulative DIs are more applicable for evaluating the damage state of the structure, which is experiencing an earthquake or cyclic loading. Some popular DIs introduced by different researchers are explained here.

A-1-1 Park and Ang (1985)

Amongst all the cumulative DIs, the very widely adopted one for the seismic loading is the one proposed by (Park and Ang 1985). The concept of the index is based on the combination of the strength, ductility and energy dissipation. The DI for a single degree of freedom (SDOF) system is defined by the following equation:

1. $$\boldsymbol{DI = \frac{u_m}{u_u} + \beta \frac{\int dE_h}{m r_y u_u} = \frac{u_m}{u_u} + \beta \frac{E_h}{F_y u_u}}$$

where, u_m is the maximum displacement of an SDOF system under seismic loading, u_u is the ultimate displacement under monotonic loading, E_h is the hysteretic energy dissipated by the SDOF system, r_y is the yield resistance of the system, F_y is the yield force, β is the parameter to include the effect of repeated loading and m is the mass of the system.

A-1-2 Banon and Veneziano (1982)

Banon & Veneziano (1982) defined a DI based on the normalised cumulative rotation (Banon and Veneziano 1982), which is addressed based on the flexural damage by the following function:

2. $\boldsymbol{DI = \frac{\sum_{i=1}^{n} \emptyset_{im} - \emptyset_y}{\emptyset_u}}$

where ϕ_m is the rotation value of m^{th} element, and ϕ_y and ϕ_u respectively represent the rotation function of curvature at the yield and ultimate states.

Based on flexural damage ratio (FDR), Banon et al. (1981) developed a DI regarding stiffness degradation.

3. $\boldsymbol{DI = \frac{M_u \emptyset_m}{M_m \emptyset_u}}$

where, M_m is the moment in m^{th} element and M_u represents the moment at ultimate state.

A-1-3 Stephen and Yao (1987)

Stephens and Yao (1987) expressed the fatigue damage sustained during each cycle of response using cumulative displacement ductility according to:

4. $\boldsymbol{DI = \sum_{i=1}^{n} \left[\frac{\Delta d^+}{\Delta d_f}\right]^{1-br}}$

where Δd is the displacement ductility, and Δd_f represents fatigue displacement. Using this approach, the relative damage attributed to each inelastic cycle of response is a nonlinear function of the shape and size of the cycle and coefficient b_r can be calculated based on the shape and size of the cycle (Stephen and Yao 1987).

A-1-4 Jeang and Iwan (1988)

Jeang and Iwan (1988) calculated DI based on the accounting of the effect of combining cycles with various amplitudes.

5. $$DI = \sum_{i=1}^{n} \left[\frac{n_i u_i^2}{C} \right]$$

where n represents the number of cycles, u is the relative deflection and C is the amplitude defined in Saleemuddin and Sangle (2017).

A-1-5 Cao et al. (2011)

Cao and colleagues explained that the damage in an earthquake depends on two factors –the structure characteristic and applied loadings. For a monotonic loading, they proposed the following equation

6. $$DI = \left[\frac{E_h}{E_h + E_{rec}} \right]^{N-i}$$

where E_h represents the cumulative hysteretic energy until the i^{th} cycle, and E_{rec} is the cumulative recoverable energy until the i^{th} cycle, i is the number of cycles that satisfy the condition $u_m > u_{cr}$, u_{cr} is the deformation at cracking and N is an equivalent number of yield cycles defined by the following equation:

7. $$N = \frac{E_{non-rec,collapse}}{E_{non-rec,y}}$$

where, $E_{non-rec,y}$ is non-recoverable energy at yield, and $E_{non-rec,collapse}$ is the non-recoverable energy at collapse under monotonic loading.

8. $\boldsymbol{E_{non-rec,collapse} = F_y(u_u - u_y)}$

where F_y is the yield force. For structure, the DI is defined according to

9. $\boldsymbol{DI_{structure} = \sum(\lambda_{n,element} \cdot DI_{n,element})}$; $\boldsymbol{\lambda_{n,element} = \left[\frac{E_{h,n}}{\sum E_{h,n}}\right]_{element}}$

where, $DI_{n,element}$ is the DI of n^{th} elements and $\lambda_{n,element}$ is the weighting factor based on hysteretic energy (Cao Van *et al.* 2011).

A-2 NONCUMULATIVE DAMAGE INDICES

In monotonic loadings the non-cumulative damage models are more appropriate in which the simplest concept is the ductility ratio, expressing the rate of the deformation in the load time history to the ultimate or the yield deformation of the structure. The non-cumulative DIs which can be used for monotonically increasing load, usually have been used to determine the local damage and may not be useful for the system's general damage.

A-2-1 Rafuaiel and Meyer (1988)

The global damage parameter (GDP) has been proposed to define the strength-based overall degree of damage in a frame building, according to

10. $\boldsymbol{DI = GDP = \frac{d_r - d_y}{d_f - d_y}}$

where d_r is the maximum roof displacement, d_y represents the roof displacement, and d_f denotes the roof failure displacement (Roufaiel and Meyer 1987).

A-2-2 Massumi and Moshtagh (2013)

Based on the percentage of the nonlinear fundamental period of the structure, and the variation of the structural period due to seismic loads, the following DI was proposed for reinforced concrete flexural frames (Massumi and Moshtagh 2013),

$$\textbf{11. } \boldsymbol{DI = 1 - \left(\frac{T_{initial}}{T_{final}}\right)^2}$$

in which, $T_{initial}$ is the fundamental period of the structure, and T_{final} represents the primary period of a structure subjected to cyclic loads (Massumi and Moshtagh 2013).

The concept of vibration-based structural damage detection and health monitoring as an essential factor in safety, reliability and durability of the system has been addressed by Doebling *et al.* (1996) and reviewed and monitored by Montalvao *et al.* (2006) and Farrar and Worden (2007)

A-2-3 Ghobarah et al. (1999)

Ghobarah et al. (1999) used the concept of the final softening for determining the damage value. They proposed a practical method based on the static pushover analysis to assess the damage of the structures when subjected to earthquakes of different intensities

$$\textbf{12. } \boldsymbol{(DI)_K = 1 - \left(\frac{K_{final}}{K_{initial}}\right)}$$

where $K_{initial}$ is the initial slope of the base shear-top deflection relationship resulting from the pushover analysis of the frame before being subjected to the earthquake ground motion

and K_{final} is the initial slope of the same relationship but after the structure is subjected to the earthquake time history (Ghobarah *et al.* 1999).

C. Estimating the Stable Time Increment Size

An approximation to the stability limit is often written as the shortest transit time of a dilatational wave across any of the elements in the mesh

13. $\Delta t \approx \frac{L_{min}}{c_d}$,

where L_{min} is the smallest element dimension in the mesh and c_d is the dilatational wave speed in terms of λ_0 and μ_0 , defined below.

14. $c_d = \sqrt{\frac{\hat{\lambda}+2\hat{\mu}}{\rho}}$

Where ρ is the density of the material. In an isotropic, elastic material the effective Lamé's constants can be defined in terms of Young's modulus, E, and Poisson's ratio, ν , by

15. $\hat{\lambda} = \lambda_0 = \frac{E\nu}{(1+\nu)(1-2\nu)}$

and

16. $\hat{\mu} = \mu_0 = \frac{E}{2(1+\nu)}$

In general, for beams, conventional shells, and membranes the element thickness or cross-sectional dimensions are not considered in determining the smallest element dimension; the stability limit is based upon the mid-plane or membrane dimensions only. When the transverse shear stiffness is defined for shell elements, the stable time increment will also be based on the transverse shear behaviour.

This estimate for Δt is only approximate and in most cases is not a conservative (safe) estimate. In general, the actual stable time increment chosen by Abaqus/Explicit will be less than this estimate by a factor between $1/\sqrt{2}$ to 1 in a two-dimensional model and between $1/\sqrt{3}$ to 1 in a three-dimensional model. The time increment is chosen by Abaqus/Explicit also accounts for any stiffness behaviour in a model associated with penalty contact (Kulkarni and Shah 1998) (ABAQUS 6.14 2013).

Based on the above description, the total analyses time-period can be calculated and is assumed 0.04(s).

17. $c_d = \sqrt{\frac{E}{\rho(1-\nu^2)}} = \sqrt{\frac{23500}{2.4e^{-9}(1-0.15^2)}} = 9009$

where elements' size $l = 20\ (mm)$

for the stability of analysis: $\Delta t = \frac{l}{C} = 0.002\ (s)$

$T \leq 50 * \Delta t$

$T = 0.04\ (s)$

D. How time-period of the analysis influence on the response of the structure under impact

Experimental results for a reinforced concrete beam subjected to a drop hammer loading were used for calibrating this simulation (Fujikake et al., 2009). A significant issue which could be raised in Dynamic/Explicit analysis is to select the appropriate time-period for the study of the impact phenomenon, time-step option in ABAQUS. In the impact analysis, based on the concepts of FE techniques, if the methodology of impact modelling is applying initial velocity to the impactor, the time-period of analysis, T, cannot affect the structural response. While the time-period, *t*, of the impact, P(t), which is dependent on the velocity and the impulse of the induced forces, T, could influence the results and structural responses. The general response of the system can be calculated from the differential equation.

To understand the concept and to consolidate the findings, analysis with different Time-Periods of (a) T=0.01s, (b) T=0.05 s, (c) T=0.1s, has been conducted to examine how the selection of time-period, T, can influence the response of the structure under the impact loading of a MO. **Figure D-1** illustrates three simulations where the mass, velocity and the structure were kept the same with the time-period as the major variables. It is noted that the response of the crack patterns is not different, and the crack path is aligned with the initiated cracks, and

the growth of the cracks is observed with increase in time-period from 0.01 to 0.1 second.

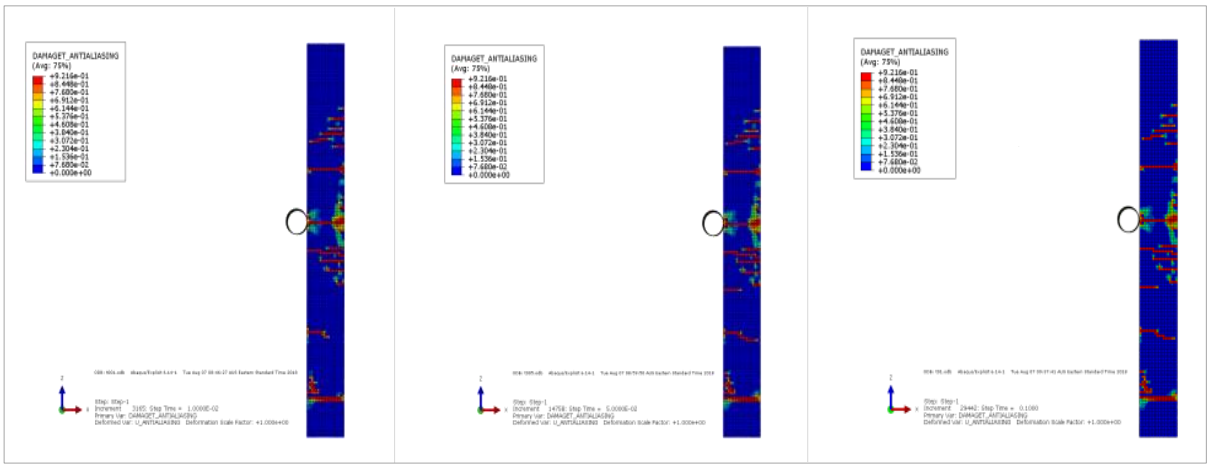

Figure D-1: Crack pattern and responses of a simulated model utilising ABAQUS with time-period of (a) T=0.01s, (b) T=0.05 s, (c) T=0.1s**.**

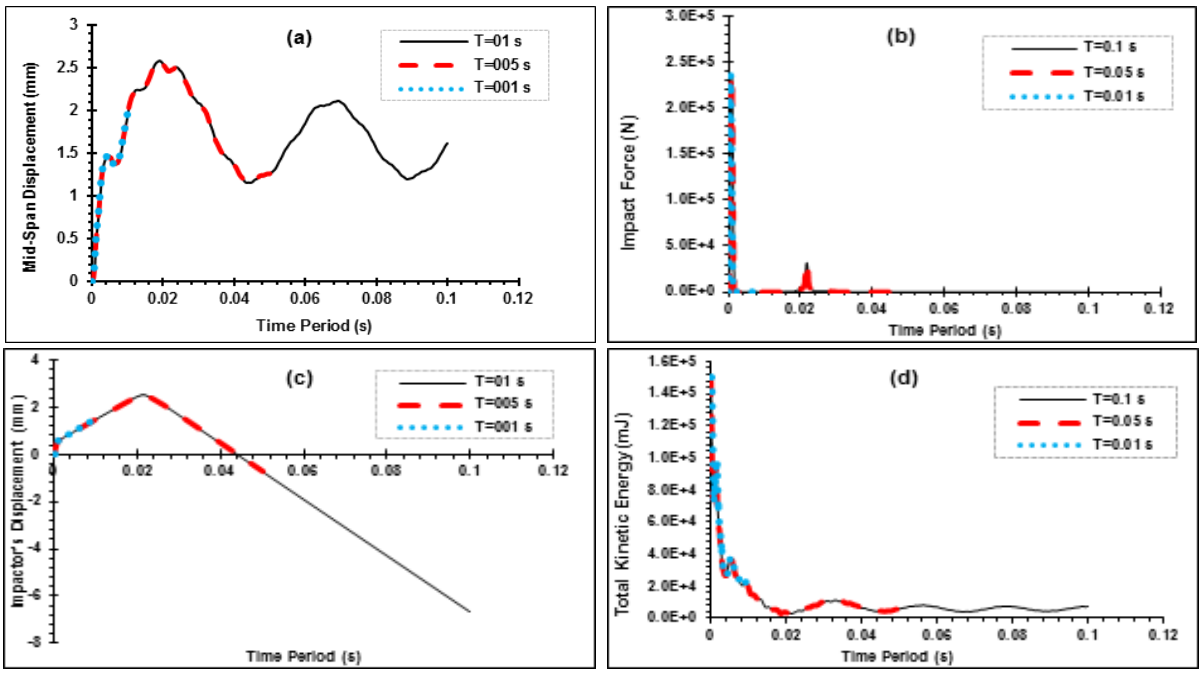

Figure D-2: Structural responses for different time-periods of 0.01 (s), 0.05 (s) and 0.1 (s), in various aspects; Time history of (a) the deformation of the mid-span, (b) impulse of the loading, (c) the displacement of the object and (d) total kinetic energy.

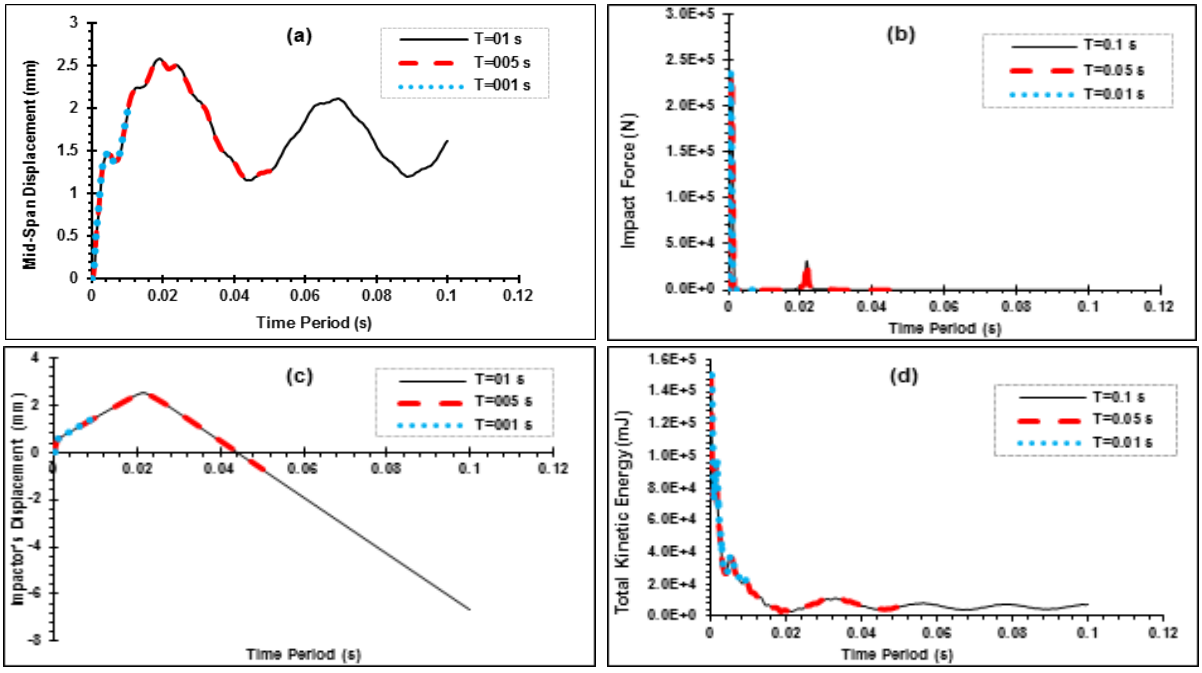

Figure D-2 illustrates different aspects of structural responses for selected time-periods. Time history of the deformation of the mid-height, impulse of the loading, the displacement of the object and the total kinetic energy shows how the time-period selection in this case study can affect the responses. In other words, does not support the hypothesis that the time-period influences the structural responses. This is applicable in the case where the structure is under the impact of MO, and the impact loading is applied with free boundary conditions and velocity to the object. The reason for adopting the velocity approach for implementing an impact loading to the structure is that the velocity is time-independent, and it doesn't affect the structural response. This analysis has been conducted to determine what time-period is appropriate for this numerical analysis.

Based on the above analysis, it is observed that time steps will affect when the load is applied incrementally on the structure. However, time-step doesn't influence the results if the load is applied using it as velocity or inertia for the MO.

E. Comparison of the dimensionless factor of the peak impact forces (φ_{pi}) with AASHTO and AS5100

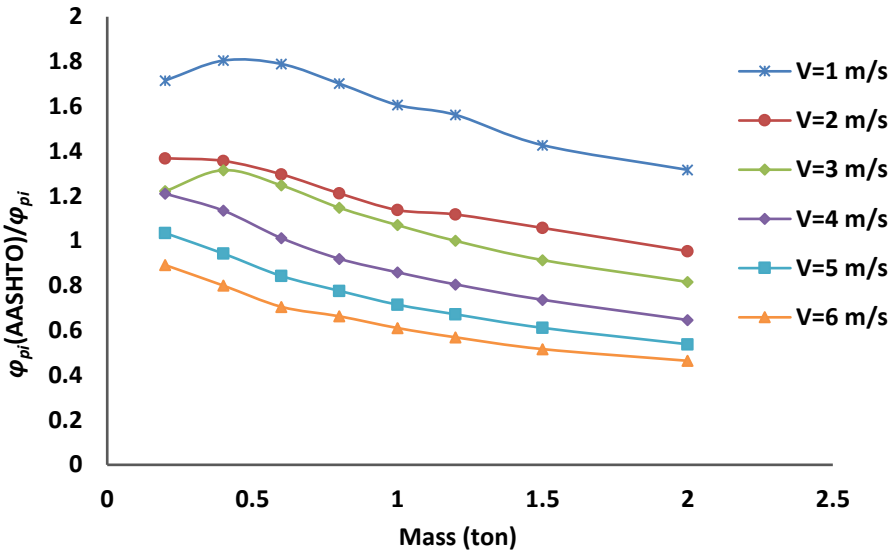

Figure E-1: The ratio of the coefficient of horizontal impact forces resulting from the impact of the MO to the bridge pier and calculated based on AASHTO and the current study

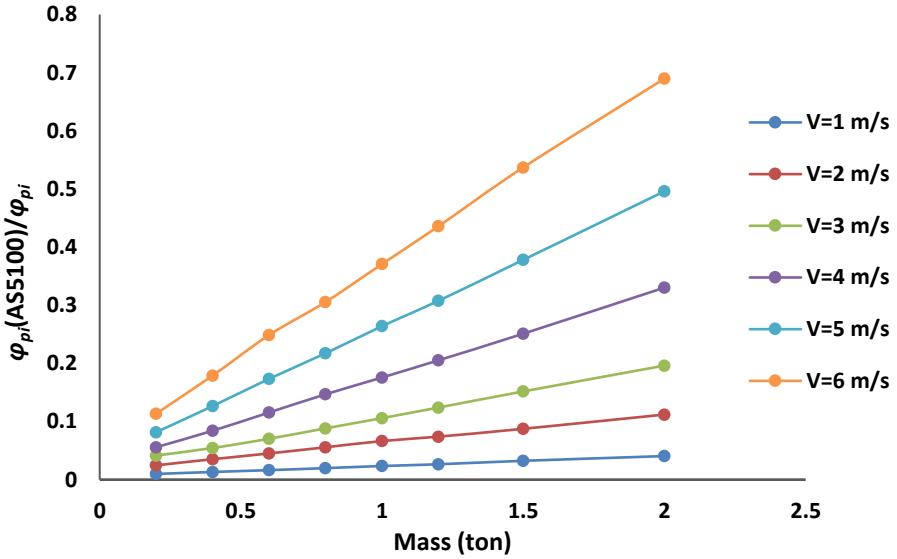

Figure E-2: The ratio of the coefficient of horizontal impact forces resulting from the impact of the MO to the bridge pier and calculated based on AS5100 and the current study